# Evolution of the Arabian Nubian Shield and Snowball Earth

7

Nathan R. Miller and Robert J. Stern

**Abstract**

Neoproterozoic evolution of the Arabian-Nubian Shield (ANS) and East African Orogen (EAO), 870–541 Ma, spanned revolutionary changes in Earth Systems, including a supercontinent cycle (Rodinia break-up, opening/closing of the Mozambique Ocean, Gondwana assembly), extreme climate fluctuations between long-lived glacial episodes as postulated by the Snowball Earth Hypothesis (1992–2002), marked increases in oceanic and atmospheric oxygen levels, and expansion of the biosphere from simple microbial life to the inclusion of larger and more diverse multicellular organisms. Understanding of these Earth System transitions has advanced tremendously over the past two decades through the integration of global studies of Neoproterozoic sedimentary successions with refined geochronologic techniques. This approach applied to Neoproterozoic Snowball Earth (NSE) localities now indicates that Neoproterozoic glaciations included two global-scale (panglacial) episodes, the ~717–659 Ma Sturtian and ~650–640 to 635 Ma Marinoan glaciations—which together comprise the Cryogenian Period, and more regional episodes during the Ediacaran Period and possibly, albeit controversially, during the earlier Tonian Period. Recent geochronologic, geochemical, and sedimentologic studies of low metamorphic grade ANS successions substantially contribute to the global Neoproterozoic dataset and, along with recently revised age constraints for the Cryogenian Period, facilitate an updated assessment of how Neoproterozoic glaciations may have influenced the sedimentary record of the ANS during its development. Tonian and Sturtian glaciations would have occurred following Rodinian break-up and major phases of juvenile crust formation in arc/island arc settings of the Mozambique Ocean (870–690 Ma), while latent terrane accretion and magmatism were still active. Paleogeographic reconstructions for these intervals generally place the ANS at tropical latitudes, where chemical weathering rates of juvenile crust terranes would have been high. Evidence supporting Tonian glaciation in the ANS is unresolved, with banded iron formation (BIF) and possible glacial diamictite scattered over the Central Eastern Desert (CED) of Egypt, NW Arabia, and possible correlative units in NE Sudan, as strongest candidates based on available age control (~780–740 Ma) and lithologic compatibility with NSE episodes. New age constraints for some of these localities (i.e., Atud diamictite and Um Nar, El-Hadid, Um Ghamis, and Wadi Kareim BIF localities in the CED) now demonstrate that deposition coincided with the Sturtian panglacial interval. Strong evidence of Sturtian glaciation in the ANS also occurs at the top of the Tonian-early Cryogenian Tambien Group in Northern Ethiopia, where polymict diamictite (<719.7 ± 0.5 Ma) bearing clasts consistent with glacial transport transitionally overlies limestone with pre-Sturtian $^{87}Sr/^{86}Sr$ values of 0.7066. Diamictite clast compositions similar to lower Tambien Group units suggest derivation from Tambien Group source terranes within the ANS, such as may have developed during early structural emergence of the EAO and/or associated eustatic sea-level fall. Carbonate units preserving negative carbon isotope excursions correlated to the ~800 Ma Bitter Springs anomaly, ~737 Ma Islay anomaly, and ~720 Ma pre-Sturtian transition, demonstrate that the Tambien Group is an important archive for studying the Tonian transition to extreme climates of the Cryogenian. The Marinoan (~645–635 Ma) glaciation overlapped with incipient development of the EAO, resulting from convergence, uplift, and structural

N. R. Miller (✉)
Department of Geological Sciences, University of Texas at Austin, Austin, TX 78712-1722, USA
e-mail: nrmiller@jsg.utexas.edu

R. J. Stern
Geosciences Department, University of Texas at Dallas, Richardson, TX 75083-0688, USA



Z. Hamimi et al. (eds.), *The Geology of the Arabian-Nubian Shield*, Regional Geology Reviews,
https://doi.org/10.1007/978-3-030-72995-0_7

deformation of earlier formed arc and accreted arc terranes, as the Mozambique Ocean closed between cratonic fragments of West and East Gondwana. Because most of the ANS was likely elevated above sea level, the ANS/EAO had few depocenters capable of preserving Marinoan sedimentation. Some peripheral margin basins, such as Murdama and Furayh basins in Arabia, overlapped with the Marinoan glaciation, but their sedimentary records have not been systematically studied for glacigenic characteristics. The onset of sedimentation in some post-amalgamation basins of the northern ANS (e.g., Jibalah Group of NW Arabia and possible equivalents in Jordan and Israel) may have overlapped with the Marinoan glaciation or Marinoan sediments could have been subsequently reworked in alluvial systems and redeposited during early basin formation. Following continental collision (~630–600 Ma), Ediacaran glaciations would have coincided with continued shortening and orogenic uplift (~600–540 Ma), when vast alluvial fan systems transported sediments away from EAO highlands. Ediacaran paleogeographic reconstructions generally place the ANS at higher tropical or temperate latitudes in the S. Hemisphere that may have supported regional scale glaciation. Within post-amalgamation basins of the northern Arabian Shield, the Jibalah Group sedimentary record includes polymict conglomerate, matrix-supported diamictite, and occasional dropstones that could be glacigenic. Regional deposition, constrained between underlying shield rocks (likely $\leq 605 \pm 5$ Ma) and the overlying Lower Cambrian basal unconformity (~540–520 Ma) and confirmed by U–Pb zircon dating of volcanic intervals within several basins, would have spanned the ~580 Ma Gaskiers glaciation, the ~575–567 Ma Shuram negative carbon isotope excursion, and younger Ediacaran glaciations. Although highly variable, sedimentary fill in many basins begins as polymict conglomerate with increasing limestone abundance in the higher succession, possibly consistent with a marine transgression. Carbonate $\delta^{13}C$ values in combination with detrital zircon ages indicate that the basal conglomerate units pre-date the Shuram anomaly and could correlate with the ~580 Ma Gaskiers glaciation. Post-glacial supersequences may have been similarly deposited throughout northern Gondwana (Israel, Jordan, Saudi Arabia, Oman). Metazoan trace and probable body fossils are documented in Dhaiqa and Jifn basins above conglomeratic strata (Mataar Fm and Jifn Polymictic Conglomerate) that have been prospectively correlated with the Gaskiers glaciation. The lowest fossil horizons are no younger than 577 ± 5 Ma (Jifn) and 569 ± 3 Ma (Dhaiqa), similar to the Newfoundland record, where Ediacaran fauna appear ~9.5 myr after the ~580 Ma Gaskiers glaciation (Pu et al. in Geology 44:955–958, 2016). Follow-up studies are needed to assess the timing and glacigenic affinity of conglomerate and diamictite units, and to establish if and when marine deposition occurred within the Jibalah Group. A conspicuous stratigraphic feature of the northern Gondwanan margin is the widespread occurrence of an erosional unconformity throughout North Africa and Arabia separating Neoproterozoic basement from Cambro-Ordovician age sandstone that was principally sourced from erosion of the EAO. Although EAO erosion would have initiated as soon as regional uplift began, the exceptional power of Marinoan and Ediacaran ice sheets acting on a Himalaya-scale orogen may have contributed to ~650–540 Ma beveling of the Afro-Arabian Peneplain.

**Keywords**

Arabian-Nubian Shield • East African Orogen • Afro-Arabian Peneplain • Neoproterozoic glaciation • Snowball Earth • Sturtian • Marinoan • Gaskiers

## 7.1 Introduction

The Arabian-Nubian Shield (ANS) is a vast tract of variably deformed and metamorphosed juvenile Neoproterozoic crust, forming Precambrian basement terranes that outcrop over substantial areas of NE Africa and Arabia. The intersection of ANS evolution with late Neoproterozoic glaciations, as popularized by the Snowball Earth Hypothesis (SEH) (Kirschvink 1992; Hoffman et al. 1998; Hoffman and Schrag 2002) and as defining the Cryogenian Period (Knoll et al. 2004, 2006; Rooney et al. 2015) is the topic of this chapter. To appreciate the timing of this intersection over Earth history, consider the length of an outstretched arm as an analogy for Earth's 4.54 Ga timeline, with the nail edge of the longest (index) finger being today. ANS evolution roughly occurred within the palm of the hand. The Cryogenian Period is where a snowball (or slushball) would rest on the upper palm of the outstretched arm. This is also about the time that life became more complex. From the hand to the shoulder, the record of life is simple and microbial. From the palm to the fingernail, the size and complexity of multicellular life increased dramatically with the rise of multicellular organisms. Clearly, Neoproterozoic development of the ANS spanned a dynamic and fascinating interval of Earth history. The ANS stands out in that early Cryogenian glaciation occurred within a regionally active intra-oceanic arc setting, compared with more typical passive margin successions that dominate the Neoproterozoic Snowball Earth (NSE) literature.

Both volcanism and chemical weathering are potential triggering mechanisms for Neoproterozoic glaciations (Stern and Miller 2018). Compared to continental crust, juvenile crust is more susceptible to chemical weathering in subaerial and submarine environments, particularly in low latitude settings, and may have fostered reverse greenhouse cooling by burying carbon in sediments (Goddéris et al. 2003; Donnadieu et al. 2004; Horton 2015; Gernon et al. 2016). Thus, it is of particular interest to understand how the magmatic and weathering history of ANS terranes relates to Neoproterozoic climate. Within the tectonomagmatic evolution of the ANS, depositional, chemical, and isotopic characteristics of associated sedimentary rocks, especially those of low metamorphic grade, are essential for understanding the history of Neoproterozoic interactions between the evolving geosphere, hydro/cryosphere, atmosphere, and biosphere. That sediments of this age and metamorphic grade are preserved in the ANS is increasingly recognized and has begun to attract international scientific attention to its sedimentary archives. As a reference for further considering ANS development in relation to Neoproterozoic glacial episodes, it is useful to first introduce the chronological framework and significant global events of the Neoproterozoic Era.

The Neoproterozoic Era (1000–541 Ma), subdivided into Tonian (1000–720), Cryogenian (720–635.5 Ma), and Ediacaran (635.5–541 Ma) Periods, was a revolutionary time interval in Earth history, involving tremendous changes in Earth Systems (Fig. 7.1). Tectonically, Neoproterozoic time witnessed a supercontinent cycle involving the break-up of Rodinia in the first half of the era, and the reassembly of a new supercontinent (Greater Gondwana or Pannotia) near the end of the era (Stern 1994). Rocks bearing definitive evidence of modern plate tectonic processes become abundant during the Neoproterozoic (Stern 2018; Stern and Miller 2018). Climatically, Neoproterozoic Earth experienced multiple extreme swings between exceptionally widespread and enduring glacial states and greenhouse conditions (Kirschvink 1992; Hoffman et al. 1998). The redefined Cryogenian Period (Knoll et al. 2004, 2006; Rooney et al. 2015; Shields-Zhou et al. 2016) denotes the interval of most intense glaciation: ~717–659 Ma Sturtian glaciation and ~650–640 to 635 Ma Marinoan glaciation. More regional shorter-lived glaciations occurred during the Ediacaran, notably the Gaskiers glaciation. Potentially (albeit controversially) regional glaciations may also have occurred earlier, during the Tonian.

Marked increases in oceanic and atmospheric oxygen levels occurred during the Neoproterozoic (Fig. 7.1C), termed the Neoproterozoic Oxygenation Event (NOE) (Och and Shields-Zhou 2012). During the NOE, the redox profile of deep Neoproterozoic oceans, as proxied by sulfur isotopes in pyrite and gypsum of marine sediments, transitioned from largely anoxic, ferruginous, and sulfate-poor [with episodic euxinia (free-$H_2S$) at mid-depths and oxygenated surface waters] (Canfield et al. 2008; Poulton and Canfield 2011; Guilbaud et al. 2015) to a more oxygenated sulfate-rich and Fe-poor state by the end of the Ediacaran, conditions which have prevailed in Phanerozoic oceans (Canfield et al. 2007; Och and Shields-Zhou 2012; Sahoo et al. 2012; Planavsky et al. 2014; Shields et al. 2019; Tostevin et al. 2019; Wu et al. 2020).

The carbon and strontium isotopic composition of Neoproterozoic seawater, as proxied by marine carbonates (Fig. 7.1A–B), respectively demonstrate multiple deep negative carbon isotope excursions (CIEs) from background values ~5–8‰ higher than modern seawater, considered to reflect major perturbations to the carbon-cycle (Halverson et al. 2005; Grotzinger et al. 2011; Halverson et al. 2018), and an overall, but still poorly resolved, increase in $^{87}Sr/^{86}Sr$—consistent with increased weathering of continental crust (Kaufman et al. 1993; Squire et al. 2006), but with intermittent input of less-radiogenic Sr before and during Rodinian break-up (Zhou et al. 2020).

Finally, the Neoproterozoic separates relatively simple microbial ecosystems of the previous three-billion years from larger and more complex multicellular organisms of the Phanerozoic biosphere (Fig. 7.1C) (Butterfield 2015). Although molecular-clock estimates suggest Tonian origins (Dohrmann and Wörheide 2019), rocks close to the Cryogenian-Ediacaran transition first document the presence of metazoans as (sponge) biomarkers (McCaffrey et al. 1994; Love et al. 2009; but see Antcliffe 2013) and a ~600 Ma specimen of probable poriferan affinity is described from the Doushantuo Formation of South China (Yin et al. 2015). Key increases in metazoan size and diversity occurred during the Ediacaran Period. Recent age constraints indicate that Ediacaran biota in Canada likely appeared after the ~580 Ma Gaskiers glaciation (Pu et al. 2016) and before the ~575–567 Ma Shurum negative CIE (Rooney et al. 2020).

The SEH is constantly modified as new information amasses. The intersection of ANS evolution with evidence for Neoproterozoic Snowball Earth (NSE) glaciations was earlier explored in Stern et al. (2006), where diagnostic evidence supporting glacial processes and post-glacial warming was described, and the occurrence of ANS sedimentary rocks with characteristics of NSE successions was demonstrated. Since then much new has been learned about Neoproterozoic glaciations, notably including the number and timing of panglacial episodes that have redefined the onset and termination of the Cryogenian Period, the stratigraphic frequency and timing of negative CIEs and their relationship to glacial intervals, the mainly pre- and syn-Sturtian occurrence of sedimentary iron formation, idiosyncratic characteristics of Sturtian and Marinoan cap

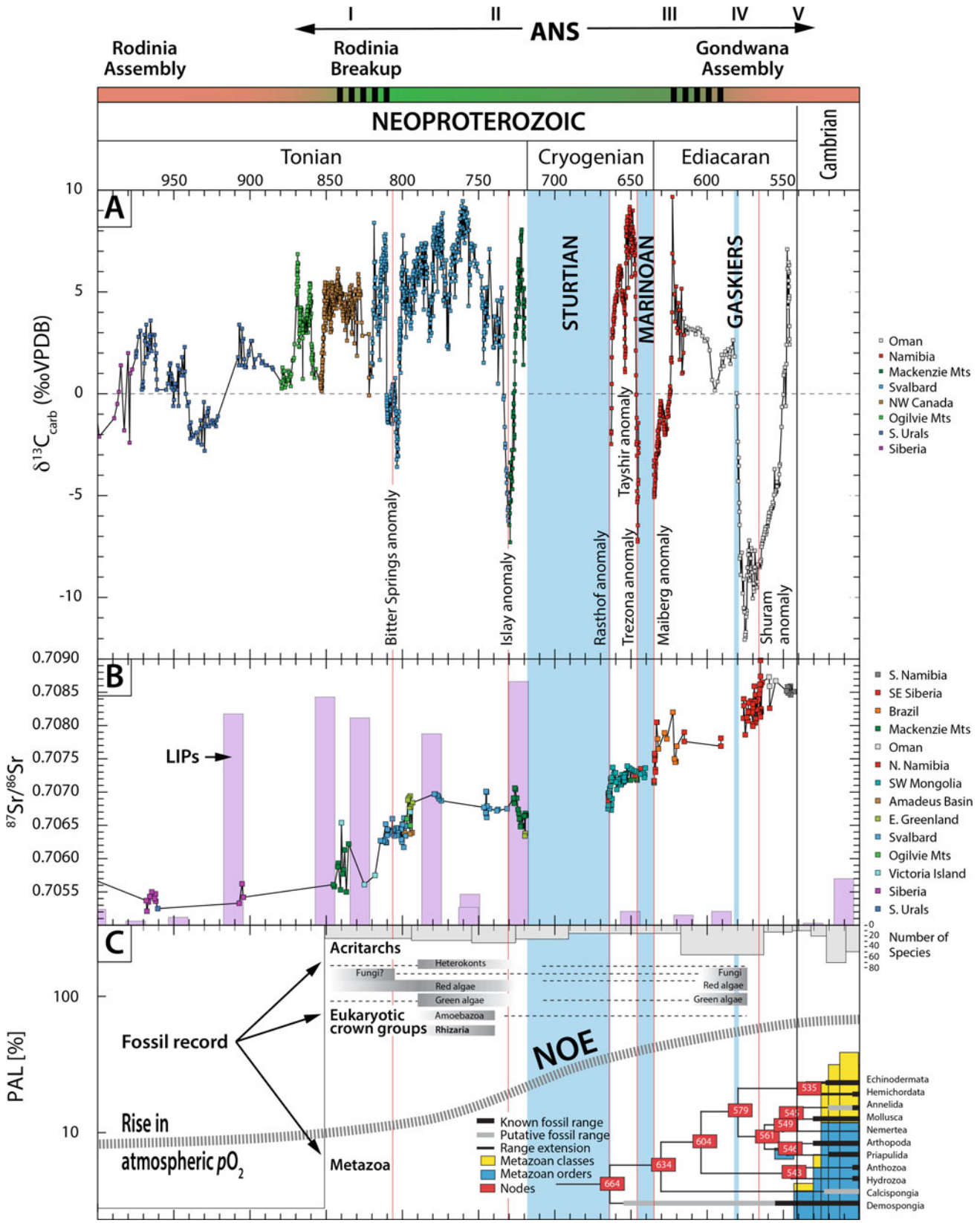
I
II
ANS
III
IV
V
Rodinia Assembly
Rodinia Breakup
Gondwana Assembly
NEOPROTEROZOIC
Tonian
Cryogenian
Ediacaran
Cambrian
950
900
850
800
750
700
650
600
550
A
δ13Ccarb (‰VPDB)
STURTIAN
MARINOAN
GASKIERS
Bitter Springs anomaly
Islay anomaly
Rasthof anomaly
Tayshir anomaly
Trezona anomaly
Maiberg anomaly
Shuram anomaly
Oman
Namibia
Mackenzie Mts
Svalbard
NW Canada
Ogilvie Mts
S. Urals
Siberia
B
87Sr/86Sr
LIPs
S. Namibia
SE Siberia
Brazil
Mackenzie Mts
Oman
N. Namibia
SW Mongolia
Amadeus Basin
E. Greenland
Svalbard
Ogilvie Mts
Victoria Island
Siberia
S. Urals
Number of Species
C
PAL [%]
Fossil record
Rise in atmospheric pO2
Acritarchs
Heterokonts
Fungi?
Red algae
Green algae
Eukaryotic crown groups
Amoebazoa
Rhizaria
Fungi
Red algae
Green algae
NOE
Metazoa
Known fossil range
Putative fossil range
Range extension
Metazoan classes
Metazoan orders
Nodes
Echinodermata
Hemichordata
Annelida
Mollusca
Nemertea
Arthopoda
Priapulida
Anthozoa
Hydrozoa
Calcispongia
Demospongia

◀ **Fig. 7.1** Earth system transitions and glacial episodes (light blue columns) during the Neoproterozoic supercontinent cycle, involving the breakup of Rodinia and assembly of Gondwana, and geologic evolution of the Arabian-Nubian Shield (ANS). **A** Carbon isotopic composition of seawater based on marine limestones for localities compiled by Cox et al. (2016). Red vertical lines mark globally recognized negative carbon isotope excursions (CIEs) or anomalies, as labeled. Horizontal dashed line shows $\delta^{13}C$ composition of modern sea water. **B** Strontium isotopic composition of seawater based on marine limestones for localities compiled in Cox et al. (2016). Light purple bars show timing and relative magnitude of Neoproterozoic large igneous provinces (LIPS) based on the compilation of Ernst et al. (2008). **c** Neoproterozoic biotic evolutionary advances (modified after Spence et al. 2016, and references therein) and proposed rise in atmospheric oxygen concentration relative to present atmospheric levels after Canfield (2005). Specific timing and magnitude of the Neoproterozoic Oxygenation Event (NOE) are poorly constrained (Och and Shields-Zhou 2012). Roman numerals (I–V) correspond with mid-points of key phases of ANS development described in Sect. 7.3 (cf. Fig. 7.4)

carbonates, and possible triggering mechanisms for global-scale glaciations. Important assessments of NSE glaciation in new and established ANS localities have also occurred since Stern et al. (2006). Here, we update what we know about ANS successions that contain evidence of Neoproterozoic climate and oxygenation events or whose deposition may have been contemporaneous with Neoproterozoic glaciations but have not been systematically studied for glacigenic influences (Fig. 7.2). For background on evidence supporting Neoproterozoic glacigenic activity (i.e., glacial deposits such as diamictites and dropstones, regional-scale unconformities, cap carbonates, sedimentary iron formation, and globally synchronous low paleolatitude glaciation and deglaciation), the reader is referred to Stern et al. (2006), Hoffman et al. (2017), and Stern and Miller (2019). For background on triggering mechanisms of NSE episodes, the reader is referred to the synthesis in Stern and Miller (2018). To encourage future work in the region, we consider possible roles of ANS evolution (rapid and prolific magmatism/volcanism production of juvenile continental crust, amalgamation and orogenic uplift, weathering, and erosion) as contributing factors (e.g., atmospheric $pCO_2$ sequestration via the silicate weathering thermostat) for climate deterioration in the lead-ups to Neoproterozoic glaciation.

## 7.2 Snowball Earth and Late Neoproterozoic Glaciation

Earth's most extreme icehouse intervals occurred twice during Precambrian time, during Paleoproterozoic and Neoproterozoic Eras, when ice sheets possibly extended to equatorial latitudes (Fig. 7.3). Earth's surface temperature regime is controlled by several interrelated factors operating on different time scales, the interplay of which has been sufficient to maintain liquid water over most of Earth history (Feulner 2012). Solar luminosity increases through time (Newman and Rood 1977) and insolation would have been ~6–7% lower during the Cryogenian (Hoffman et al. 2017). The inclination of Earth's rotational axis with respect to its orbital plane (obliquity) controls the latitudinal distribution of solar energy arriving at its surface (insolation), and the surface reflectivity (albedo) affects the amount of solar energy absorbed and reflected back into space. Earth's surface temperatures are also regulated by atmospheric greenhouse gas concentrations, which absorb outgoing reflected solar radiation and infrared radiation given off by the Earth at night. Greenhouse gas concentrations are regulated by the balance of sinks (formation of $CaCO_3$ and photosynthesis) and sources (volcanic emissions, metamorphic decarbonation). Over millions of years, the fixing of $CO_2$ by silicate weathering buffers greenhouse gas concentrations. Times of enhanced silicate weathering promote atmospheric cooling by reducing greenhouse gas concentrations. This occurs because of an increased transfer of carbon from the atmosphere to sediments in the form of carbonates (carbonic acid in rainfall promotes crustal weathering, delivery of dissolved Ca ions to oceans, and carbonate formation) and organic matter (photosynthesis removes atmospheric and dissolved $CO_2$ during formation and burial of marine biomass). The ensuing cooling reduces the amount of silicate weathering through the buildup of polar ice and reduced the intensity of the hydrologic cycle, until $CO_2$ levels rise through volcanic and metamorphic degassing to resume warming. Perturbations to surface warming mechanisms via extraterrestrial, geodynamic, oceanographic, and biotic factors have been variously proposed as possible causes of NSE (see summary in Stern and Miller 2018).

Most triggering schemes for low-latitude glacial advances presume that Neoproterozoic Earth had similar obliquity to modern Earth; but an alternative explanation not requiring global scale glaciation suggests that Neoproterozoic Earth instead had much higher obliquity (>54°), such that the equator was cooler than the poles (Williams 2008; Williams et al. 2016). Global energy budget models for Earth with modern obliquity (22.1–24.5°) indicate that glacial advances into tropical latitudes would increase Earth's albedo to a critical tipping point where more solar energy was lost than absorbed, resulting in rapid atmospheric cooling and global coverage by ice sheets and sea ice (aka runaway albedo effect). With global ice cover, $CO_2$ sinks (silicate weathering, photosynthesis) would become less vigorous and possibly cease to function but, lacking a rapid means of increasing greenhouse gas concentrations, severe icehouse states would have persisted for millions of years and have

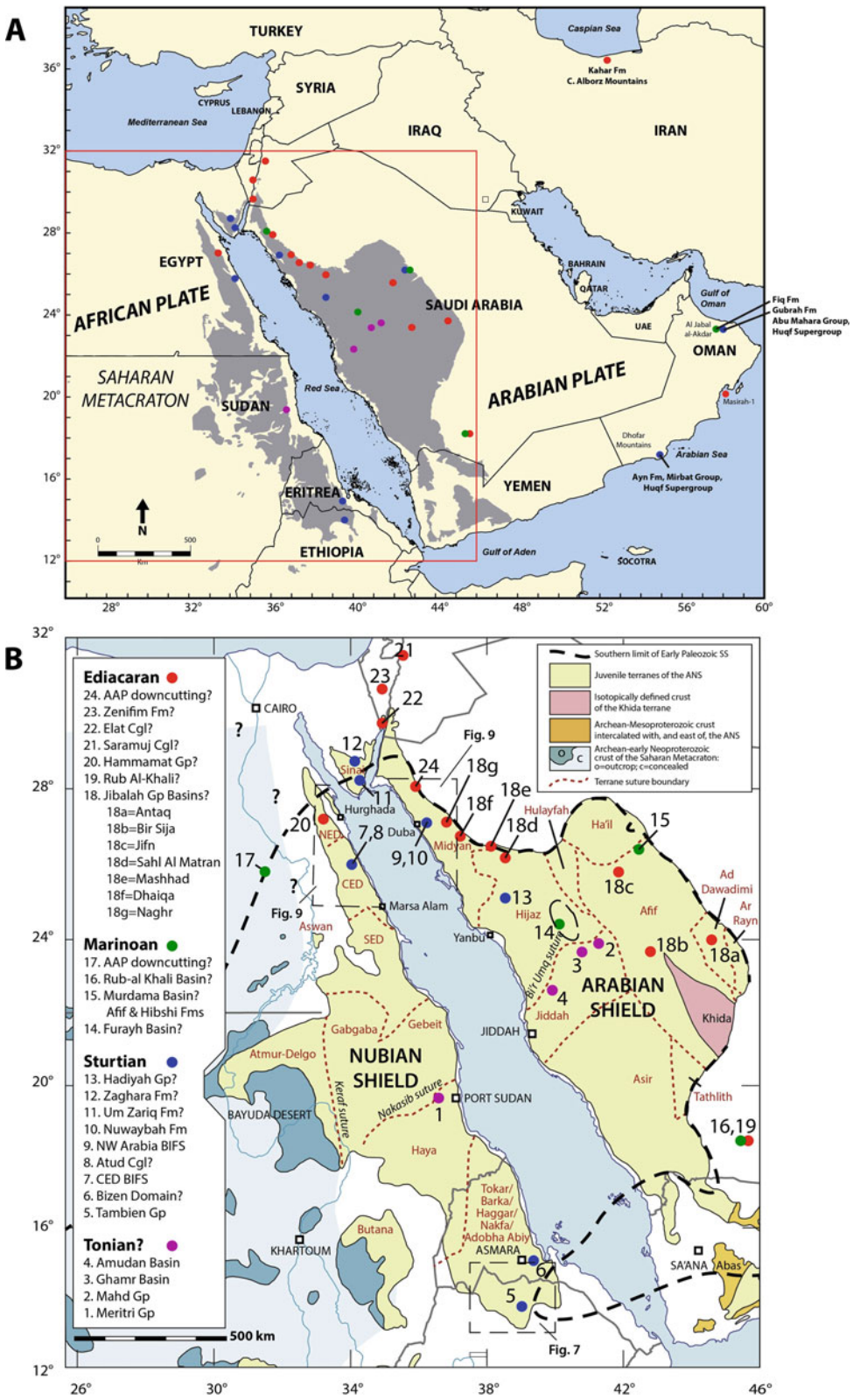


**Fig. 7.2** Arabian-Nubian Shield (ANS) localities with evidence or prospective evidence of Neoproterozoic snowball Earth episodes. **A.** Distribution of Neoproterozoic basement exposures of the ANS (grey area) in countries flanking the Red Sea, with prospective glacigenic localities discussed in the text; red box corresponds to area shown in (**B**), below. Map modified from Al-Husseini (2014). Well-documented Sturtian and Marinoan glacial deposits occur in Huqf Supergroup of SW and NE Oman (Mirbat and Abu Mahara Groups), but Oman was likely removed from the ANS until amalgamation in the latest Cryogenian and Ediacaran time (645–544 Ma; Rieu et al. 2007). Evidence of Ediacaran glaciation also occurs in the Kahar Formation of N. Iran and prospectively within the Nafun Group at the base of the Shuram Formation in offshore Oman (Misarah-1 well; Al-Husseini 2014), which along with ANS localities were distributed over the northern Gondwana margin (present coordinates). **B** Tectonostratigraphic terrane map of the ANS (after Johnson et al. 2013; De Sauza Filho and Drury 1998) showing prospective Tonian, Sturtian, Marinoan, and Ediacaran glacigenic localities (purple, blue, green, and red numbered points, respectively). Dashed line marks the southern limit of Early Paleozoic sandstone, where the Afro-Arabian Peneplain is exposed (from Avigad et al. 2005)

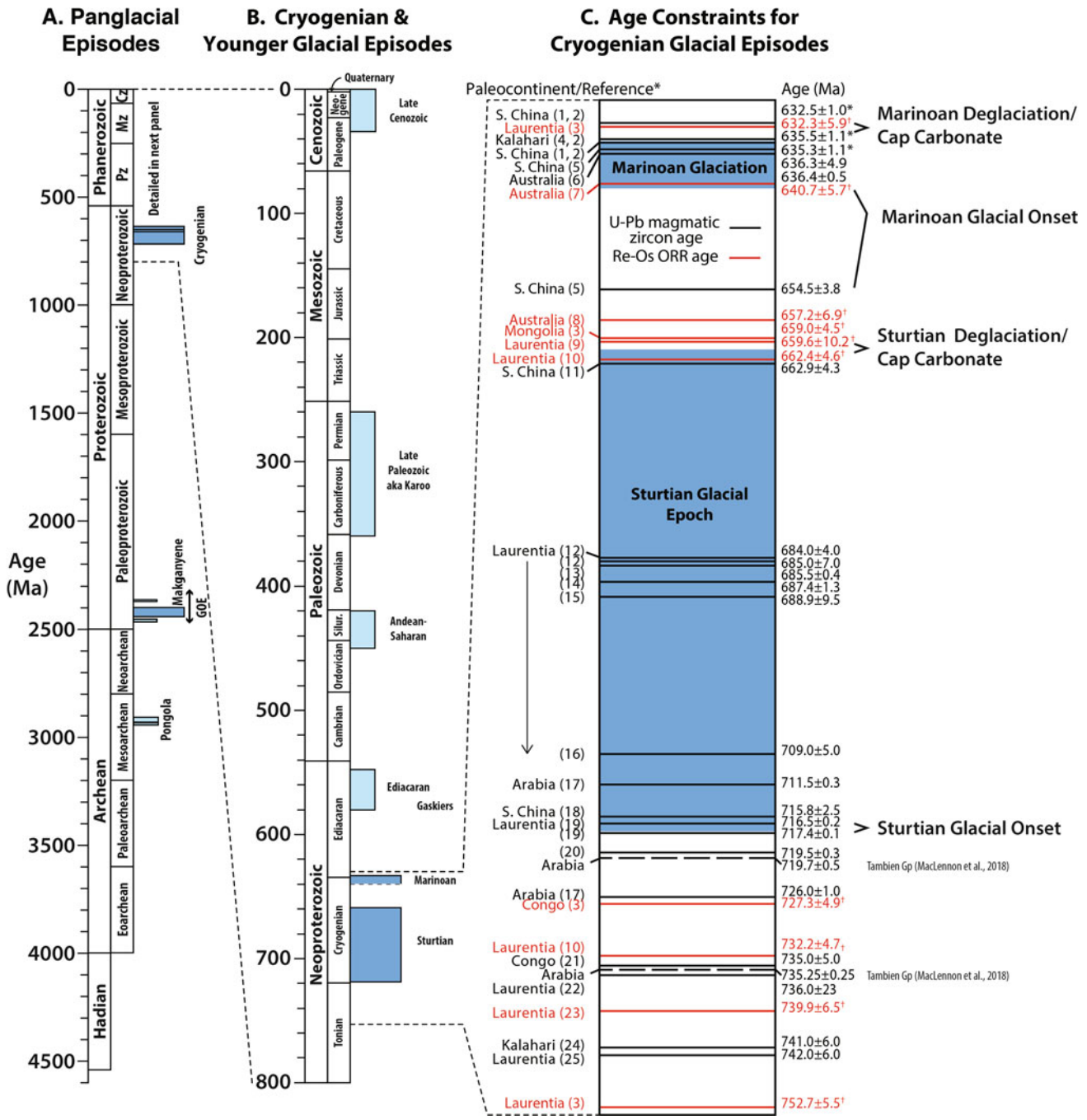


**Fig. 7.3** Occurrence of regional scale (light blue boxes) and panglacial (dark blue boxes) episodes in Earth history and geochronological constraints supporting the synchroneity and long durations of Cryogenian icehouse episodes (modified from Stern and Miller 2019 and Rooney et al. 2015). **A** Geological evidence supports two possible panglacial icehouse states, each involving global or near-global glacial episodes lasting multiple millions of years: (1) Paleoproterozoic glacial strata on six cratons are constrained between 2.45 and 2.26 Ga (Hoffman 2013) and (2) Cryogenian glacial units on all continents range between ~0.720 and 0.635 Ga. **B** Cryogenian (Sturtian and Marinoan) glacial episodes include an abundance of low paleolatitude localities and have distinctive deglacial cap carbonate successions. Ediacaran glacial episodes (~581–547 Ma) are documented on several paleocontinents, but low latitude settings have yet to be confirmed and durations are comparable to Paleozoic and Cenozoic glaciations (e.g., the ~580 Ma Gaskiers glaciation had a ~340 kyr duration; Pu et al. 2016). **C** U–Pb magmatic zircon ages (black line datums) and Re–Os organic-rich rock ages (red line datums) from different paleocontinents constrain the timing of onsets and deglaciations for the Sturtian and Marinoan panglacial episodes (see Rooney et al. 2015 for supporting references). Black dashed datums show zircon U–Pb ID-TIMS ages determined in strata shortly underlying Sturtian diamictite topping the Tambien Group of N. Ethiopia (MacLennan et al. 2018). Such age compilations demonstrate that Cryogenian glacial onsets and deglaciations were essentially synchronous in low latitude settings and had long durations (Sturtian ~717–659 Ma: ~58 myrs; Marinoan ~650–639 to ~635 Ma; ~4–15 myrs), with a non-glacial interim of <25 myrs (Hoffman et al. 2017; Rooney et al. 2015)

been termed "Snowball Earth" states or panglacial episodes to distinguish them from more common regional scale icehouse episodes, such as occurred in Paleozoic and Cenozoic Eras (Fig. 7.3).

Kirschvink (1992) first coined the term "Snowball Earth" and formulated the SEH as a mechanism to account for: (1) the long-noted abundance of Neoproterozoic glacigenic strata on most continents (Harland 1964), including evidence of widespread continental glaciers within a few degrees of the equator; (2) the common but odd lithostratigraphic association of glacial deposits (indicating cold climate) sharply bracketed by thick carbonate sequences, including later-defined cap carbonates, or containing carbonate fragments (suggesting warm climate); and (3) the recurrence of banded iron formation (BIF) in some glacigenic successions after a billion-year absence from the geologic record. That runaway albedo icehouse transitions ever occurred was originally rejected for lack of a known recovery mechanism. Kirschvink (1992) realized that Earth's climate would eventually recover from Snowball Earth icehouse states following protracted build-up of atmospheric carbon dioxide from volcanic and metamorphic outgassing and reduced weathering. Once reaching critical levels of greenhouse gas concentrations and albedo, he envisioned transitions to and from glacial conditions would both have been rapid. To test this hypothesis, he proposed that (1) glacial units for a given episode should be globally synchronous; (2) that shallow marine environments should record similar glacial-deglacial successions around the world; and that (3) iron formation recurrence could be explained by ocean-wide changes in redox state-related to ice cover, whereby dissolved ferrous iron built-up over millions of years of ice cover would subsequently oxidize upon deglacial resumption of ocean-atmosphere exchange. Detailed sedimentologic and carbon isotope investigations of Cryogenian sequences in northern Namibia (Hoffman et al. 1998; Hoffman and Schrag 2002) attracted further attention and extended the SEH, notably documenting the odd characteristics of post-glacial cap carbonate units, the coincidence of negative CIEs approaching typical mantle-outgassing values (e.g., −5 to −8‰; Javoy et al. 1986) leading into glacial episodes and recoveries to near pre-excursion values within the overlying cap carbonate sequence, and suggesting that negative CIEs followed from decreased biological fractionation during transitions to icehouse states and associated biosphere collapse. The common occurrence of thick "cap-carbonate" sequences directly overlying glacigenic sediments further suggested that cap limestone and dolomite successions may have been deposited very rapidly, as the warming deglacial ocean became intensely supersaturated in carbonate. The Neoproterozoic marine $\delta^{13}C$ evolution curve has since been greatly refined through integration of global correlations with varying levels of age control (e.g., Asmerom et al.1991; Brasier et al.1996; Bartley et al. 2001; Kuznetsov et al. 2006; Halverson 2006; Halverson et al. 2005, 2007a, b; Maloof et al. 2005; Fike et al. 2006; Jones et al. 2010; Macdonald et al. 2010a; Sawaki et al. 2010; Swanson-Hysell et al. 2010, 2015; Rooney et al. 2014; Bold et al. 2016; Cox et al. 2016; Park et al. 2019; Canfield et al. 2020), and globally synchronous negative CIE events have been proposed within Tonian (**Bitter Springs, Islay**), Cryogenian (Rasthof, **Taysh ir**, Trezona), and Ediacaran (Maiberg, **Shuram, end-Ediacaran**) Periods (Fig. 7.1A). These negative CIEs, some with nadirs well below mantle-outgassing levels (e.g., ∼−12‰ for the Shuram CIE nadir; Burns and Matter 1993), are mainly interpreted to reflect large variations in release, burial and oxidation of organic carbon (e.g., Kaufman et al. 1997; Hoffman et al. 1998; Rothman et al. 2003; Tziperman et al. 2011; Schrag et al. 2013) and/or a sampling depth-dependent $\delta^{13}C$ gradient in the water column (e.g., Fairchild et al. 2000; Klaebe et al. 2018), but not all (**bold** above) coincided with panglacial episodes (e.g., Hill et al. 2000; Halverson et al. 2005; Bold et al. 2016; Husson et al. 2015).

It remains controversial whether or not the entire Earth ever became ice-covered (e.g., Runnegar 2000; Hyde et al. 2000; Pollard and Kasting 2005), but it is largely accepted that Neoproterozoic glaciations were more extensive than the late Cenozoic "ice ages." Efforts to test and refine the SEH have progressed through the integration of regional stratigraphy and sedimentology with improved dating of events through radiometric, paleomagnetic, and geochemical techniques. Precise determination of glacial unit age is often difficult because of the absence of datable materials, such as interbedded ash beds, within glacigenic units. Determinations of paleolatitude face comparable preservational challenges, but paleomagnetic evidence now supports that substantial volumes of glacial debris were deposited in low-latitude settings (Harland 1964; Hoffman and Schrag 2002; Evans 2000; Evans and Raub 2011). Early work raised the possibility of multiple (2–4) panglacial episodes between ∼800 and 580 Ma. The present consensus (Fig. 7.3) benefits from the recent addition of high-resolution U–Pb and Re–Os ages (e.g., Rooney et al. 2015) and now supports two panglacial episodes, the Sturtian (*c.* 717–659 Ma) and the Marinoan (*c.* 645–635.5 Ma); named for glacigenic successions in Australia but extended globally in modern usage. The Sturtian episode (>55 myr) seems to have encompassed a time span that was nearly as long as the Cenozoic Era, whereas the Marinoan episode was briefer, lasting for ∼15–5 myr.

Evidence for pre-Sturtian (*c.* 740 Ma) panglacial intervals suggested for localities on cratons including the Kalahari (Kaigas glaciation), Tarim (Bayisi diamictite), Egypt (Atud diamictite) and Congo (Kundelungu Basin) are controversial because of questionable age constraints, glacigenic origins,

and/or demonstrable overlap with nonglacial sedimentation in Laurentia (Rooney et al. 2015). These older prospective glaciations have often been generalized as the Kaigas glaciation after exposures mapped as the Kaigas Formation in Southern Namibia, but the stratigraphy of this placename locality has since been reinterpreted to correlate with the younger Sturtian (Numees Formation) glaciation (Macdonald et al. 2010b).

The possibility that Late Neoproterozoic panglacial episodes served as evolutionary bottlenecks for the appearance of Ediacaran biota has stimulated paleontological investigations of post-Marinoan (Ediacaran) glacial strata. The occurrence of Ediacaran glacial deposits on multiple (8) paleocontinents (Evans and Raub 2011), including some with apparent low-paleolatitudes (10–30°; Gostin et al. 2010; Pisarevsky et al. 2011), led to the concept of a post-Marinoan panglacial event often referred to as the "Gaskiers" glaciation (after well-dated glacigenic deposits in eastern Newfoundland). With the addition of high-precision radiometric age constraints, many Ediacaran glacial localities have since been shown to be diachronous or to have had short durations inconsistent with multimillion-year-long durations required for panglacial episodes, and glacial episodes definitely younger than the Gaskiers glaciation are documented in eastern and western peri-Gondwana (e.g., *c.* 560 Ma glaciation in Iran, Etemad-Saeed et al. 2016; *c.* 565 Ma Weesenstein-Orellana glaciation, Linnemann et al. 2018). Recent radiometric dates now constrain the Gaskiers glacial episode in Newfoundland between 580.90 ± 0.04 Ma and 579.63 ± 0.15 Ma, ~9.5 myr prior to the appearance of Ediacaran fauna (Pu et al. 2016). The Shuram anomaly, Earth's longest duration non-glacial, negative CIE, is constrained by new Re–Os dates between 574 ± 4.7 and 567.3 ± 3.0 Ma, and thus at least 5.2 ± 4.8 myr younger than the Gaskiers deglaciation (Rooney et al. 2020).

## 7.3 Overview of ANS and EAO Development

The Arabian-Nubian Shield (ANS) is a complex of juvenile Neoproterozoic basement terranes (Fig. 7.2) that formed in an accretionary orogen that comprises the northern sector of the East African Orogen (EAO) (Johnson et al. 2013). The ANS outcrops in nine countries around the Red Sea and NE Africa (Israel, Jordan, Egypt, Saudi Arabia, Sudan, Yemen, Eritrea, Ethiopia, and Kenya), with an areal extent of ~$2.7 \times 10^6$ km$^2$ (Johnson 2014)—slightly larger than the Mediterranean Sea ($2.5 \times 10^6$ km$^2$). From the narrowest exposures in S. Kenya and N. Tanzania that mark its southern termination against high-grade rocks of the Mozambique Belt, the ANS widens northwards over distance of 3500 km, with widest exposures (~1500 km) between Sudan and Saudi Arabia (Johnson 2014). The ANS formed during the early Neoproterozoic to early Cambrian supercontinent cycle (aka Pan African Orogenic Cycle) involving the breakup of Rodinia, opening and closure of the Mozambique Ocean, and assembly of Greater Gondwana, through phases of convergence and amalgamation of arc terranes generated in the Mozambique ocean (Hoffman 1999; Stern 1994; Johnson and Kattan 2008; Johnson et al. 2011; Cox et al. 2012). ANS assembly also involved suturing of terranes and emplacement of syntectonic and posttectonic granitoids (Johnson et al. 2013). Arc terranes of the ANS constitute significant growth of juvenile crust, possibly the largest single tract of Neoproterozoic juvenile crust on Earth (Patchett and Chase 2002), and would have had a much larger areal extent prior to ocean closure.

ANS tectonostratigraphic terranes (Fig. 7.2B) are differentiated on the basis of common formation age, stratigraphy, isotopic composition, and structural style (Johnson 2014). Evidence of juvenile oceanic crust affinities for arc assemblages is supported by a diversity of volcanic and volcaniclastic rocks and large epizonal TTG-type intrusions with tholeiitic to calc-alkaline and MORB chemistries (Zimmer et al. 1995; Hargrove et al. 2006; Johnson 2014), in addition to Nd (and Hf) isotopes which yield positive age-adjusted εNd values (Stern 1994, 2002; Shang et al. 2010; Morag et al. 2011a, b; Johnson and Kattan 2012; Johnson et al. 2013; Johnson 2014). Sutures between terranes, many with dated ophiolites and metamorphic assemblages, document collisional deformation and help constrain the timing of terrane amalgamation. Many sutures have appreciable strike–slip offsets, and these may broadly relate to ~600 Ma escape tectonics (Burke and Sengör 1986), during which ANS terranes were progressively sandwiched by, and offset between, obliquely converging Gondwana cratonic blocks (De Souza Filho and Drury 1998, and references therein). Fault translations of uncertain extent accompanied closure of the Mozambique Ocean and the ensuing Gondwanan collisional orogeny, as indicated by contrasting tectonostratigraphic basement terranes of the southern ANS (Vail 1983; Drury and Berhe 1993; Tadesse 1997; De Souza Filho and Drury 1998; Tsige and Abdelsalam 2005). The ANS largely escaped high-grade metamorphism because terminal collision was most intense in the south, allowing the EAO to escape northward (Bonavia and Chorowicz 1992; Abdelsalam and Stern 1996). In contrast, the southern EAO (Tanzania and Madagascar) was more intensely deformed and metamorphosed and contains abundant granulite-facies rocks, many with pre-Neoproterozoic protolith ages (Kröner et al. 2003). These rocks represent the intensely overprinted margins of the colliding continents and testify to greater thickening of the crust in the south and correspondingly deeper erosion.

ANS evolution can be simplified into five phases as shown in Fig. 7.4(I–V); more comprehensive reviews by

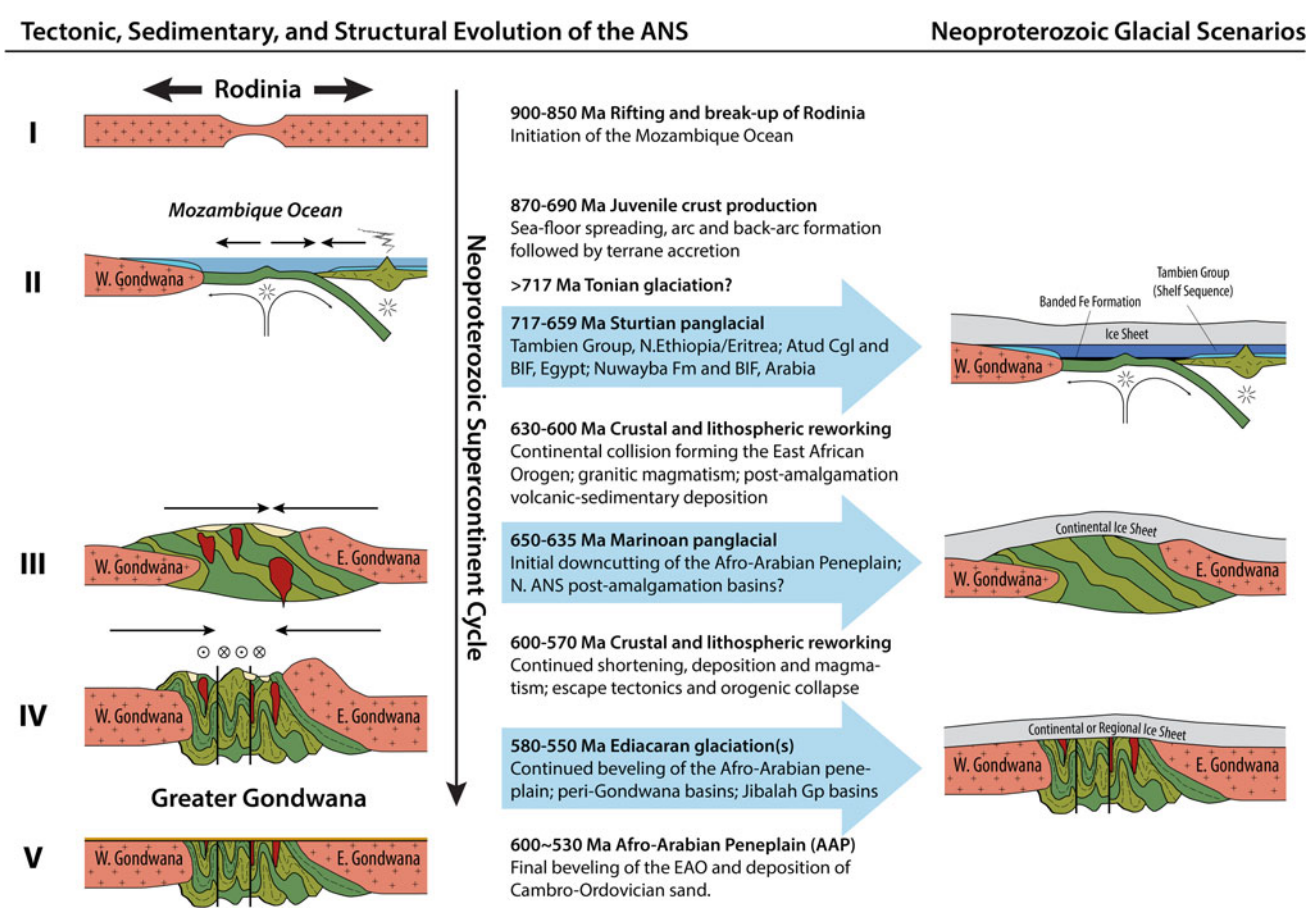


**Fig. 7.4** Schematic illustration of ANS geological development relative to the Neoproterozoic supercontinent cycle spanning the break-up of Rodinia and Gondwana assembly, and timing of Cryogenian and Ediacaran glacial episodes (modified from Stern et al. 2006; Stern and Johnson 2010)

Johnson et al. (2011) and Fritz et al. (2013) further elaborate on the orogenic history of the ANS.

(I) *900–850 Ma Rifting and Break-up of Rodinia:* Rodinian breakup during the Tonian Period between 900 and 800 Ma is inferred from the oldest (~870 Ma) juvenile Neoproterozoic rocks in the ANS (Stern 1994; Küster et al. 2008) and events in eastern Gondwana (Cawood 2005). This part of ANS history is poorly understood.

(II) *870–690 Ma Seafloor Spreading, Arc and Back-arc basin Formation, Ocean Closure, and Terrane Accretion:* ANS juvenile crust was generated within spreading systems, and subduction-related oceanic island arcs of the Mozambique Ocean, which formed between rifting cratonic fragments of Rodinia (Stern 1994; Johnson 2014), likely separating Neoproterozoic India from the Saharan Metacraton and Congo-Tanzania-Bangweulu block (Johnson et al. 2011). Oceanic plateaux may also have formed above mantle plumes within the ocean (Stein 2003). Oceanic crust generation occurred from ~870 to 600 Ma, as indicated by dated ophiolite complexes (~845–675 Ma) and arc assemblages (~870–615 Ma) (Johnson and Kattan 2012). Juvenile arc and plateau terranes collided and were welded into larger tracts of juvenile crust as the Mozambique ocean closed between fragments of East and West Gondwana, forming arc-arc sutures, composite terranes, and ultimately the ANS (Johnson and Woldehaimanot 2003). Ocean closure was diachronous, beginning ~650 Ma (Squire et al. 2006). ICP–MS U–Pb ages on detrital zircons and felsic magmatism intruding ophiolites suggest final amalgamation and Mozambique Ocean closure was complete ~620 Ma in the Ediacaran Period (Cox et al. 2012, 2018; Johnson 2014).

(III) *630–600 Ma Continental Collision (EAO formation):* Consolidation and amalgamation of ANS terranes culminated with the protracted collision between Eastern (Indian craton) and Western (Saharan, Congo-Tanzanian cratons) Gondwana, resulting in the EAO and the newly fused Greater Gondwana or

Pannotia supercontinent at the end of Neoproterozoic time (Stern 1994; Kröner 2001; Collins and Windley 2002; Meert 2003; Jacobs and Thomas 2004). In reconstructed Gondwana, the EAO extends from the Mediterranean (Tethys) southward along the eastern margin of Africa and across East Antarctica (Stern 1994; Jacobs et al. 2003). The regional orogen, thought to have been ~8000 km long and >1000 km wide, has also been termed the Transgondwanan Supermountains (Squire et al. 2006). The ANS represents the northern sector of the EAO.

(IV) *600–570 Ma Continued Shortening, Escape Tectonics, Post-Amalgamation Basin Formation, and Orogenic Collapse:* Collisional orogenesis involved considerable compression and shortening that continued during the first ~50 million years of the Ediacaran Period (Veevers 2003). Deformation included strike-slip shear zones and tectonic collapse structures in the northern EAO (Egypt, Sudan, and northern Arabia), formation of N-trending upright tight folds and shear zones in the central EAO (Ethiopia, Eritrea, and southern Arabia), and formation and uplift of high-grade gneisses and granulites in the southern EAO (Abdelsalam and Stern 1996). The most intense collision occurred in the southern EAO, which had the thickest crust, highest mountains, and the deepest erosion. Accordingly, metamorphic grade of exposed ANS rocks decreases northward, compared to higher grade granulite facies further south (Stern 1994). By ~570 Ma, ANS assembly had accreted to the Saharan Metacraton and evolution continued within the southern Paleotethys realm of northern Gondwana (Abdelsalam et al. 2003; Johnson et al. 2013). Greater Gondwana began to break up almost as soon as it formed at the end of Neoproterozoic time, shedding microcontinents into especially Asia all through Paleozoic and early Mesozoic time, with the core of Gondwana finally rupturing in Late Jurassic time.

(V) *600–530 Ma Formation of the Afro-Arabian Peneplain:* Extensive erosion of the EAO resulted in cutting of a widespread regional unconformity prior to Cambro-Ordovician time (Avigad et al. 2005), herein termed the Afro-Arabian Peneplain (AAP) (see Powell et al. 2015). This peneplain is recognized throughout northern Gondwana (Fig. 7.5D), extending from Morocco to eastern Arabia and Oman (Stern 1994; Meert and Van Der Voo 1997; Garfunkel 1999; Avigad et al. 2005; Squire et al. 2006; Avigad and Gvirtzman 2009; Al-Husseini 2014). Although the timing of the initial downcutting of the AAP is unknown, erosion would have begun as soon as regional uplift began. Some regional uplift could have initiated during the Sturtian glaciation, but more regional erosion of the ANS is likely to have spanned Marinoan and Ediacaran glaciations. Relief would have been enhanced by glacial eustasy, with isostatically adjusted sea level falls on the order of ~500 m or more estimated for the Sturtian and Marinoan panglacial episodes (Hoffman et al. 2007; Liu and Peltier 2013). Glaciation of the developing EAO would have accelerated erosion, and we speculate here that it could have contributed to initial peneplain formation. As a singular erosion surface, the AAP principally corresponds with deeply eroded highlands of the EAO, but along the northern periphery of the EAO at least two separate regional unconformities are recognized: (1) the ~585 Ma Sub-Jibalah Unconformity in N. Arabia (with equivalents in Iran, Jordan, and Oman) and (2) the a ~530–520 Ma unconformity correlated in Jordan (known as the Ram Unconformity), Saudi Arabia (Sub-Siq Unconformity), Iran (Sub-Lalun Unconformity and Oman (Angudan Unconformity) (Al-Husseini 2011). We use the term AAP inclusively to represent the significant erosional episodes that affected the EAO prior to Cambro-Ordovician time and consider it equivalent to the globally recognized Great Unconformity. See Sect. 6.3.3 for further discussion.

Neoproterozoic paleogeographic reconstructions (720–550 Ma, Fig. 7.5) generally place the ANS (as inferred oceanic arcs) within the greater Mozambique Ocean between India and Congo cratons. For example, Collins and Pisarevsky (2005) place ophiolite-bearing strata of the Adola Belt (southern Ethiopia) outboard of the Congo Craton at 750 Ma. As the Adola Belt lies in the southern EAO, it is reasonable to infer a similar outboard location for the ANS. The earliest reliable regional palaeomagnetic data for the ANS derive from the time of Gondwana amalgamation (Fig. 7.5C–D); late Cryogenian (593 ± 15 Ma) Dokhan volcanics of Egypt (Davies et al. 1980; Wilde and Youssef 2000), interpreted to have a subtropical paleolatitude (20.6 ± 5.08°, Trindade and Macouin 2007; but see Nairn et al. 1987). Low subtropical paleolatitudes (9–13°) are also reported for Huqf Supergroup units in Oman between 722 and 544 Ma (Kempf et al. 2000; Kilner et al. 2005; Allen 2007), with Oman likely amalgamating with the ANS between 645 and 544 Ma (Rieu et al. 2007). To the extent that the ANS occupied a latitudinal range similar to the Congo- Sào Francisco and/or East-Sahara cratons during the early Cryogenian (*c*. 750 Ma), as implied by various paleogeographic reconstructions (e.g. Trindade and Macouin 2007; Li et al. 2013; Pisarevsky et al. 2008), and Oman was latitudinally adjacent, possibly along the margin of the Indian craton (Denèle et al. 2012; Johnson 2014; Whitehouse et al. 2016; Alessio et al. 2017), the ANS may have occupied low to intermediate paleolatitudes during much of

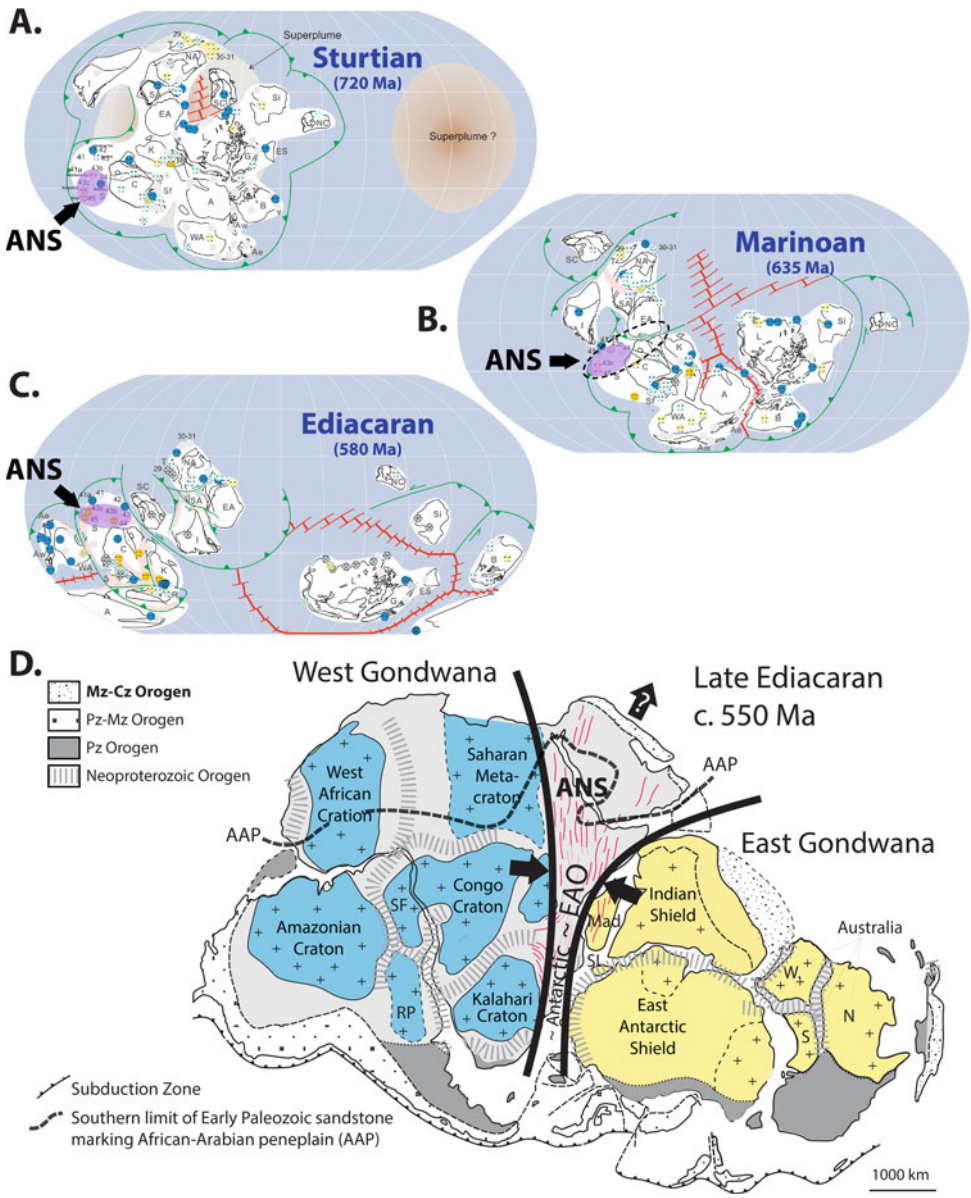


**Fig. 7.5** Global paleogeographic reconstructions showing the inferred position of the ANS during Neoproterozoic glacial intervals. **A**–**C**. Paleogeographic reconstructions (Li et al. 2013) indicate that the ANS (purple shaded ellipses) generally occupied tropical to subtropical latitudes during the Sturtian, Marinoan, and Ediacaran (Gaskiers) glaciations; see original reference for numbered localities. Rifting and break-up of Rodinia (*c.* 900–750 Ma) were associated with seafloor spreading, arc and back-arc basin formation, and terrane accretion in the Mozambique Ocean—the birthplace of juvenile Neoproterozoic crustal terranes that characterize the ANS. Accommodation space in most of the ANS likely inverted by 630 Ma in response to the closure of the Mozambique Ocean between converging elements of West (Sahara, Congo) and East Gondwana (Indian) and emergence of the EAO (aka Transgondwanan Supermountain, Squire et al. 2006, dashed ellipse in **B**). Craton/terrane name abbreviations in **A**–**C**: *A* Amazonia; *Ae*—Avalonia (east); *Aw*—Avalonia (west); *B*—Baltica; *C*—Congo; *CAFB*—Central Asian Fold Belt; *EA*—East Antarctica; *ES*—East Svalbard; *G*—Greenland; *I*—India; *K*—Kalahari; *L*—Laurentia; *NA*—Northern Australia; *NC*—North China; *R*—Rio Plata; *S*—Sahara; *SA*—Southern Australia; *SC*—South China; *Sf*—Sao Francisco; *Si*—Siberia; *T*—Tarim; *WA*—West Africa. **D** Paleogeographic and structural setting of the ANS at *c.* 550 Ma within the context of Greater Gondwana amalgamation and continued structural shortening of the EAO (modified from Meert and Lieberman 2008; Gray et al. 2008). Sedimentary records of extensional post-amalgamation basins, possibly formed in association with escape tectonics (?) along the Gondwanan margin (e.g., Jibalah Group basins), may preserve indications of Ediacaran glaciation. The modern southern limit of Early Palaeozoic sandstone (dashed bold line) documents the continent-scale extent of the Afro-Arabian Peneplain (AAP) that developed following uplift and erosion of the EAO (Avigad et al. 2005)

the Neoproterozoic (Fig. 7.5A–C; Miller et al. 2011). The closest modern analog to the ANS may be the Indo-Australian Archipelago, the islands and shallow submerged regions of which constitute portions of volcanic island arcs and volcanic arcs within a tropical climate.

## 7.4 Expected Manifestations of Neoproterozoic Glaciations in the ANS and EAO

Age constraints for Neoproterozoic glaciations have implications for the accumulation and preservation of Snowball Earth episodes within the ANS and EAO (Fig. 7.4). The long-duration Sturtian and Marinoan panglacial episodes are particularly likely to have impacted depositional systems within the evolving ANS and EAO. Because of the lack of direct paleolatitude evidence constraining a low latitude for the pre- ~600 Ma ANS (Davies et al. 1980; Wilde and Youssef 2000), any Tonian (pre-Sturtian) glacial activity in the ANS could have been regional at higher latitudes similar to Phanerozoic icehouse episodes. As mentioned above, evidence of Tonian panglacial intervals is controversial (Rooney et al. 2015). Nonetheless, the possibility of regional glacial activity preceding the Sturtian panglacial episode cannot yet be entirely refuted. Tonian and Sturtian episodes (e.g., 800 ~ 660 Ma) would have occurred while ANS juvenile crust was being generated by magmatism associated with seafloor spreading, volcanic arcs, back-arc basins, and oceanic plateaus within and around the Mozambique Ocean (Fig. 7.4II). Such glacial episodes could also have accompanied or followed arc terrane accretion (~870–690 Ma), possibly including early phases of contractional tectonics associated with Mozambique Ocean closure prior to ~630 Ma Gondwana fusion (Avigad et al. 2007). The recurrence of Neoproterozoic BIF, now considered to have been largely a Sturtian phenomenon (Cox et al. 2013), would have overlapped with this phase of ANS development. The physiography of continental shelves, oceanic plateaux, arcs, and accreted arc terranes within the Mozambique Ocean provided numerous basins with accommodation space capable of holding sediments that reflected glaciation. A wide range of water depths similar to those associated with modern back-arc basins and intraoceanic forearcs is probable, from shallow depths of a few hundred meters within the photic realm of continental shelves, oceanic plateaus, and island arcs, to abyssal depths (2500–5000 m). Sedimentation may also have involved marine carbonate deposition away from significant siliciclastic/volcaniclastic input—perhaps outboard of or along margins of magmatically dormant accreted arc terranes. We note that Neoproterozoic carbonate successions are particularly rare in the northern ANS but poorly studied candidates exist in the Keraf and Nakasib sutures of Sudan (Abdelsalam and Stern 1993; Abdelsalam et al. 1998) and in N. Ethiopia. Because of the value of marine C and Sr chemostratigraphy for Neoproterozoic correlation, low-grade marine carbonate successions in the ANS are of particular importance. Any sediments deposited in association with pre-Sturtian or Sturtian glacial episodes would have been deformed during later accretion and collision events (Fig. 7.4III–IV). Because of the southward increase in metamorphic grade within the ANS, optimal preservation of any glacigenic successions is most likely to occur within low grade greenschist the successions of middle (e.g., N. Ethiopia) and northern portions of the ANS.

Preservation potential is lowest for Marinoan and Ediacaran glacial episodes because these occurred when the ANS began to rise out of the sea in response to collisions between various terrane fragments within the Mozambique Ocean, culminating in terminal collision between E. and W. Gondwana with full development of the EAO (Fig. 7.4III). Most of the ANS was likely above sea level by ~630 Ma. As continental collision got underway, basins capable of preserving syn-glacial sediments moved away from the EAO to its flanks. By the end of the Neoproterozoic, the EAO may have been located at intermediate (~30–60 °S) latitudes (e.g., Dalziel 1997; Li et al. 2008) capable of hosting a thick continental ice sheet. In addition, the EAO was the site of the Transgondwanan Supermountains, which are thought to have been Himalayan in relief (Squire et al. 2006) and these were prone to glaciation. Continental glaciers are powerful agents of erosion, thus Marinoan and/or Ediacaran ice sheets could have contributed to erosion and downcutting of EAO hinterlands, as initial phases of AAP beveling (Fig. 7.4III–V). Associated glacial deposits could be preserved in deep grabens around the margins of the ANS, such as those preserving glacigenic successions of the Huqf Supergroup in Oman (Stewart 2016), or possibly also in continental shelf deposits on the northern flank of the end-Neoproterozoic supercontinent, such as may exist beneath Israel and N. Iran (Etemad-Saeed et al. 2016). Reworking of Marinoan and Ediacaran glacial deposits by alluvial processes may obfuscate definitive field evidence of primary glacial associations. Evidence that clasts were transported over great distances from terranes outside of the ANS may support an earlier glacial association, for example in the case of the Atud/Nuwaybah diamictite (Ali et al. 2010a). Minimum ages from detrital zircons recovered from clasts and matrix constrain when these glacial deposits were reworked.

## 7.5 Evidence for Glaciation in the ANS

Prospective Neoproterozoic glacigenic deposits in the ANS are reviewed below. These are presented in terms of four glacial episodes: Tonian (~780–755 Ma), Sturtian (720–

660 Ma), Marinoan (~645–635 Ma), and Ediacaran (~585–550 Ma), of which the Sturtian and Marinoan episodes define most extreme global climate fluctuations of the Cryogenian Period. Outside the ANS, the closest Neoproterozoic glacial localities are known in NW Africa (Shields-Zhou et al. 2011), central Africa (Master and Wendorff 2011; Tait et al. 2011), and Oman (Allen et al. 2011a, b). Glacial deposits in NW and central Africa were hosted by different cratonic blocks outside of the Mozambique Ocean. The relationship of Oman to the ANS (and Mozambique Ocean) is poorly understood but Oman is thought to be related to buried crust in eastern Arabia (e.g., Johnson and Stewart 1995). Although Oman's crystalline basement contains juvenile Neoproterozoic rocks similar to the ANS, contrasts in the timing of magmatism and sedimentation suggest Oman had a different geologic setting (Johnson et al. 2011) prior to Gondwana amalgamation during the latest Cryogenian and Ediacaran Periods (Rieu et al. 2007). Gondwana consolidation shortened the W-E distance (present coordinates) between the ANS northern sector of the EAO and some of these terranes within the northern peri-Gondwana margin. For brevity in the case of occurrences reported in Stern et al. (2006) for which there is no new information, this is simply stated.

### 7.5.1 Evidence for Tonian (*c.* 780–755 Ma) Glaciation

#### 7.5.1.1 ~780 Ma Diamictite in Eastern Sudan (Meritri Group) and Central Arabian Shield (Mahd Group)

Indications of possible Tonian glacial sedimentation in the ANS include ~780 Ma diamictite deposits on the southern margin of the Nakasib-Bi'r Umq Suture Zone in the Meritri group of E. Sudan (Fig. 7.2, locality 1) and Mahd Group of the central Arabian Shield (Fig. 7.2, locality 2) (Stern et al. 2006, 2011). These were deposited in a passive margin setting ~30 million years prior to ~750 Ma collision between terranes (Hijaz-Gebeit, Jiddah-Haya) forming the suture zone. Both groups are dominated by volcanic and volcaniclastic rocks but contain basal polymict conglomerate units. Exposures of the ~2 km thick Meritri group are located within the suture zone, and both the internal stratigraphy of the Meritri group and its contact relationships with bracketing units are unclear due to folding, faulting, and shearing. Oldest Meritri group deposits consist of polymict conglomerate bearing deformed clasts ($\leq$70 cm length) of granite, granodiorite, diorite, rhyolite, ignimbrite, and carbonate (Abdelsalam and Stern 1993). Mahd group outcrops occur further south of the suture zone, so stratigraphic relationships are less affected by structural complexities (Johnson et al. 2003; Stern et al. 2011). Oldest Mahd group deposits are matrix-supported diamictite (1–5 m in thickness), with abundant angular to sub-angular clasts ($\leq$30 cm length) of granitic and felsic volcanic rocks (Fig. 7.6A–B) (Stern et al. 2011). Ages bracketing the Meritri group (790 $\pm$ 2 Ma to 779 $\pm$ 3 Ma; Stern and Absdelsalam 1998) and Mahd group (785 $\pm$ 6 Ma to 777 $\pm$ 5 Ma; Hargrove et al. 2006b) suggest that diamictite deposition was largely contemporaneous over a ~10 myr interval. The Mahd group unconformably overlies diorite and tonalite of the ~811 Ma Dhukhr batholith (Stoeser and Stacey 1988) indicating a substantial erosional interval at ~810–780 Ma, which could be associated with glaciation (Johnson et al. 2003). The ~790–780 depositional window for basal diamictite in the Meritri and Mahd groups coincides with deposition of the lower Tambien Group in the southern ANS (Sect. 6.2.1); for example, Tsedia Slate deposition was ongoing at 778.72 $\pm$ 0.24 Ma in Tsedia synclinorium and followed the Bitter Springs CIE (Swanson-Hysell et al. 2015). Additional mapping and study Meritri and Mahd group deposits are required to understand the origin of the unconformity at the base of the Mahd group

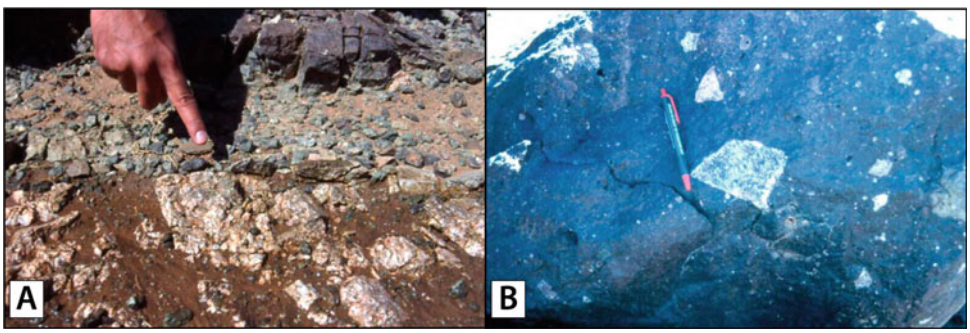


**Fig. 7.6** Outcrop photographs of possible Tonian glacial diamictite at the base of the Mahd Group (from Stern et al. 2011). **A** Nonconformity of ~770 Ma Mahd Group basal diamictite resting on truncated 806 Ma Dhukhar batholith, Saudi Arabia (Fig. 7.2, locality 2). **B** Mahd Group basal diamictite with dark matrix-supported angular granitic clasts

and determine if they preserve evidence of glacial deposition. C and Sr isotope analysis of least altered carbonate units, if present, could aid in regional correlation.

#### 7.5.1.2 ~750 Ma Ghamr and Amudan Volcanosedimentary Basins, Central Arabian Shield

In the central Arabian Shield, Ghamr and Amudan basins (Fig. 7.2, localities 3–4) contain 400–600 m thick, weakly metamorphosed, volcano sedimentary successions that are discontinuously exposed along and southward of Bi'r Umq suture zone in west-central Arabian Shield. Named for the Ghamr group (Kemp et al. 1982) and Amudan formation (Ramsay 1986), these successions unconformably overlie truncated 816–775 Ma arc-related basement rocks (Calvez and Kemp 1982; Hargrove 2006a) and contain polymict conglomerate and matrix-supported pebble conglomerate units, with clasts sourced from underlying arc volcanic and plutonic basement (Johnson et al. 2013). Deposition may have occurred near volcanic centers in terrestrial (alluvial fan, drainage channels) and near-shore marine environments near a convergent margin, possibly in a retroforeland basin setting (Johnson et al. 2013). The basal contact for the Ghamr group is an angular unconformity where it overlies eroded arc rocks, and a nonconformity where it overlies plutonic rocks. Ages constraining Ghamr group deposition derive from a Rb–Sr whole-rock isochron age of 748 ± 22 Ma for subvolcanic rhyolite (Calvez and Kemp 1982) and U–Pb zircon SHRIMP condordia ages of 753 ± 6 Ma, 752 ± 4 Ma, and 746 ± 6 for dacite and andesite (n = 2) lavas, respectively (Hargrove 2006a). The Amudan basin succession is structurally conformable above arc rock basement but dating of the latter demonstrates a 15 myr erosional hiatus (Hargrove 2006a). Collectively ~745–755 Ma Ghamr and Amudan deposition followed an extended erosional hiatus over older arc terranes. This time interval would have partially overlapped and followed ~780–750 Ma collision and amalgamation of the Bi'r Umq suture zone (Johnson et al. 2013). The lengthy hiatus preceding Ghamr and Amudan deposition, along with basal diamictite units, could be associated with glacial erosion. No glacigenic deposits have been reported, but such evidence has not been sought. The association of Tonian arc-terrane collisional settings with intense erosional episodes (similarly applicable to the older Meritri and Mahd group deposits) could bear on greenhouse gas concentrations in the lead up to the Cryogenian, as juvenile crustal terranes located at low latitudes would have been particularly susceptible to chemical weathering and drawdown of $pCO_2$ through the burial of carbon in carbonates and organic matter. The ~775–750 Ma erosional interval preceding Ghamr/Admudan deposition corresponded with deposition of carbonate-rich facies in the S. ANS (Tambien Group), as next discussed.

### 7.5.2 Evidence for Sturtian Glaciation (~717–659 Ma)

#### 7.5.2.1 Ethiopia/Eritrea—Tambien Group

Evidence of Sturtian glaciation in the ANS occurs in the Tambien Group of northern Ethiopia (Tigrai province; Fig. 7.2, locality 5). The Tambien Group is a mixed siliciclastic and carbonate succession of Tonian and early Cryogenian age, preserved mainly in N–NE trending synclinoria and related thrust belts. The most-studied localities include the Shiraro region, Mai Kenetal, Tsedia, and Chemit synclinoria in western Tigrai, and Negash and Samre synclinoria in the eastern Tigrai (Fig. 7.7A–D). Prospectively equivalent upper Tambien Group strata of the Gulgula Group occur in western Eritrea (west-directed arrow above Fig. 7.7A) just west of the Shiraro area, as well as in the Adobha Abi terrane and Bizen Domain to the north in Eritrea (north-directed arrows above northern extent of Fig. 7.7). Carbonate transitioning upward into polymict diamictite attributed to the Sturtian glaciation is documented at the top of the Tambien Group in eastern Negash (Miller et al. 2003, 2009; Alene et al. 2006; Avigad et al. 2007; Swanson-Hysell et al. 2015) and Samre synclinoria (MacLennan et al. 2018; Park et al. 2019). No post-Sturtian cap carbonate succession has been discovered, making Tambien Group diamictites Ethiopia's youngest known Neoproterozoic metasediments. Tambien Group exposures are unconformably overlain by Ordovician Enticho Sandstone, and this unconformity corresponds with the AAP (Fig. 7.4E).

Tambien Group deposition followed magmatism and volcaniclastic deposition of the Tsaliet Group (~850–755 Ma), corresponding with volcanic arc activity in the Tigrai sector of the Mozambique Ocean (Fig. 7.4II). Terminal collision between western and eastern fragments of Gondwana to form the EAO deformed the Tsaliet-Tambien Group supracrustal assemblage, producing tight upright folds (Fig. 7.4III–IV) that host the studied inliers. This collisional time interval overlapped with the long-duration Sturtian glaciation. Subsequent crustal thickening and melting of lower crustal rocks induced a phase of late- to post-orogenic igneous activity (so-called "Mereb" granitoids) that peaked around 620 Ma (Teklay et al. 2001; Bentor 1985; Stein 2003). Undeformed "Mereb" granitoids penetrate the entire Tsaliet-Tambien Group supracrustal sequence. The age of Tambien Group deposition is crudely constrained between deformed syn-tectonic granitoids and metavolcanics of the Tsaliet Group (~850–755 Ma) and the post-tectonic emplacement of undeformed "Mareb"

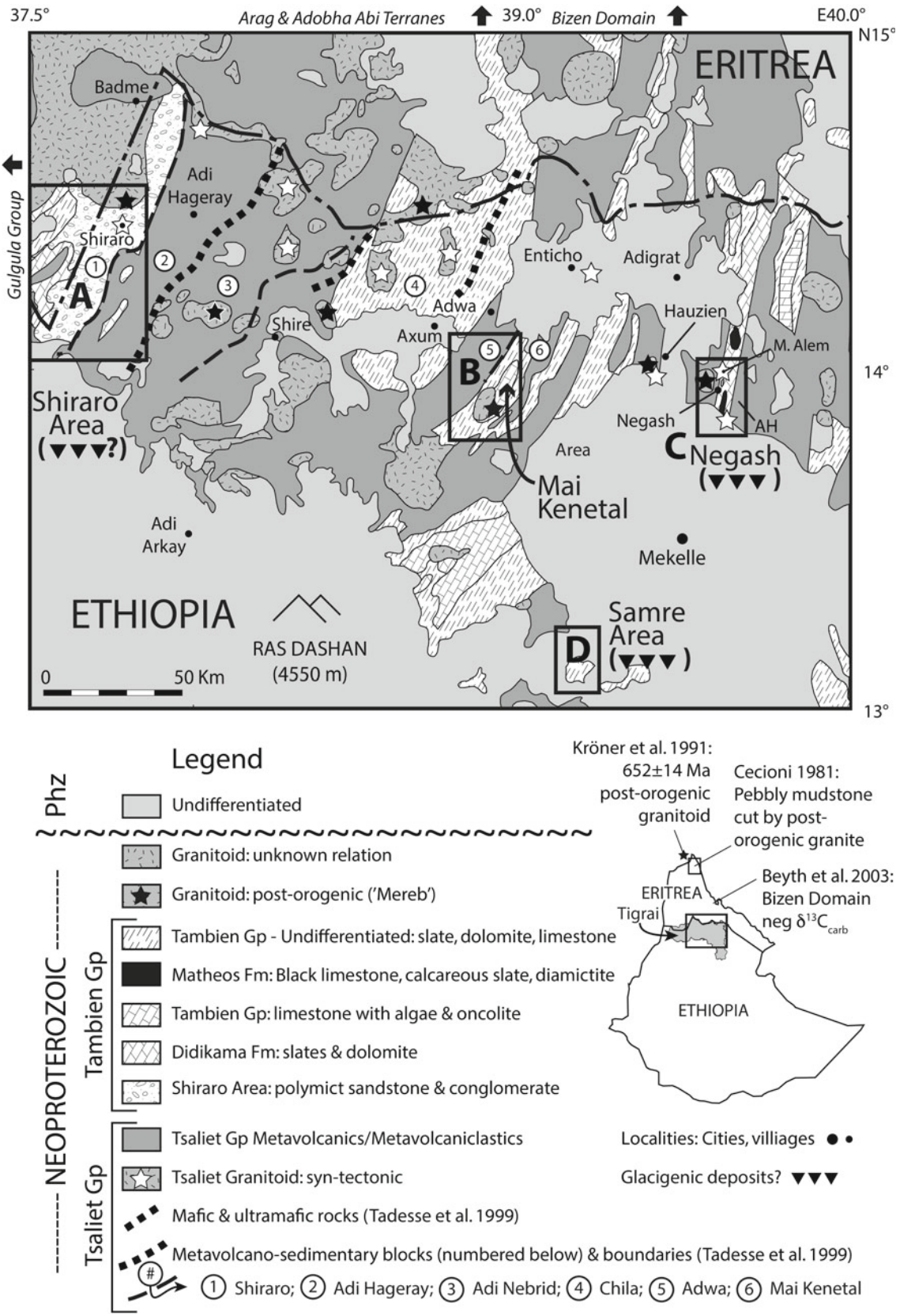
37.5°
Arag & Adobha Abi Terranes
39.0°
Bizen Domain
E40.0°
N15°
ERITREA
Badme
Adi Hageray
Shiraro
Gulgula Group
A
Enticho
Adigrat
Adwa
Hauzien
Shire
Axum
B
M. Alem
14°
Shiraro Area (▼▼▼?)
Negash
AH
C Negash (▼▼▼)
Area
Mai Kenetal
Adi Arkay
Mekelle
ETHIOPIA
RAS DASHAN (4550 m)
Samre Area (▼▼▼)
D
0
50 Km
13°
Legend
Phz
Undifferentiated
Granitoid: unknown relation
Granitoid: post-orogenic ('Mereb')
Tambien Gp
Tambien Gp - Undifferentiated: slate, dolomite, limestone
Matheos Fm: Black limestone, calcareous slate, diamictite
Tambien Gp: limestone with algae & oncolite
Didikama Fm: slates & dolomite
Shiraro Area: polymict sandstone & conglomerate
NEOPROTEROZOIC
Tsaliet Gp
Tsaliet Gp Metavolcanics/Metavolcaniclastics
Tsaliet Granitoid: syn-tectonic
Mafic & ultramafic rocks (Tadesse et al. 1999)
Metavolcano-sedimentary blocks (numbered below) & boundaries (Tadesse et al. 1999)
① Shiraro; ② Adi Hageray; ③ Adi Nebrid; ④ Chila; ⑤ Adwa; ⑥ Mai Kenetal
Kröner et al. 1991: 652±14 Ma post-orogenic granitoid
Cecioni 1981: Pebbly mudstone cut by post-orogenic granite
Beyth et al. 2003: Bizen Domain neg δ13Ccarb
ERITREA
Tigrai
ETHIOPIA
Localities: Cities, villiages
Glacigenic deposits? ▼▼▼

◀ **Fig. 7.7** Location of key Tambien Group exposures (unshaded units) within northern Ethiopia (Tigrai Province): **A** Shiraro area; **B** Mai Kenetal Synclinorium; **C** Negash Synclinorium; **D** Samre area). Metavolcano–sedimentary block boundaries (Tadesse et al. 2000) occur only within the Tsaliet Group and are inferred to represent accreted arc terranes or slivers in a supra-subduction zone setting. Stars show geochronological localities for syn-tectonic intrusives (white), post-orogenic intrusives (black), and detrital zircons (white stars with black dots) discussed in the text. Prospectively equivalent upper Tambien Group strata of the Gulgula Group occur in western Eritrea (arrow) just west of the Shiraro area, as well as in the Adobha Abi terrane and Bizen Domain (arrows) to the north in Eritrea. M. Alem (Madahne Alem) marks the western limb locality in the Negash Synclinorium bearing 774.7 ± 4.8 Ma zircons in slate ~16 m below lowest Tambien Group carbonate beds (Avigad et al. 2007). Negash Synclinorium is structurally bounded to the east by the Atsbi Horst (AH). Inset map (below) shows the location of an unnamed pebbly mudstone unit in northeastern Eritrea (Cecioni 1981) that could correlate to the Tambien Group. Figure modified from Miller et al. (2011)

granitoids (~660–580 Ma) (see Avigad et al. 2007 and Miller et al. 2011 for specific ages).

*Previous work*—The determination of Sturtian age glacial deposits follows from the first investigations of prospective NSE glacigenic sediments within the ANS, in metasediments of the Bizen Domain (Fig. 7.2, locality 6) and Tambien Group in E. Eritrea and N. Ethiopia by Beyth et al. (2003) and Miller et al. (2003) (Fig. 7.7). Early mapping in this region by Verri (1909), Bibolini (1920, 1921, 1922), Cecioni, 1940-41 (in Cecioni 1981) and Beyth (1972), well before the concept of Snowball Earth had emerged (Kirschvink 1992), identified putative Proterozoic glacigenic sediments (variously termed: pebbly mudstones, conglomerate, arkosic sandstone, pebbly slate) in NE Eritrea, the Shiraro region, and core of Negash syncline in N. Ethiopia. From a small sampling of widespread carbonate units, some with negative $\delta^{13}C$ values, Beyth et al. (2003) suggested that the Tambien Group might preserve evidence of NSE episodes. From reconnaissance sampling, Miller et al. (2003) established rudimentary C and Sr isotope stratigraphies for the Tambien Group in Negash Syncline and concluded that the diamictite was likely glacial and attributable to the Sturtian glaciation. Prior to this study, the closest known Sturtian glacial locality was in the Huqf Supergroup of SE Oman, where glacigenic diamictite occurs in the basal Ghubrah Member of the Ghadir Manqil Formation (Tschopp 1967; Glennie et al. 1974). Brasier et al. (2000) determined a U–Pb zircon age of 723 + 16/−10 Ma for zircon recovered from tuffaceous wackes interbedded within the Ghubrah diamictite, providing one of the earliest age constraints for the onset of Sturtian glaciation. Resampling of this bed subsequently yielded zircons producing a more precise CA–TIMS U–Pb age (Bowring et al. 2007; $^{206}Pb/^{238}U$ date of 711.52 ± 0.20 Ma and $^{207}Pb/^{206}Pb$ date of 714.2 ± 0.6 Ma), indicating that glaciation began prior to ~713 Ma in Oman.

More systematic studies of the Tambien Group over the past 15 years have since confirmed its association with the Sturtian panglacial episode, extended understanding of its regional litho- and chemostratigraphy and depositional age, and now establish the Tambien Group as an exceptional archive of environmental change during the Tonian transition to Cryogenian Earth systems (Fig. 7.8). In Mai Kenetal synclinorium, Alene et al. (2006) identified a negative $\delta^{13}C$ excursion in the lower carbonate unit (Assem limestone) of the Tambien Group, with likely equivalents in Tsedia and Chemit synclinoria to the east, and suggested it correlated with the non-glacial ~800 Ma Bitter Springs negative CIE. Avigad et al. (2007) published SHRIMP U–Pb ages for magmatic and detrital zircons in units below, within, and above the Tambien Group that further constrained its depositional age. Miller et al. (2009, 2011) documented more detailed C and Sr isotope stratigraphies for Tambien Group exposures in the Shiraro Area, Mai Kenetal and Negash synclinoria, and the Samre area, proposed a regional chemostratigraphic correlation scheme, and suggested from field reconnaissance and satellite imagery that the Samre region might also host Sturtian diamictite above black limestone (Matheos Fm) similar to Negash. Subsequent investigations of the Samre region verified the occurrence of stratigraphic units equivalent to the Negash facies, including glacial diamictite (Bussert 2010; MacLennan et al. 2018; Park et al. 2019). Recent studies have also enhanced C- and Sr-isotope stratigraphies and added important absolute age constraints for deposition of Tambien Group units, including the diamictite (Swanson-Hysell et al. 2015; MacLennan et al. 2018; Park et al. 2019).

*Characteristics, age, and origin of glacigenic deposits*—The transition from Matheos Formation black limestone to diamictite appears to be conformable in Negash and Samre inliers, involving increasing proportions of non-calcareous phyllitic slate that pass upward into pebbly slate without interbedded carbonate (Fig. 7.8). At Negash, the diamictite interval is ~200 m thick above its transitional base. Diamictite clasts, initially sub-centimeter in scale, increase in abundance and size (up to 20 cm in diameter) upward (Fig. 7.8C–E). Clasts are matrix-supported and the finer matrix retains horizontal layering (1–3 cm), with lateral pinching and swelling. Syn-orogenic compression deformed the diamictite to varying extents, including elongated clasts with pressure shadows and foliation of pelitic intervals. Despite this, clasts that appear to preferentially deform underlying matrix laminae (possible dropstone textures) are common (Fig. 7.8F). Larger diamictite clasts have sub-rounded, elongate, and angular shapes (including some bullet-nosed clasts; Fig. 7.8E) and striated clast surfaces

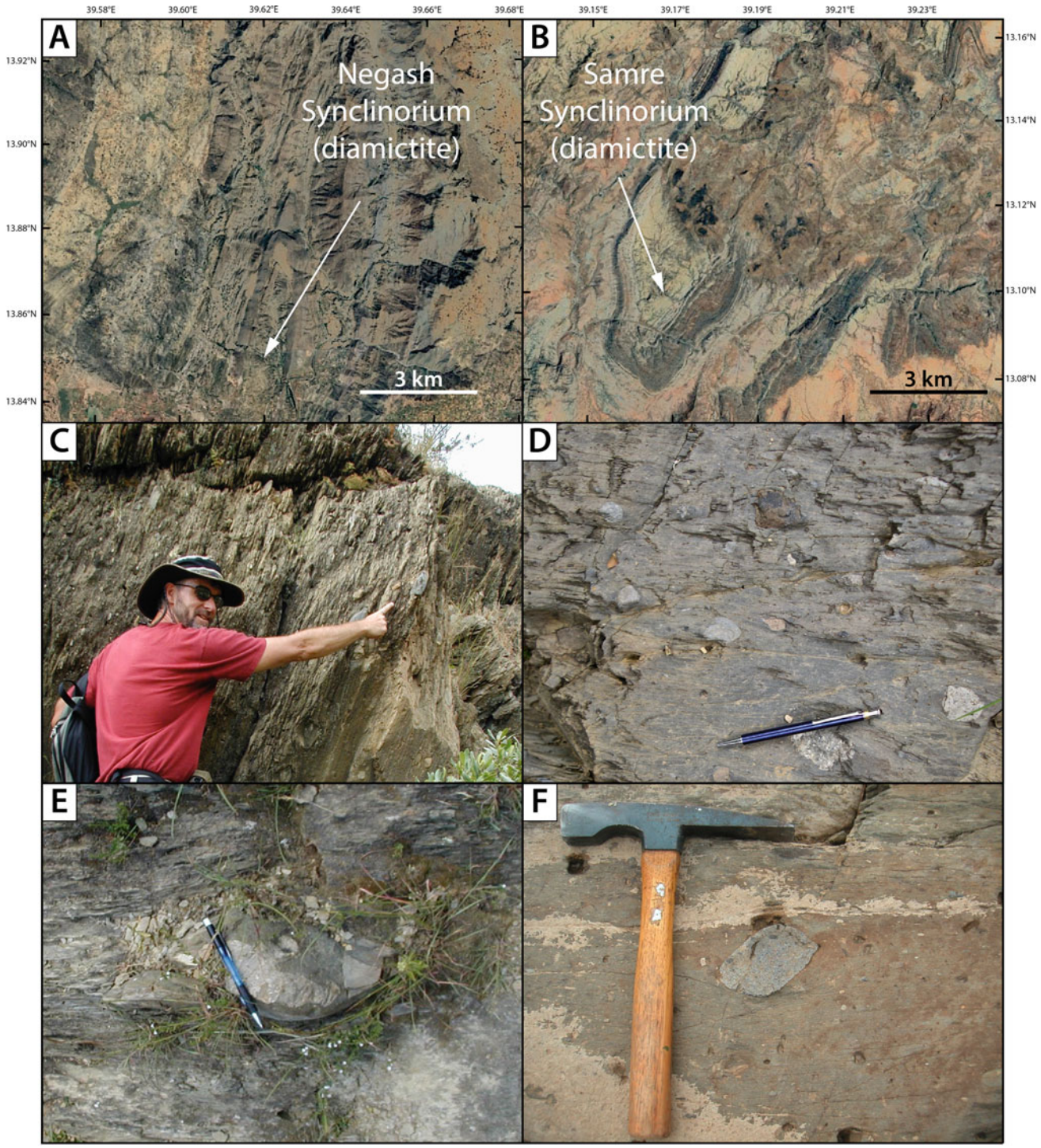


**Fig. 7.8** Sturtian glacial diamictite of the Tambien Group exposed in the cores of Negash (**A**) and Samre (**B**) synclinoria. **C–F** Diamictite photos from Negash Synclinorium: **C** Steeply bedded diamictite with matrix-supported clasts (N. Miller for scale). **D.** Polymictic matrix-supported pebbles. **E** Outsized rounded cobble in fine-grained weakly-foliated pelitic matrix. **F** Probable dropstone (well-rounded volcaniclastic cobble)

have been reported (Miller et al. 2003; MacLennan et al. 2018). Clast lithologies are polymictic, including felsic volcanic rocks, granite, fine-grained limestone retaining primary depositional textures, and dolomite, low-grade semipelitic sediments, and rare volcanic conglomerate consistent with the upper Tsaliet Group (Miller et al. 2011). Carbonate clasts in the diamictite show a wide range of $\delta^{13}C$ values consistent with derivation from older Tambien Group

carbonate units, including negative $\delta^{13}C$ values similar to negative CIE intervals identified in western (e.g., Mai Kenetal, Tsedia, Chemit; Miller et al. 2006; Alene et al. 2006) and eastern (Negash, Samre; Swanson-Hysell et al. 2015; MacLennan et al. 2018; Park et al. 2019) inliers.

SHRIMP U–Pb detrital zircon analysis of the Ordovician Enticho Sandstone, interpreted to reflect the proximal crustal composition of the southern ANS in Ordovician time, demonstrates two magmatic modes, an older mode at ~800 Ma (major concentration between 820 and 760 Ma) consistent with contributions from Tsaliet-like crust generated in island arc settings, and a younger mode at 620 Ma (major concentration between 660 and 580 Ma), consistent with contributions from late- to post-tectonic "Mereb" granitoids formed in association with Gondwana collision and crustal thickening (Avigad et al. 2007). The ~688 Ma midpoint of the Sturtian glacial interval (~717–659 Ma) is conspicuously centered within this ~100 myr interval of reduced igneous activity. Subsidence and deposition of shallow marine carbonates and mudrocks of the Tambien Group therefore likely occurred in the magmatic lull of waning arc volcanism. Detrital zircon analysis of the Negash diamictite (and prospectively equivalent arkosic sandstone in the Shiraro region) found no zircons younger than ~740 Ma, suggesting glacial deposition occurred between ~740 Ma and the onset of "Mereb" magmatism (660–580 Ma; Avigad et al. 2007). In the Samre area, the culminating diamictite has recently been constrained to be younger than 719.7 ± 0.5 Ma, based on nearly identical U–Pb ID–TIMS dates from tuffaceous siltstones 74 and 84 m lower in the underlying transition (Marian Bohkakho Fm) from Matheos Formation black limestones (MacLennan et al. 2018). These ages, in addition to $^{87}Sr/^{86}Sr$ values of 0.7066 in uppermost carbonate intervals (Miller et al. 2003, 2009), strongly support that the Negash and Samre diamictite intervals are products of the ~717–659 Ma Sturtian panglacial episode and potentially correlative with the Atud/Nuwaybah diamictites of Egypt and Saudi Arabia.

The diamictites appear to have been derived from a proximal source, as neither clast inventory nor the detrital zircon spectra indicate significant contributions from pre-Neoproterozoic sources outside the ANS (Avigad et al. 2007). Clast lithologies consistent with derivation from underlying Tambien group carbonate and Tsaliet volcanics could mean the entire Tambien Group (~1500 m) was locally uplifted or tectonically inverted to generate the diamictite source terrane. Dramatic eustatic sea-level lowering on the order of >500 m related to expansion of the Sturtian cryosphere (Hoffman et al. 2007; Liu and Peltier 2013) would have enhanced erosion of shallow marine terranes.

*Regional lithostratigraphy and timing of Tambien Group deposition*—There remain many unanswered questions about the timing of Tambien Group deposition and its regional lithostratigraphy prior to diamictite deposition. The most complete successions occur in Mai Kenetal and Negash synclinoria, but they have differing lithostratigraphies and it has proven difficult thus far to establish radiometric ages to definitely establish how they may correlate. The Mai Kenetal sequence involves successive alternations between slate and dark limestone, the lower limestone unit (Assem Limestone) of which is associated with a sharp basal contact and negative $\delta^{13}C$ compositions. The Negash succession begins with slate and increasing proportions of dolomite (Didikama Formation), below a sharp contact with overlying dark limestone (Matheos Formation) that in turn grades upward into glacial diamictite. Some regional correlation challenges follow from different lithostratigraphic frameworks used in compiling four map sheets (Mekele: Arkin et al. 1971; Adi Arkay: Hailu 1975; Adigrat: Garland 1980; and Axum: Tadesse 1999) that cover Tambien Group exposures in Tigrai. Regional facies differences are possible, if not likely, because Tambien Group deposition may have occurred while arc terranes were still amalgamating and/or during Mozambique ocean closure and relief differentiation from early compressional shortening. There are two broad schools of interpretation for regional correlation, related to how depositional units in Mai Kenetal synclinorium correlate to those exposed in Negash and Samre synclinoria. Several workers have established chemostratigraphic arguments, consistent with the suggestion of Beyth (1972) that the Mai Kenetal and Negash successions, both of which begin above Tsaliet Group metavolcanics, must somehow correlate laterally (Miller et al. 2003, 2009, 2011; Alene et al. 2006), although a significant unconformity may occur in the Negash succession below its contact with upper dark limestone unit (Garland 1980). The other interpretation is gleaned from the Adi Arkay map, which in one key area interprets the entire Mai Kenetal succession to underlie the Negash succession. The field relationships underlying this interpretation should be confirmed, as these map compilations were substantially made from aerial photography with ground-truthing in selective field traverses.

$^{87}Sr/^{86}Sr$ chronostratigraphy could help rectify lithostratigraphic relationships if all Tambien Group carbonate units were deposited in open marine basins of the Mozambique Ocean. The Tonian seawater evolution curve is still in an early stage of refinement (Fig. 7.1B), but the dominant trend over 850–700 Ma indicates increasing $^{87}Sr/^{86}Sr$ values from ~0.7055 to 0.7068 by ~770 Ma, followed by somewhat lower values 0.7067 before further decreasing near the onset of the Sturtian glaciation (Zhou et al. 2020). Sr isotope data in Miller et al. (2009) show increasingly radiogenic compositions up-section in the most-studied Negash and Mai Kenetal inliers. In Negash, values increase within the Didikama Fm, from ~0.7055 ± near

the base to ~0.7062 near its top, before abruptly jumping to 0.7066 in overlying Matheos Fm black limestones. This jump, in addition to the abrupt lithologic change (dolomite to black limestone) may indicate an unconformity in the Negash sequence at this level (as previously indicated by Garland 1980). In the higher Matheos transition to diamictite, $^{87}Sr/^{86}Sr$ values decrease to values approaching 0.706. In Mai Kenetal, a nearly comparable range of $^{87}Sr/^{86}Sr$ values are documented. Values in the Assem Limestone (~0.7062) and Tsedia Slate (0.7063) are less radiogenic than the culminating Mai Kenetal Limestone (0.7067). If the Negash facies are younger than the Mai Kenetal facies, and the measured $^{87}Sr/^{86}Sr$ values are close to depositional values, then the Tonian seawater $^{87}Sr/^{86}Sr$ evolution curve requires a strong decrease of 0.0012 following Mai Kenetal Limestone deposition to reach values obtained in the lower Didikama Formation. In addition to similar $^{87}Sr/^{86}Sr$ compositions, the Mai Kenetal LS, and Matheos Formation limestones have comparable $\delta^{13}C$ values and uniquely enriched Sr concentrations. Although $^{87}Sr/^{86}Sr$ values could be differentially affected by dolomitization/alteration, they could indicate that Negash Didikama strata are older than the Mai Kenetal Limestone.

The addition of absolute age constraints for Tambien Group units in key inliers, particularly from ash falls that can provide depositional ages, is critically needed and has recently begun using U–Pb ID–TIMS dates in recent publications. In Mai Kenetal synclinorium, deposition of Tsaliet Group volcanics was ongoing at 822.2 ± 1.3 Ma (Swanson-Hysell et al. 2015; Park et al. 2019). In eastwardly adjacent Tsedia syncline, tuff samples correlated within the Werri Slate and Tsedia Slate respectively indicate ongoing deposition at 815.29 ± 0.32 Ma and 778.72 ± 0.24 Ma (Swanson-Hysell et al. 2015). The lower limestone unit (Assem Limestone) at Mai Kenetal and its negative CIE is inferred to have been deposited between these ages (Swanson-Hysell et al. 2015). Consistent with this interpretation are U–Pb zircon and Re–Os dates from the Fifteenmile Group of northwest Canada, which constrain a maximum age for the onset of the Bitter Springs CIE of 811.51 ± 0.25 (Macdonald et al. 2010a) and 810.7 ± 6.3 Ma (Cohen et al. 2017), respectively. In Negash synclinorium, Tsaliet Group metavolcanic deposition was ongoing at 794.3 ± 0.6 Ma (Park et al. 2019) and detrital zircons in the overlying Amota Formation (considered within the Didikama Formation by Beyth 1972; Miller et al. 2003, 2009; Alene et al. 2006) indicate that overlying deposition was younger than 794.2 ± 0.7 Ma (Swanson-Hysell et al. 2015).

The Tambien Group appears to contain at least three negative CIE events, which have been linked to the ~800 Ma Bitter Springs event, the ~737 Ma Islay anomaly, and the ~720 Ma transition into the Sturtian diamictite (Fig. 7.1A). Interestingly, the Bitter Springs event has been linked to an episode of true polar wander (Maloof et al. 2006), suggesting a rapid reorientation of Earth's magnetic field relative to its lithospheric shell. If the correlation is accurate, this perturbation followed deposition of the basal Tambien Group (Werii Slate) in western inlier exposures (Mai Kenetal, Chemit, Tsedia). In eastern inliers (Negash and prospectively Samre), basal Tambien Group deposition (Amota Formation, Negash E. Limb) is younger than 794.3 ± 0.6 Ma (Park et al. 2019) and deposition of lowest dolomite beds of the overlying Didikama Formation (Negash W. Limb) was younger than 774.7 ± 5.7 Ma (Miller et al. 2009). These dates bracket the 788.1 ± 0.2 Ma age of ongoing deposition of the Tsedia Slate in the Tsedia inlier (Swanson-Hysell et al. 2015), which followed recovery from the prospective Bitter Springs negative CIE in the Assem Limestone in Mai Kenetal synclinorium. The other two negative CIE events are currently only resolved in eastern inliers (Negash and Samre). A negative CIE prospectively correlated with the Islay anomaly, which precedes the Sturtian glaciation by >10 myr (Rooney et al. 2014) appears to be reasonable based on age constraints (U–Pb ID–TIMS data of 735.25 ± 0.25 Ma for tuff layers within basal Matheos Formation; MacLennan et al. 2018). However, the anomaly in Negash and Samre inliers begins within the uppermost Didikama Formation and recovers in overlying black limestone of the Matheos Formation. The abrupt lithologic change, previous reporting of a possible angular unconformity (Garland 1980), and abrupt jump in $^{87}Sr/^{86}Sr$ (Miller et al. 2009, 2011) across this contact may indicate a considerable hiatus. The uppermost negative CIE occurs in the transition to diamictite deposition. This negative excursion from positive values following recovery from the Islay Anomaly is represented in other Sturtian glacigenic successions (e.g., Halverson et al. 2005; Rooney et al. 2011; Fairchild et al. 2018). Future efforts can greatly clarify Tambien Group regional lithostratigraphy by further constraining the age of units associated with negative CIEs, in least altered successions with minimal structural complications.

*Opportunities for further study*—As a relatively continuous Tonian to Cryogenian succession, greenschist grade metasediments of the Tambien Group offer valuable opportunities to understand the lead up to extreme climate transitions of the Cryogenian. Although Tambien Group deposition occurred in a period of reduced magmatic activity, volcanic ashes occur sporadically throughout the sequence providing samples suitable for absolute age dating. The occurrence of shallow marine carbonate intervals with well-preserved primary depositional textures allows C and Sr isotopic determinations on least altered samples, whereas slate intervals may reveal the extent of chemical weathering.

The onset of the Cryogenian may have been driven by consumption of atmospheric $CO_2$ and reverse greenhouse cooling associated with weathering of large volumes of juvenile Neoproterozoic crust and/or flood basalts emplaced at low latitudes (Goddéris et al. 2003; Donnadieu et al. 2004). Carbonate and organic carbon in the Tambien Group may constitute a portion of this sequestered greenhouse carbon, and the associated siliciclastic intervals may represent weathering of volcanic arc terranes generated in the Mozambique basin. Preliminary work on thick slate units comprising the lower Tambien Group demonstrates high chemical weathering indices, consistent with Tsaliet arc accretion complexes undergoing protracted and intensive and silicate weathering prior to carbonate deposition (Sifeta et al. 2005; Miller et al. 2009). The contribution of weathering of ANS arc terranes to initiation of Cryogenian glaciation is a topic worthy of future studies. The paleolatitude of Tigrai during Tambien Group deposition is still poorly constrained. Extensive paleomagnetic testing of Matheos Formation limestone in the core of Negash syncline proved unsuccessful due to probable Quaternary remagnetization (Kidane et al. 2014). Further paleomagnetic testing of other inliers may reveal valid depositional paleolatitudes for the Tambien Group.

#### 7.5.2.2 Banded Iron Formation of Egypt and Arabia

BIFs are found in the Central Eastern Desert of Egypt and in the Silasia Formation of the Midian region in NW Saudi Arabia (Fig. 7.2, localities 7, 9; Fig. 7.10A–D). These distinctive sedimentary rocks occur as centimeter- to meter-scale interbeds in wackes distributed over a 200 × 100 km area (Fig. 7.9), possibly representing portions of an extended ANS BIF basin (Stern et al. 2006). They are metamorphosed into greenschist facies.

BIF deposition occurred in a marine basin associated with arc/backarc basin volcanism and immature clastic sedimentation. Beds are composed of alternating iron- and silica-rich laminae (Fig. 7.10D), which may reflect seasonal changes in deposition of Fe vs. Si. Fe-rich layers are dominantly composed of primary fine-grained hematite "dust" and minor apatite, with abundant secondary magnetite. Rapid deposition is revealed by (1) major and trace element data indicating that ANS–BIF are very pure (<20% detrital input) chemical sediments in spite of being deposited in a basin with high sedimentation rates, and (2) pervasive evidence for soft-sediment deformation, suggesting that rapid sedimentation of dense, weak materials caused slumping (Fig. 7.10C). Nd and Pb isotopic compositions are predominantly mantle-like, indicating the dominance of hydrothermal sources or weathering of juvenile ANS crust for these elements. REE data show HREE-enriched patterns typical of modern seawater, with small positive Eu and small negative Ce anomalies. Low abundances of transition elements that are commonly abundant in proximal hydrothermal deposits of modern oceans indicate that ANS–BIF formed at some distance from hydrothermal vents (El-Shazly et al. 2019; Kiyokawa et al. 2020). REE data and Zn/Co share characteristics of both modern seawater and hydrothermal vent fluids suggesting derivation from a mixture of shallow suboxic seawater with a dilute, low-T hydrothermal vent fluid. Considered in conjunction with BIF of similar age on other paleocontinents, these observations support that rapid and widespread re-oxygenation of $Fe^{+2}$ in previously anoxic or suboxic seawater led to rapid precipitation of hematite "dust" and BIF deposition.

A similar conclusion about the origin of ANS BIF was provided by Abd El-Rahman et al. (2020) for BIF at Wadi Hamama in the Egyptian CED. They suggested that the BIF may have formed as low-temperature hydrothermal fluids on the floor of an island-arc basin. The iron formations were deposited during periods of volcanic quiescence, with metals having been derived from low-temperature pervasive hydrothermal alteration of volcanic and volcaniclastic rocks exposed on the seafloor. Precipitation took place due to mixing of metal-bearing hydrothermal fluids and cold, oxygenated seawater.

Until very recently, ANS BIF was thought to have formed ~750 Ma, prior to the Sturtian glacial episode (which began ~717 Ma). Age constraints obtained by Ali et al. (2009, 2010b) come from ages of underlying Ghawjah Formation metavolcanic rocks in Saudi Arabia and "Younger Metavolcanics" of the CED. Ghawjah metavolcanic rocks are mostly basalts and andesites with tholeiitic to calc-alkaline affinities. These erupted in an arc or back-arc basin and yield a U–Pb zircon age of 763 ± 25 Ma (Ali et al. 2010b). Ghawjah metavolcanic rocks are correlated with the "Younger Metavolcanic" rocks from the CED of Egypt, in terms of stratigraphic relations, chemical compositions, Nd-isotopic compositions, and U–Pb zircon ages (~750 Ma; Ali et al. 2009). These volcanic rocks showed a wide range of U–Pb zircon ages due to inherited zircons, so ages are not tightly constrained. A younger age constraint for Silasia Fm BIF comes from the observation that it is intruded by 725–710 Ma plutons of the Muwalylih suite (Hedge 1984). With the onset of the Sturtian glaciation at ~717 Ma, these constraints were taken to indicate that ANS BIFs were pre-Sturtian deposits.

The inference that BIF deposition occurred ~750 Ma has recently been challenged by U–Pb zircon age constraints of El-Shazly and Khalil (2016), for zircons in intrusions and metavolcaniclastic rocks interpreted as magmatic, and zircon overgrowths in metavolcaniclastic rocks interpreted as metamorphic or hydrothermal, and Abd El-Rahman et al. (2020), for zircons in metavolcaniclastic units interpreted as magmatic. These results indicate that ANS BIF formed

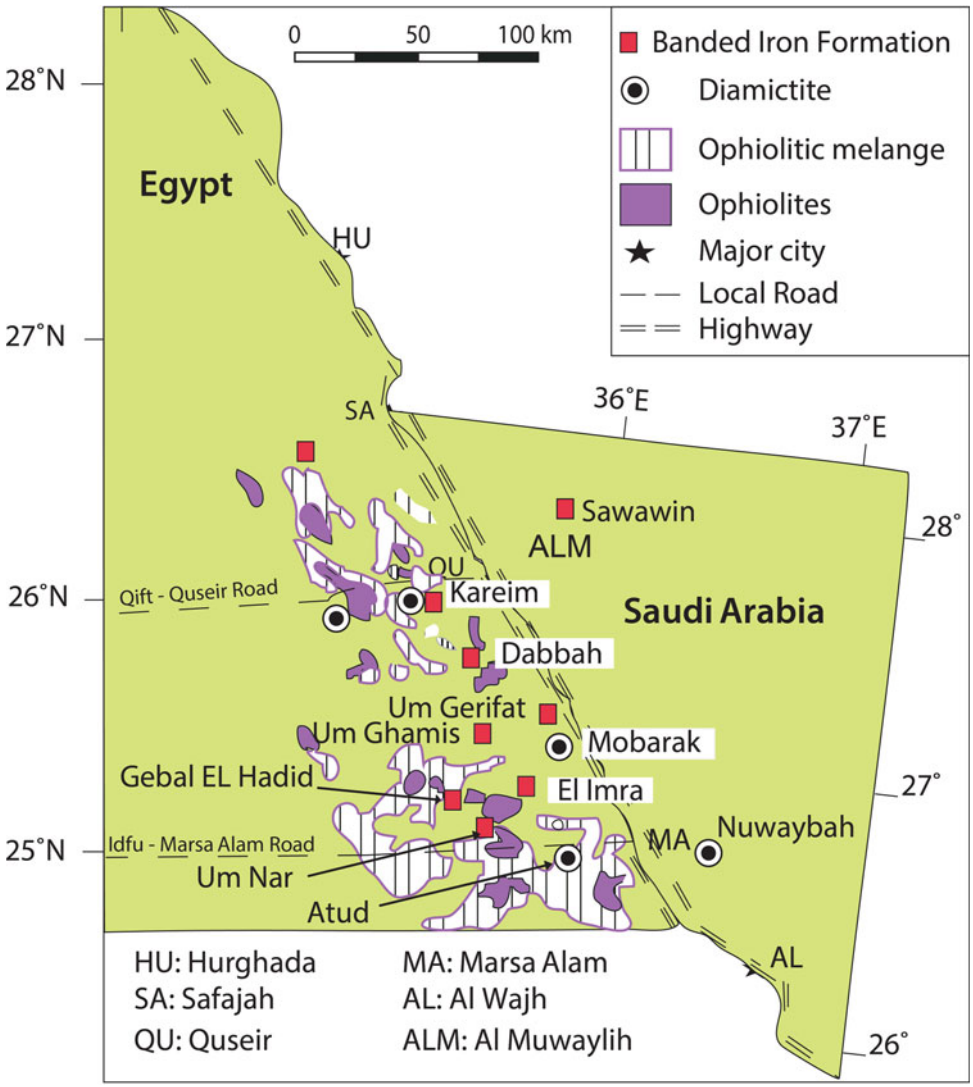


**Fig. 7.9** Location of the Atud and Nuwaybah diamictite and associated BIF, as well as ophiolitic rocks in Egypt and Saudi Arabia, northern ANS, with the Red Sea closed. Diamictites and BIFs in this area are thought to be early Cryogenian in age. See Fig. 7.2 for regional location (modified after Ali et al. 2010a, b) and Stern et al. 2011) for geographical coordinates of sites

during the Sturtian (*c*. 717–659 Ma) glaciation. El-Shazly and Khalil (2016) dated interbedded volcaniclastic sediments at Um Nar, El-Hadid, Um Ghamis, and Wadi Kareim BIF localities in the CED. These gave a wide range of ages but youngest ages of 725 ± 9 Ma, 687 ± 10 Ma and 689 ± 15 Ma (N = 10, 8, 4, respectively) at Um Nar, 718 ± 11 Ma (N = 15) at El Hadid, and 722 ± 4.5 Ma (N = 20) at Wadi Kareim suggest deposition at 687–725 Ma, indicating a Sturtian age for ANS–BIF. Abd-El Rahman et al. (2020) confirm a Sturtian age for ANS BIF. They dated three samples from volcaniclastic sedimentary rocks that host the BIF at Hamama using U–Pb zircon SIMS techniques. Twenty-two analyses of banded tuff underlying the BIF gave an age of 693.0 ± 4.1 Ma. Forty-six analyses of zircons from dacitic cobble from a conglomerate above the BIF gave an age of 696.8 ± 2.9 Ma. A third sample from tuffaceous matrix of conglomerate overlying the BIF yielded two zircon populations, both concordant: an older group of 12 zircons at 841.4 ± 5.8 Ma and a younger group of 6 zircons at 701 ± 8 Ma. These results tightly constrain the Hamama BIF to be ~695 Ma, well within the Sturtian glaciation interval.

Further detailed studies like those of Abd-El Rahman et al. (2020) are needed in other localities to determine the age range of ANS-BIF deposition, but presently these seem to be Sturtian in age.

#### 7.5.2.3 Atud Diamictite (Egypt) and Nuwaybah Formation (Zaam Group) (NW Arabia)

The Atud diamictite and Nuwaybah Formation are part of the same metasedimentary succession as ANS–BIF (Fig. 7.2, localities 8, 10; Fig. 7.9). Originally called the Atud Conglomerate, the term diamictite is more appropriate because the clasts are very poorly sorted in size. Clasts up to 1 m across of granitoid, quartz porphyry, quartzite, basalt, greywacke, marble, arkose, and microconglomerate are set

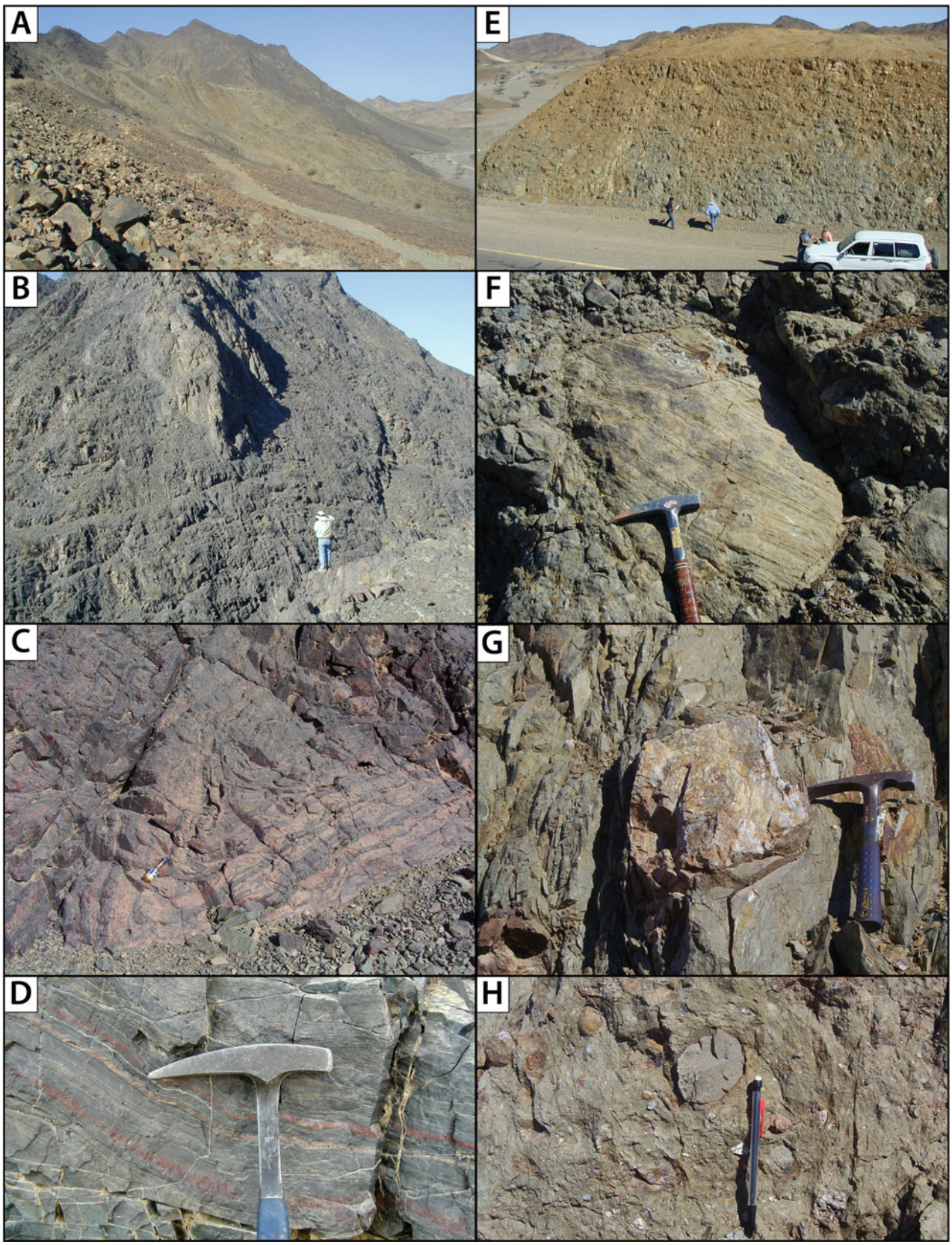
A
E
B
F
C
G
D
H

◀ **Fig. 7.10** Outcrop photos of banded iron formation and diamictite from Saudi Arabia. Photos **A–D** Silasia Formation banded iron formation. **A** Dark high ridge is Silasia formation. **B** Closer view of steeply dipping well-bedded iron formation (P. Johnson for scale). **C** Internal folding is likely related to slope deposition of iron formation. Banding corresponds to alternating silica-rich (lighter) and iron-rich (darker) layers. **D** Close-up view of banded iron formation. Photos **E–H** Nuwaybah Formation diamictite outcrop on the Midyan Red Sea highway. **E** View eastward of Nuwaybah outcrop. **F** Possible glacial striated boulder. **G** Possible dropstone in vertically bedded matrix-supported diamictite; note deformed bedding to right of clast. **H** Matrix-supported diamictite with variably rounded and angular polymict clasts

in a wacke matrix. Stratigraphic relations indicate that the diamictite was deposited in a marine environment. Atud diamictite is associated with ANS BIF at the Wadi Kareim locality; elsewhere BIF and diamictite are found separately but within the ANS BIF basin. Ali et al. (2010a) studied the Atud diamictite in Wadi Kareim and Wadi Mobarak in the Eastern Desert of Egypt and the Nuwaybah Formation in NW Saudi Arabia (Fig. 7.10E–H). They concluded from U–Pb zircon analyses (igneous zircon from Ghawjah volcanic rocks) that ~750 Ma ages are dominant with a significant component of older materials, characterized by minor Mesoproterozoic and more abundant Paleoproterozoic and Neoarchean material. Ali et al. (2010a) found that some matrix and metasedimentary clast zircons yield 713–722 Ma ages that are significantly younger than the youngest clast (754 ± 15 Ma) but considered these anomalous. They concluded that Atud/Nuwaybah diamictite deposition occurred ~750 Ma or slightly later.

Li et al. (2018) reported zircon U–Pb age and Hf–sO isotopes for a felsic volcanic cobble and wacke matrix samples from the type locality of the Atud Formation near Gebel Atud in the CED. They interpreted their results for 110 detrital zircons in wacke matrix to indicate that the Atud Formation was deposited between *c*. 720 and 700 Ma. The origin of pre-Neoproterozoic zircon in the Atud Formation has been variously interpreted. Citing a lack of known source areas for Neoarchean and Paleoproterozoic clasts within the ensimatic Arabian Nubian Shield, Ali et al., (2010a) suggested allogenic transport from erosion of flanking tracks of older crust, whereas Li et al. (2018) interpreted pre-Neoproterozoic zircon ages as relicts of old continental crust substrate in this part of the shield. However, the distribution of pre-Neoproterozoic ages in the Atud/Nuwaybah diamictite is similar to the distribution of the pre-Neoproterozoic basement ages in Yemen and the Saharan Metacraton, suggesting that these clasts were transported hundreds of kilometers, maybe by ice-rafting.

The conclusion of Ali et al. (2010a) that the Atud diamictite was deposited ~750 Ma needs to be reassessed. Determining the age of diamictites depends on correctly identifying the age of the youngest clast and/or zircon and even this only provides a maximum age constraint. If diamictite and ANS BIF are approximately correlative in age —as they seem to be at Wadi Kareim—then the tight ~695 Ma age for Hamama BIF make it likely that the Atud/Nuwaybah diamictite is also about this age. Further studies focused on the age of the youngest clasts and zircons in wacke matrix are needed to more tightly constrain the age of Atud diamictite and determine whether or not this is indeed a Sturtian deposit.

#### 7.5.2.4 Um Zariq and Zaghara Formations, Sinai Peninsula, Egypt, Northern ANS

Helmy et al. (2021) report evidence of possible Sturtian glaciation in the amphibolite-grade Um Zariq Formation (UZF) of SE Sinai Peninsula, Egypt (Fig. 7.2, locality 11), a metasedimentary stratigraphic succession that may be equivalent to BIFs and diamictite exposures further south in the CED and northern Arabia. The 1.5 km thick UZF sequence, within the highly deformed Kid metamorphic complex, is mainly volcanic-free pelitic schist and subgreywacke, but the upper formation contains diamictite, conglomerate, and possible dropstones, which are overlain by a thinly laminated pink-buff metacarbonate unit that is 10 s of meters in thickness. BIF is reported near the base of the exposed sequence (Gad and Kusky 2007), but its stratigraphic relationship with the UZF is uncertain due to structural complexities (faulting, folding, and shear zones). Fowler et al. (2015) reported dropstone boulders in the nearby (~45 km NNW) Zaghara Formation, within the Sa'al metamorphic complex (Fig. 7.2, locality 12), which may correlate within the upper UZF. Age constraints for UZF deposition support deposition during the latest Tonian and Cryogenian. Moghazi et al. (2012) reported concordant SIMS $^{206}Pb/^{238}U$ ages for detrital zircons recovered from a UZF metapelitic schist sample, suggesting maximum and minimum depositional ages of 813 ± 16 Ma (n = 19) and 647 ± 12 Ma, respectively. Eyal et al. (2014) obtained magmatic SIMS U–Pb age peaks of 885, 825, 760, and 735 Ma for zircons (n = 21 with <10% discordance) isolated from schist near the center of the UZF formation, suggesting a maximum depositional age of ~730 Ma. Zircons from an undeformed granitic vein intruding UZF metasediments provided a concordia age of 611 ± 4 Ma, interpreted as a crystallization age (Eyal et al. 2014). The depositional window for the UZF is thus loosely constrained between ~730 and 647 ± 12 Ma. The local association with BIF, with documented Sturtian equivalents further south in the CED and the northern Arabian Shield, could be consistent with regional Sturtian glaciation but the minimum age constraint could include the Marinoan glaciation. More stringent age control is required for the upper UZF (from

diamictite and lonestone bearing intervals in addition to the overlying metacarbonate succession), in addition to deliberate sedimentological investigations for evidence of glacigenic deposition. If a glacial association is confirmed, the metacarbonate would be the first Cryogenian cap carbonate identified in the ANS. Similar studies are required to assess the age and glacigenic association of the Zaghara Formation. The high metamorphic grades of these successions may limit interpretations of primary depositional characteristics.

#### 7.5.2.5 Hadiyah Group, NW Arabian Shield

The Hadiyah group (Pellaton 1979; Kemp 1981) is a thick (7000 m) succession of volcaniclastic and siliciclastic sediments exposed in three elongate structures that parallel the Yanbu suture in northwestern Hijaz terrane (Fig. 7.2, locality 13). This ophiolite-decorated suture marks the collision between the Midyan terrane and overriding Hijaz arc terranes, with 780–705 Ma ophiolites constraining the period of collision and the orientation of the arc trench (Johnson et al. 2013). Hadiyah group basins are located 25–50 km inboard of the suture and mainly overly sedimentary arc rocks assigned to the 735–705 Ma Al Ays magmatic arc, the magmatic axis of which trends >100 km east of the suture. This configuration suggests that Hadiyah group deposition occurred between the arc trench and the magmatic axis, possibly as a fore-arc accretionary prism (Johnson et al. 2013). Intrusion of the suture by the ~695 Ma Jar-Salajah batholith (Pallister et al. 1988), which cuts folds of the Hadiyah group that continues into the Al Ays group, indicates that convergence was complete by ~700 Ma and that both groups were earlier affected by collisional deformation and intrusion. Despite deformation, the Hadiyah group has low greenschist grade facies.

The Hadiyah group is subdivided into three formations, the mostly volcanic Siqam followed by sedimentary Tura'ah (with lower Jammazin and upper Qaraqah members) and Aghrad formations (Kemp 1981). The basal contact with the Al Ays group has been variously interpreted as unconformable, with truncation of up to 4000 m of the Al Ays group (Kemp 1981), and intercalated with Al Ays group rocks (Johnson 1995). Zircon U–Pb ion probe ages between 708 ± 4 Ma and 736 ± 5 Ma for Al Ays group rocks and a 697 ± 5 Ma crystallization age for rhyolite in the Siqam formation (Kennedy et al. 2004, 2005) provide constraints for these interpretations. Regolith development at the contact between Al Ays and Hadiyah groups supports a period of weathering between deposition of the two groups (Johnson et al. 2013).

Of possible glacial significance are diamictite, limestone, and polymict conglomerate intervals within the Tura'ah and Aghrad formations. Hadiyah group deposition (~695 Ma) would have occurred during the Sturtian panglacial episode (717–659 Ma), for which there is strong supporting evidence of glacial influence in the S. ANS (Tambien Group). Putative 4-km incision of the Al Ays group could be consistent with the effects of continental-scale glaciation and eustatic sea-level fall (Fig. 7.4II), in addition to supplying a clast source for matrix-supported conglomeratic intervals (Johnson et al. 2013). Deliberate studies of the character and origin of matrix-supported pebble and boulder sandstone intervals (e.g., Jammazin member) are required to determine if evidence supporting glacigenic processes exists within the Hadiyah group (Johnson et al. 2013). If confirmed, these deposits (possibly along with the Um Zariq and Zaghara Formations of Sinai) would be the youngest evidence of Sturtian glaciation in the ANS. Environmental conditions of syn-Sturtian microbial limestone deposition would be relevant for understanding biotic responses to glaciation.

### 7.5.3 Evidence for Marinoan (Onset ~650–639, to ~635 Ma) and Ediacaran (~580–550 Ma) Glaciation

Orogeny associated with closure of the Mozambique Ocean, the uplift and emergence of the EAO, and the consolidation of Gondwana transformed the Cryogenian marine basin into a great Ediacaran mountain range. The so-called "Transgondwanan Supermountain" chain resulting from the protracted continent-continent collision between E and W Gondwana ~650–515 Ma extended from East Africa to Antarctica (length: >8000; width >1000 km; Jacobs and Thomas 2004) and is estimated to have shed sediments in excess of 100 $Mkm^3$ over a period of >100 Myr, as evidenced by common detrital zircon U–Pb age spectra in flanking terranes of India, Arabia, Africa, Australia, New Zealand, South America, and Antarctica (Squire et al. 2006). Widespread erosional unconformities throughout northern Africa and Arabia, separating Neoproterozoic basement from continentally derived Cambro-Ordovician quartz-rich sediments, testify to massive and sustained erosion of this vast collisional mountain range (Burke and Kraus 2000; Avigad et al. 2003). Fritz et al. (2013) argued that regions in the southern EAO experienced the greatest crustal thickening and uplift; the regions now occupied by Tanzania and Madagascar, in particular, experienced a Himalayan-type orogen with doubly thickened crust and correspondingly great uplift. Earliest orogenesis likely followed from the collision of northeastern Africa with the ANS at ~650–590 Ma (Boger and Miller 2004). By about 630 Ma, much of the ANS was probably above sea level. In orogenic hinterlands of the ANS, sediments that may have been deposited in association with the Marinoan panglacial episode would have been uplifted and increasingly eroded.

Metamorphic mineral T and P relationships, in addition to $^{40}Ar/^{39}Ar$ studies that constrain Neoproterozoic basement uplift (cooling) histories provide regional estimates of the extent of regional mountain range relief and beveling. For example, high-grade kyanite-bearing rocks in east Eritrea (Ghedem Domain) suggest formation at depths exceeding 40 km (Beyth et al. 1997; Ghebreab 1999), implying that the southern EAO had a crustal thickness of ~70 km (Beyth et al. 2003). Structurally overlying low-grade metasediments (Bizen Domain), akin to the Tambien Group, underwent burial metamorphism at considerably shallower burial depths. In Ethiopia, greenschist metamorphism of Tsaliet Group arc volcanic rocks in the northern Tigre area likely occurred at depths of 6–8 km (e.g., Asrat et al. 2004), but as a result of subsequent bevelling there is no known record of post-Sturtian sediment accumulation in Ethiopia. In the NE Arabian Shield, Cole (1988) postulated epeirogenic uplift as the cause of major 615–585 Ma erosion. Consistent with this interpretation is $^{40}Ar/^{39}Ar$ uplift histories from micas that indicate rapid cooling at ~600 Ma (Cosca et al. 1999). Most explanations for ~600 Ma exhumation invoke tectonic unroofing (e.g., Al-Husseini 2000; Blasband et al. 2000), but we suggest Marinoan and younger Ediacaran glaciation could also account for much of this deep erosion. Unroofing farther south, in Sudan and southern Egypt, may have occurred ~570 Ma, and thus could have intersected Ediacaran glaciation (Bailo et al. 2003).

Marinoan or Ediacaran glacial episodes in the ANS would have involved continental glaciations, possibly as continental ice sheets. These powerful erosional agents could have rapidly lowered relief of growing EAO mountains, shedding sediments that ultimately were deposited far from the high mountains. Greatest erosion likely occurred in the southern EAO, where high-grade metamorphic terranes indicate relief was highest and unroofing has removed any post-Sturtian sedimentary record, but how and when this region was beveled is not understood. The extent of EAO uplift was not limited to juvenile terranes of the ANS, but also included bounding cratonic terranes of east and west Gondwana. The provenance of sediments shed across northern Gondwana was therefore not exclusively limited to uplifted ANS terranes (e.g., Dor et al. 2018). Any late Cryogenian or Ediacaran marine sediments in the ANS would have been deposited on the margins of consolidated Gondwana or in later-formed structural basins (e.g., Najd Fault Basins; Stern 1985, 1994; Johnson et al. 2011, 2013). In marginal marine settings, Marinoan and Ediacaran glacioeustasy likely played a role in controlling the composition and architecture of sediment packages. As carbonate rocks of this age are uncommon in the ANS, their chemostratigraphic records are of particular importance for comparison with well-calibrated marine basinal records.

#### 7.5.3.1 Post-amalgamation (Ediacaran) Basins

Although definitive evidence of glacial deposition has not yet been reported, ANS depocenters capable of preserving evidence of Marinoan and/or Ediacaran glacigenic sedimentation include post-amalgamation basins of the northern Arabian Shield (Johnson 2003). Candidates capable of preserving evidence of the Marinoan glaciation include Furayh and Murdama basins in the Arabian Shield and buried basins in the Rub-al Khali (Stewart 2016) (Fig. 7.2, localities 14-16). Furayh basin contains <665 Ma volcaniclastic, epiclastic, and carbonate sediments that were deposited in shallow water to subaerial settings until convergence during the Nabitah orogeny (680–640 Ma) eliminated accommodation space. Some record of the Marinoan glaciation could be preserved in clastic and carbonate rocks (Johnson et al. 2013). Murdama basin is filled by sediments of the Murdama group and volcanic units (Afif and Hibshi formations). U–Pb SIMS zircon ages in tuffs from these units range from 649 ± 6 Ma to 624 ± 6 Ma (Kennedy et al. 2010b) and thus deposition would have intersected the Marinoan glaciation (Johnson et al. 2013). Ediacaran age sediments of the Jibalah Group (Delfour 1970) might provide evidence of Ediacaran glaciation(s) in the northern ANS. The Jibalah Group, together with the overlying Kurayshah Group (known only in the Al 'Ula area; Nicholson et al. 2008), represent youngest Precambrian depositional units in the Arabian Shield.

*Jibalah Group Basins*—In the northern Arabian Shield, the Ediacaran (post-Marinoan) age Jibalah Group (Delfour 1970) is preserved in more than 10 isolated pull-apart basins caused by strike- and dip-slip movements of the NW-trending Najd fault system (Sultan et al. 1988) (Fig. 7.2, localities 18a–g). These small basins are spread out over 100 s of kilometers. Jibalah basin sedimentary fill, with thicknesses ranging from ~500 to >3300 m, is largely volcano-sedimentary but also includes carbonate units. Probable metazoan trace and body fossils are reported in two Jibalah Group basins (Dhaiqa and Jifn) (Vickers-Rich et al. 2013). Volcanic flows and pyroclastic beds demonstrate that the region was magmatically active during deposition. Jibalah Group regional correlation is not straightforward owing to high lithologic variability from basin to basin. Basal fill in many basins begins as polymict conglomerate (Fig. 7.11A) and limestone generally increases in abundance in the upper succession (Vickers-Rich et al. 2013). Matrix supported cobble and boulder diamictite intervals (Fig. 7.11H–J) are reported in at least one basin (Dhaiqa; Miller et al. 2008). Possible dropstones (Fig. 7.11B–C) have also been noted in Jifn Basin (Kusky and Matsah 2003) and in the Naghr Formation (Shagab Quadrangle, NW Arabia; presumed to be correlative with the Jibalah Group (Vickers-Rich et al. 2010). Jibalah Group intervals

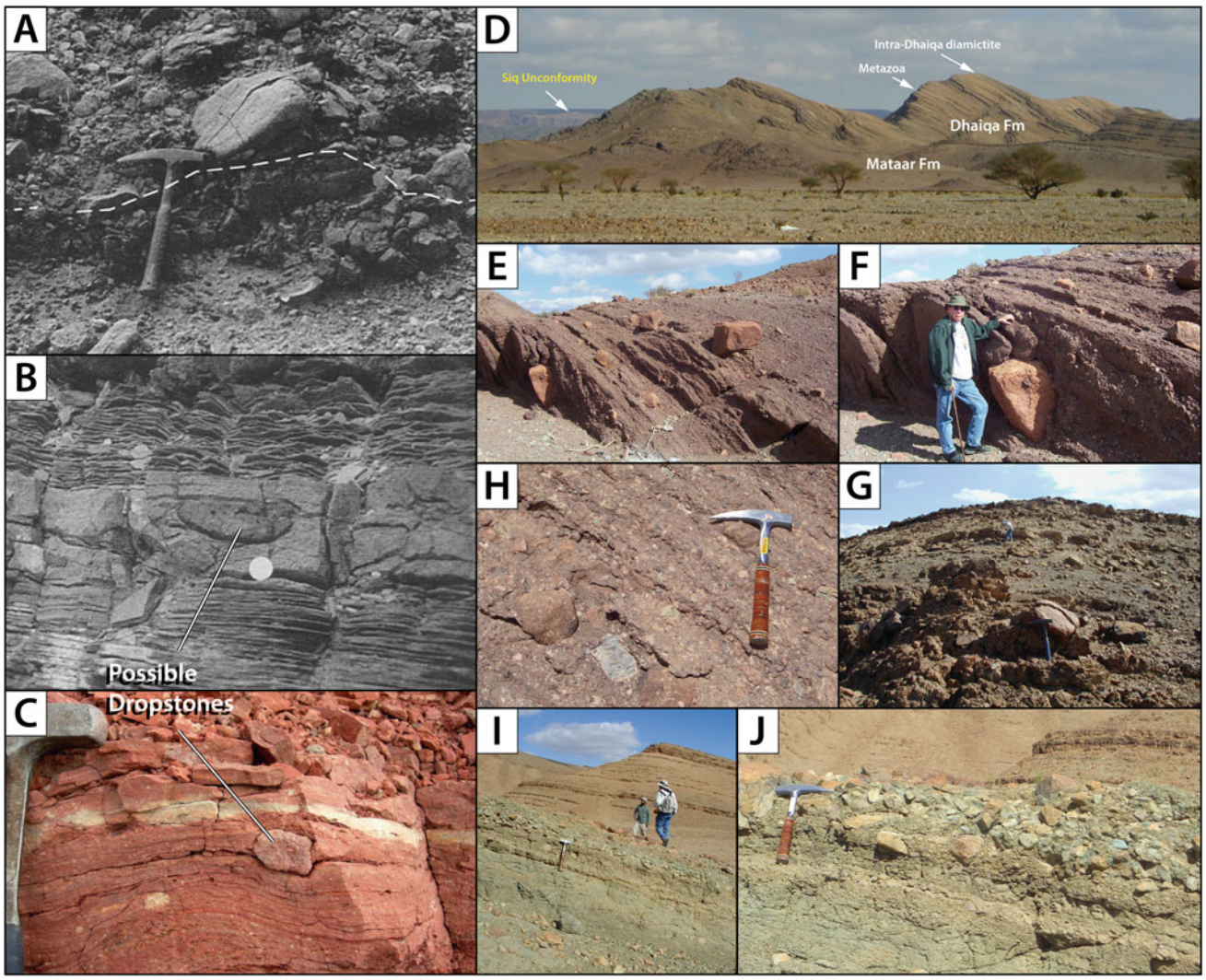


**Fig. 7.11** Outcrop photographs of prospective glacigenic intervals in the Ediacaran Jiabalah Group, Arabian Shield. **A** Polymict basal conglomerate unconformably overlying Murdama rhyolite basement; photo from Kusky and Matsah (2003). **B–C** Possible dropstones in Jifn (Kusky and Matsah 2003 and Naghr basins (Vickers-Rich et al. 2010; photo from Cui et al. 2020). Photos **D–J** Dhaiqa basin. **D** Eastward view of well-bedded carbonate in the Dhaiqa Formation, showing underlying Mataar Formation siliciclastics, positions of metazoa and a diamictite interval, and the Siq Unconformity. **E–F** Outsized boulders in the ferruginous basal Mataar Formation (R. Stern for scale). **G** Closer view of Mataar polymictic conglomerate. **I** Stratigraphic transition from the Mataar Formation to initial carbonate beds of the Dhaiqa Formation. **I–J** Intra-Dhaiqa diamictite interval

associated with polymict conglomerate, matrix-supported diamictite, and dropstones are prime targets for follow-up studies of possible glacigenic sedimentation. Jibalah Group correlatives could be found in rift basins buried beneath the Rub Al-Khali (Fig. 7.2, locality 19; Stewart 2016) and similar buried basins beneath the Western Desert of Egypt. Jibalah Group sediments may also be correlative with Hammamat sediments of Egypt, Saramuj Conglomerate of Jordan, and Elat Conglomerate of Israel (Fig. 7.2, localities 20–22). An unresolved problem is whether Jibalah Group deposition directly followed basin subsidence from local sediment sources or if the deposition was more regionally sourced and only subsequently preserved in down-dropped basins (Johnson 2003). The upward increase in carbonate units among basins suggests a marine transgression, but the prior isolated character of each basin could alternatively indicate a series of fault-controlled lakes (Johnson et al. 2003). Basin development could also have been diachronous along different Najd fault zones. The occurrence of metazoan trace fossils demonstrate that Ediacaran animals were present in some Jibalah Group basins, raising intrigue about their origins in marine vs. non-marine environments.

Jibalah Group regional deposition is constrained to be younger than underlying shield rocks ($\leq$618 Ma; Nettle et al. 2013) and likely $\leq 605 \pm 5$ Ma;) and older than the overlying Lower Cambrian basal unconformity ($\sim$540–

520 Ma) formed by peneplanation of the EAO. U–Pb zircon dating of volcanic intervals in several Jibalah Group basins confirm this depositional interval. Jibalah Group chronostratigraphy is currently best documented in three widely separated basins further detailed below: Jifn (aka Jif'n) basin in the NE Arabian Shield, Antaq basin in the E Arabian Shield, and Dhaiqa basin in the NW Arabian Shield (west of Al 'Ula).

In Jifn Basin (Fig. 7.2, locality 18c), deposition of a ~3 km thick sequence of conglomerate, limestone and shale, is constrained by TIMS U–Pb zircon techniques between 625 ± 4 (Murdama Group basement) and 577 ± 5 Ma (felsite dyke cutting Jifn Formation) (Kusky and Matsah 2003). The Jifn Jibalah Group succession above basement consists of Lower Conglomerate (500 m), Umm al-Aisah Limestone (~340 m), and the clastic Jifn Formation (~1870 m), which begins with ~290 m of Jifn Polymictic Conglomerate. Interestingly, Kusky and Matsah (2003) show an outcrop photo of a "possible dropstone", but its position within the stratigraphic succession was not reported and its possible significance was not further explored. Metazoan (multi-cellular; tissue grade organism; string-of-beads like; *Horodyskia*-like) macrofossils were later discovered in lime-rich dark mudstones of the Jifn formation (Vickers-Rich et al. 2013). The stratigraphic position of this sample within the Jifn formation is also unclear, but the regional interval was described as consisting of brownish conglomerates with well-rounded pebbles, thin grey limestone beds, dark red calcareous sandstones, and repetitive grey clastic sediments (sandstone to shale). Halverson et al. (2013) obtained a LA-ICP-MS U-Pb zircon age of ≤589.5 ± 0.5 Ma for an ash bed in the lower part of the Umm al-Aisah Limestone and also documented $\delta^{13}C$ values of 5–8‰ for this unit, which if marine could be consistent with deposition before the onset of the Shuram negative $\delta^{13}C$ excursion (similar to Khufai Fm of the Nafun Group in Oman; Al-Husseini 2014).

In Antaq basin (Fig. 7.2, locality 18a), the Jibalah Group consists of a ~2500 m thick conformable succession of nearly undeformed and unmetamorphosed clastic and carbonate sediments, consisting from base to top of Rubtayn, Badayi, and Muraykhah formations (Hadley 1974; Nettle et al. 2013). The succession is constrained by CA–TIMS (Nettle et al. 2013) and SHRIMP (Kennedy et al. 2010a, b) U–Pb zircon dates of Antaq Basement to be younger than 618–597 Ma. Nettle et al. (2013) established LA–ICP–MS U–Pb zircon dates for ash beds within the overlying Jibalah group of ≤596 ± 17 Ma (Rubtayn Fm, above Polymictic Conglomerate); 579 ± 17 Ma (Muraykhah Fm, 255 m); and ≤604 ± 18 Ma (Muraykhah Fm, 325 m). Carbonate $\delta^{13}C$ values for three sections of the Muraykhah Fm mainly span from −4 to 0‰, with considerable stratigraphic scatter (Nettle et al. 2013). If Muraykhah deposition occurred in a marine environment, the modestly negative $\delta^{13}C$ values could conceivably intersect the Shuram negative $\delta^{13}C$ excursion, possibly during its recovery as demonstrated in the Buah Formation of the Nafun Group in Oman (Fike et al. 2006; Nettle et al. 2013; Al-Husseini 2014). The ~1000 m thick Antaq Polymictic Conglomerate interval within the Rubtayn Fm is a prospective candidate for glacigenic deposition. It is described as blocky, with occasional cross-beds, predominantly consisting of sub-rounded white quartz clasts in a quartz-feldspathic matrix (Nettle 2009). The 596 ± 17 Ma date just above this unit (Muraykhah Fm, 255 m) could mean the conglomerate was deposited before this time; possibly during the ~580 Ma Gaskiers glaciation.

In Dhaiqa Basin (NW Arabian Shield, Fig. 7.2, locality 18f, Fig. 7.11D–J), near the confluence of Wadi al Jizl and Wadi Dayqah, the Jibalah Group begins above basement as the Mataar Formation (Davies 1985), a ~150 m thick siliciclastic unit, consisting of poorly sorted arkose and conglomerate bearing subangular to subrounded clasts, including matrix-supported outsized boulders with up to m-scale diameters, which grades upward into arkose and lithic arenite (Fig. 7.11E–G). The Mataar Formation is gradationally and conformably overlain by the Dhaiqa Formation (Davies 1985), a 300–400 m thick carbonate succession, consisting of low-relief microbial and algal structures with evidence of subaerial exposure (desiccation cracks) and high energy deposition (carbonate intraclast rip-ups/tempesites?) in the lower portion. Miller et al. (2008) logged the stratigraphic section, established baseline Sr and C isotope stratigraphies, and documented the possible occurrence of metazoan trace fossils within the middle portion of the Dhaiqa Formation. Trace fossils have since been verified and probable Ediacaran body fossils discovered at higher levels in the Dhaiqa Formation (Vickers-Rich et al. 2010, 2013).

Available U–Pb zircon ages support that Dhaiqa Jibalah Group deposition occurred between ≤609 and ~530 Ma and was ongoing at 570–560 Ma in the upper portion of the Dhaiqa Formation. The undated Mataar Formation overlies granitoids having a SHRIMP U–Pb zircon age of 609 Ma (Kennedy et al. 2010a). No upper contact is preserved in the basin, but the Dhaiqa Formation certainly unconformably underlies the Cambrian Siq Sandstone below the ~530 Ma Sub-Siq Unconformity, which correlates regionally with the Ram Unconformity in Jordan and Angudan Unconformity in Oman (Al-Husseini 2014; Powell et al. 2015). Two stratigraphic intervals within the Dhaiqa Formation provide further age constraints. A distinct 2–3 m-thick interval of glauconitic arenite overlain by poorly sorted polymict conglomerate (Intra-Dhaiqa Diamictite) with clast diameters up to 0.5 m (Fig. 7.11I–J), interrupts carbonate deposition in the upper Dhaiqa Formation (~180 m). Detrital zircons recovered from a fine-grained sandstone interval have

SHRIMP U–Pb ages as young as 599 ± 4.8 Ma and 570 ± 4.6 Ma (measured from the core and rim of the same grain, respectively; Miller et al. 2008). Above the diamictite interval, in a different area of the basin, Vickers-Rich et al. (2010) determined detrital zircon LA–ICP–MS U–Pb ages between 837 ± 25 and 555 ± 15 Ma for a suspected re-deposited volcanic ash bed. An age of 560 ± 4 Ma obtained for youngest zircons (n = 17) was interpreted as the maximum depositional age for the Dhaiqa Formation at this level. Youngest detrital zircon ICP–MS U–Pb ages of 569 ± 3 Ma were obtained for a tuff at a level above the diamictite interval in yet another locality (Vickers-Rich et al. 2013). These dates demonstrate mid-to-upper Dhaiqa limestone deposition at 570–560 Ma.

Metazoan trace fossils (Miller et al. 2008) and probable body fossils (Vickers-Rich et al. 2010, 2013) have been found in the Dhaiqa Formation, including *Beltanelloides/Nemiana, a Pteridinium*-like impression, a *Cyclomedusa/Aspidella*-like holdfast structure, rod-shaped fossils with oblique transverse marks similar to *Harlaniella* sp., and curvilinear conical tubes suggestive of frond-like taxa with a basal holdfast (e.g., *Charnia*). Lowest documented trace fossils occur ~30 m below the level of the Intra-Dhaiqa Diamictite, indicating that they are older than ~570–560 Ma, if the dated volcanic units (prospective reworked ash and tuff) higher in the Dhaiqa sequence are eruptive (depositional) ages.

On the basis of sedimentology (matrix-supported polymictic clasts and boulders), both the Mataar Formation and Intra-Dhaiqa Diamictite are candidates for glacigenic deposits. If so, the Intra-Dhaiqa Diamictite, constrained to be ≤570 Ma, must correspond to a glacial interval younger than the ~580 Ma Gaskiers glaciation (Pu et al. 2016), whereas the Mataar Formation (≤609–570 Ma) could correspond to the Gaskiers glaciation. Seawater C- and Sr-isotope evolution curves generated from least-altered marine carbonates indicate that Ediacaran oceans were characterized by large perturbations and systematic trends that provide a means for unambiguous regional correlation between marine sections. Sr isotope values of Dhaiqa formation carbonates (0.704–0.706), however, are well-below Ediacaran seawater values (Miller et al. 2008), indicating that the depositional setting may have been isolated (lake?) or that primary isotopic compositions were reset by diagenetic fluid exchange involving a predominant ensimatic Sr source—compatible with regional basement and Ediacaran volcanism, or hydrothermal alteration by juvenile fluids (Cui et al. 2020). C-isotopes in the Dhaiqa Formation, which are less susceptible to alteration, are predominantly positive (2.4 ± 2.3‰). If marine, the $\delta^{13}C$ compositions constrain deposition either before or after the long-lived Shuram negative $\delta^{13}C$ excursion. The Gaskiers glaciation is now thought to have slightly preceded the negative Shuram anomaly (574 ± 4.7 to 567.3 ± 3.0 Ma; Rooney et al. 2020). The available age control and positive $\delta^{13}C$ compositions support that Dhaiqa deposition likely followed the Shuram anomaly, and the Intra-Dhaiqa Diamictite interval is younger than the Gaskiers glaciation. The underlying Mataar Formation remains a candidate for a pre- ~570 Ma glaciation. Establishing depositional ages for Mataar Formation and extending the $\delta^{13}C$ database to include transitional carbonate beds grading into the Dhaiqa formation, which might have overlapped with the negative Shuram CIE, could further constrain regional correlations. Until then, distinguishing the lacustrine, paralic, or marine depositional setting of the Dhaiqa Formation remains to be resolved.

Ediacaran successions with similar lithologies and thicknesses, but lacking U–Pb zircon geochronology, occur in the Mashhad area near Al Ula, about 100 km ESE of Dhaiqa Basin, in addition to other basins further ESE. In the Jabal Rubtayn section, (Fig. 7.2, locality 18e) Hadley (1974) described the Mashhad area Ediacaran succession as consisting of Rubtayn (375 m), Badayi (120–150 m) and Muraykhah (330–370 m) formations. The succession is unconformably bracketed between the Shammar Rhyolite Group (~620–585 Ma, Al-Husseini 2011) and lower Cambrian Siq Sandstone. The Rubtayn Formation (375 m) consists of ascending boulder conglomerate, sandstone, red beds, and pebble conglomerate units (members), before being interrupted by m-scale amygdaloidal basalt flows of the Badayi Formation. The sedimentary succession resumes conformably in the Muraykhah Formation with deposition of basal conglomerate (similar to the upper Rubtayn Formation), followed by lower cherty (non-dolomitic) carbonate, red siltstone and mudstone, and an upper dolomitic (chert-poor) carbonate unit. Except for the volcanic interlude, the stratigraphic succession at Jabal Rubtayn is similar to the Mataar and Dhaiqa Formations in Dhaiqa Basin (Al-Husseini 2014). In the Sahl Al Matran section (Fig. 7.2, locality 18d, ~70 km ESE of Mashhad; SE Sahl Al Matran Quadrangle) Hadley (1986) described the comparable sequence as three informal members: (1) Volcanic Conglomerate (700 m), (2) Polymictic Conglomerate (1500 m), and (3) Sandstone (1000 m). In Bir Sija Basin (Fig. 7.2, locality 18b, ~590 km ESE of Mashhad; central Afif Quadrangle), the undated Jibalah Group also resides unconformably above the Shammar Rhyolite Group in eight units (Letalenet 1979): (1) Conglomerate with Shammar pebbles (500 m); (2) Andesite-Basalt (150 m); (3) Sandstone (200 m); (4) Polymictic Conglomerate (150 m); (5) Limestone (20 m), the "Bir Sija Limestone"; (6) Sandstone and Mudstone (700 m); (7) Sandstone and Limestone (300 m); and (8) Sandstone and Siltstone (m). Al-Husseini (2014) suggests that the Dhaiqa and Mashhad sequences begin with deposition of units comparable to Sija Basin unit 4 (Polymictic Conglomerate).

Recognizing that Ediacaran glacioeustasy should have had a strong effect on the character and sequence of sediments (supersequences) deposited on Gondwana margins, Al-Husseini (2014) proposed that Ediacaran strata in the Nafun Group (Huqf Supergroup) of Oman may correlate to Jibalah Group deposits in the northern Arabian Shield (Fig. 7.12). The correlation assumes that a major glacial episode, perhaps Gaskiers, caused a widespread unconformity, which may be related to the Great Unconformity (see discussion in Sect. 6.3.3). Within the Huqf Supergroup, the Ediacaran Nafun Group of Oman (635–547 Ma) is divided into Lower (635–582 Ma, and Upper (582–547 Ma) Supersequences by an unconformity at the base of the Shuram Formation and the long-lived (e.g. ~582–551 Ma, Bowring et al. 2007; ~570–557 ± 3, Zhou et al. 2018; 574 ± 4.7–567.3 ± 3.0 Ma, Rooney et al. 2020) Shuram negative $\delta^{13}C$ excursion (Condon et al. 2005; Le Guerroué 2010; Gong et al. 2017; Shields et al. 2019). The age of this unconformity is poorly constrained and controversial (see Al-Husseini 2014 for details); it is broadly related to the Great Unconformity (see Sect. 6.3.3 for further discussion). Assuming constant sedimentation rates for the thickest known Nafun Group sequence (2308 m; offshore Masirah-1 Well), Al-Husseini (2014) estimated the unconformity to have formed close to ~582 Ma, consistent with the known age of the Gaskiers glaciation in Newfoundland (Bowring et al. 2003, 2007). He suggested this putative glacial unconformity should be traceable to comparable "glacial" unconformities within the Jibalah Group and proposed that the Rubtayn Boulder Conglomerate (Jabal Rubtayn, Mashhad area), Mataar Polymict Conglomerate (Dhaiqa Basin), Antaq Polymict Conglomerate (Antaq Basin), and Jifn Polymict Conglomerate (Jifn Basin) are products of the same Ediacaran glaciation, and that limestone units overlying some of these units could be cap carbonates (Fig. 7.12B–G). In Jifn Basin, the proposed contact occurs within the Jifn Formation, separating Umm al-Aisah Limestone of the "lower Jibalah Supersequence" (605 ± 5–582 Ma) from Jifn Polymictic Conglomerate ($\geq$200 m thick) at the base of the Upper Jibalah Supersequence. In Antaq Basin, the contact is placed at the base of the Antaq Polymictic Conglomerate, based on the reasoning that immediately overlying age constraints (613–579 Ma) permit its deposition to have been synchronous with the ~582 Ma Gaskiers glaciation and $\delta^{13}C$ values (−4 to 0‰) in the overlying Muraykhah Formation being compatible with Buah Formation (Upper Nafun Supersequence, Oman) deposition at the end of the negative Shuram anomaly. In Dhaiqa Basin, the unconformity is placed at the base of the Mataar Formation, constrained to be <609 and >570 Ma, consistent with overlying Dhaiqa Formation carbonate deposition, with predominantly positive $\delta^{13}C$ values, being equivalent to Buah Formation (Oman), following the Shuram negative $\delta^{13}C$ excursion (Miller et al. 2008). He suggests the composite Mataar-Dhaiqa succession is a second-order sequence, "upper Jibalah Supersequence' that is correlative to the Upper Nafun Supersequence (582–547) in Oman.

This intriguing correlation scheme needs additional work to assess its feasibility. Considerations for follow up studies include that the Masirah-1 well unconformity, with estimated age of 582 Ma (Al-Husseini 2014) has not been directly dated and could have a different age. In fact, the Gaskiers glaciation in Newfoundland is now constrained to a 340 kyr duration between 579.63 ± 0.15 and 579.88 ± 0.44 Ma; Pu et al. 2016), and it may have been one of several regional-scale mid-to-late Ediacaran glacial episodes on eight paleocontinents. Age constraints for many of these are limited, but sufficient to demonstrate multiple Ediacaran glacial episodes (e.g., Hebert et al. 2010; Vernhet et al. 2012; Etemad-Saeed et al. 2016; Linneman et al. 2018). There is some support for Ediacaran glaciation in northern peri-Gondwana prior to the appearance of Metazoa. Evidence of 605 to ~560 Ma glaciation is reported in Morocco (Vernhet et al. 2012) and Late Ediacaran glaciation (~ $\leq$560 Ma) is suspected elsewhere on the West African Craton (Bertrand-Sarfati et al. 1995; Caby and Fabre 1981; Deynoux et al. 2006). Linneman et al. (2018) recently documented ~565 Ma glaciomarine diamictites along the periphery of the West African Craton (SW Iberia, Bohemia). Etemad-Saeed et al. (2016) reported possible $\leq$560 Ma glacial diamictite, overlying striated pavement, within the Kahar Formation of northern Iran, which they correlated within the upper Nafun Group Supersequence (Buah and Ara formations) of Oman. Prospective Ediacaran glacigenic units have also been documented in central (Mohsensi and Aftabi, 2015) and southern Iran (Aftabi 2001; Hassanlouei and Rajabzadeh 2019). These could all correlate within the Upper Jibalah Supersequence of Al-Husseini (2014). Evidence in support of Ediacaran glaciation in the northern ANS is currently limited to the occurrence of diamictites and polymict conglomerate units, some overlain by carbonate intervals (prospective cap carbonates), and rare documentation of possible dropstones within Ediacaran age Jibalah Group basins. Needed are more rigorous sedimentologic studies to confirm or reject glacigenic (post-glacigenic) associations with these units. The limited number and thickness of carbonate units, and possibility that Jibalah Group basins were non-marine or had limited marine connections during deposition, pose significant limitations for global chemostratigraphic correlations. The common stratigraphic occurrence of tuffs and ashes in Jibalah Group successions offers the potential for refined age control.

#### 7.5.3.2 Gondwanan Margin Basins

Other northern ANS sedimentary successions could represent glacial deposits or fluvial reworking of sediments from

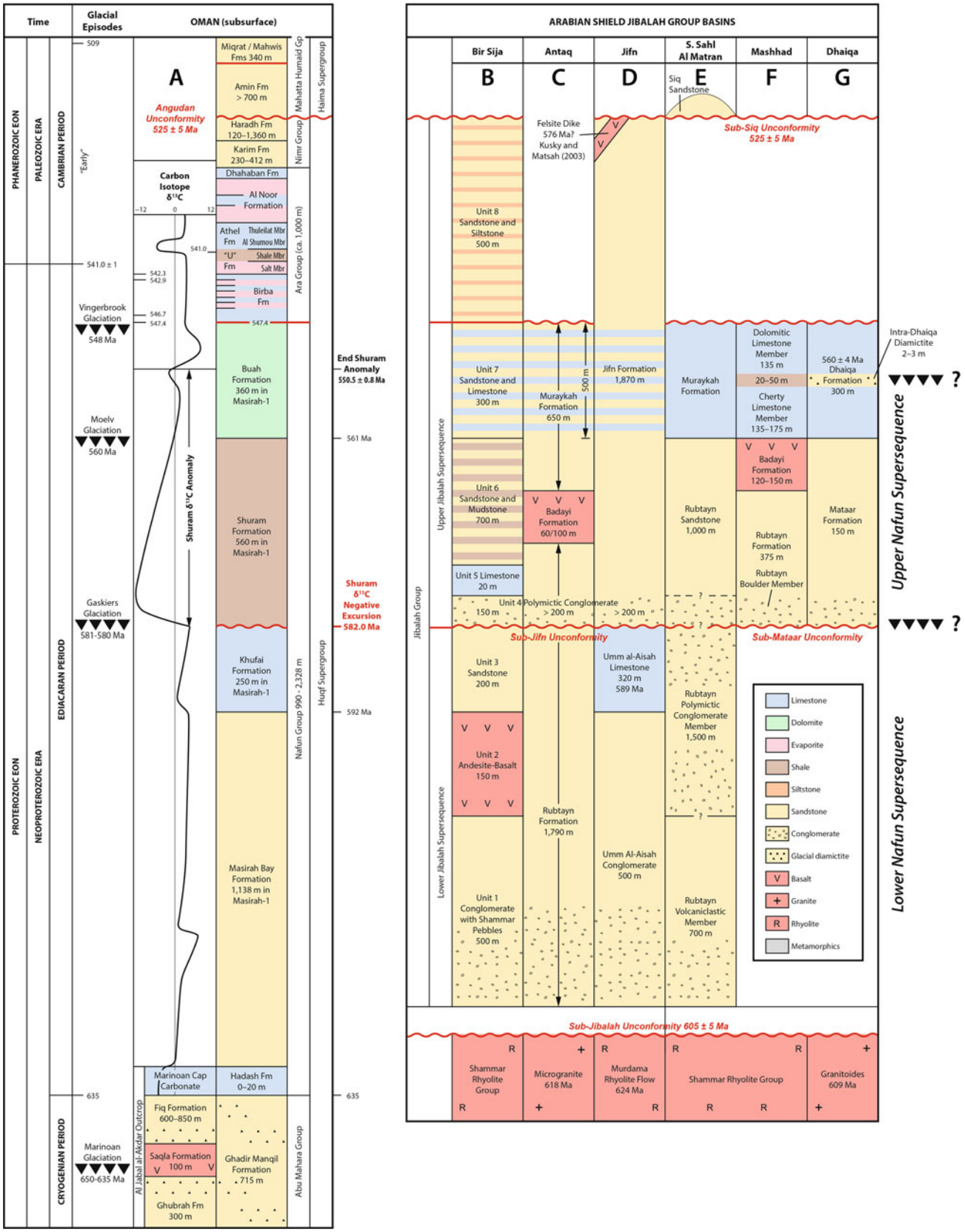
Time
Glacial Episodes
OMAN (subsurface)
PHANEROZOIC EON
PALEOZOIC ERA
CAMBRIAN PERIOD
"Early"
PROTEROZOIC EON
NEOPROTEROZOIC ERA
EDIACARAN PERIOD
CRYOGENIAN PERIOD
509
541.0 ± 1
635
A
Angudan Unconformity 525 ± 5 Ma
Carbon Isotope δ13C
−12 0 12
541.0
542.3
542.9
546.7
547.4
Vingerbrook Glaciation
548 Ma
Moelv Glaciation
560 Ma
Gaskiers Glaciation
581-580 Ma
Marinoan Glaciation
650-635 Ma
Shuram δ13C Anomaly
Miqrat / Mahwis Fms 340 m
Amin Fm > 700 m
Haradh Fm 120–1,360 m
Karim Fm 230–412 m
Dhahaban Fm
Al Noor Formation
Athel Fm
Thuleilat Mbr
Al Shumou Mbr
"U" Fm
Shale Mbr
Salt Mbr
Birba Fm
Buah Formation 360 m in Masirah-1
Shuram Formation 560 m in Masirah-1
Khufai Formation 250 m in Masirah-1
Masirah Bay Formation 1,138 m in Masirah-1
Hadash Fm 0–20 m
Ghadir Manqil Formation 715 m
Abu Mahara Group
Marinoan Cap Carbonate
Fiq Formation 600–850 m
Saqla Formation 100 m
Ghubrah Fm 300 m
Al Jabal al-Akdar Outcrop
Mahatta Humaid Gp
Nimr Group
Ara Group (ca. 1,000 m)
Nafun Group 990 - 2,328 m
Huqf Supergroup
Haima Supergroup
End Shuram Anomaly 550.5 ± 0.8 Ma
561 Ma
Shuram δ13C Negative Excursion 582.0 Ma
592 Ma
635
ARABIAN SHIELD JIBALAH GROUP BASINS
Bir Sija
Antaq
Jifn
S. Sahl Al Matran
Mashhad
Dhaiqa
B
C
D
E
F
G
Siq Sandstone
Sub-Siq Unconformity 525 ± 5 Ma
Felsite Dike 576 Ma? Kusky and Matsah (2003)
Unit 8 Sandstone and Siltstone 500 m
Unit 7 Sandstone and Limestone 300 m
Unit 6 Sandstone and Mudstone 700 m
Unit 5 Limestone 20 m
Unit 4 Polymictic Conglomerate 150 m
> 200 m
> 200 m
Sub-Jifn Unconformity
Unit 3 Sandstone 200 m
Unit 2 Andesite-Basalt 150 m
Unit 1 Conglomerate with Shammar Pebbles 500 m
Muraykah Formation 650 m
500 m
Badayi Formation 60/100 m
Rubtayn Formation 1,790 m
Jifn Formation 1,870 m
Umm al-Aisah Limestone 320 m 589 Ma
Umm Al-Aisah Conglomerate 500 m
Muraykah Formation
Rubtayn Sandstone 1,000 m
Rubtayn Polymictic Conglomerate Member 1,500 m
Rubtayn Volcaniclastic Member 700 m
Dolomitic Limestone Member 135 m
20–50 m
Cherty Limestone Member 135–175 m
Badayi Formation 120–150 m
Rubtayn Formation 375 m
Rubtayn Boulder Member
Sub-Mataar Unconformity
560 ± 4 Ma Dhaiqa Formation 300 m
Mataar Formation 150 m
Intra-Dhaiqa Diamictite 2–3 m
Upper Nafun Supersequence
Lower Nafun Supersequence
Jibalah Group
Upper Jibalah Supersequence
Lower Jibalah Supersequence
Limestone
Dolomite
Evaporite
Shale
Siltstone
Sandstone
Conglomerate
Glacial diamictite
Basalt
Granite
Rhyolite
Metamorphics
Sub-Jibalah Unconformity 605 ± 5 Ma
Shammar Rhyolite Group
Microgranite 618 Ma
Murdama Rhyolite Flow 624 Ma
Shammar Rhyolite Group
Granitoides 609 Ma

◀ **Fig. 7.12** Prospective regional correlation of Al-Husseini (2014, 2015) for Ediacaran and early Cambrian units between Oman and Jibalah Group basins of the Arabian Shield. **A** The correlation attributes the erosional unconformity at the base of the Shuram Formation (Masirah-1 well, offshore Oman) to the ~581–580 Ma Gaskiers glacial interval and postulates that similar erosional unconformities should exist within Jibalah Group sedimentary successions in the Arabian Shield. **B–G** Proposed Gaskiers-related glacigenic sediments in Jibalah Group basins include: polymict conglomerate intervals in Dhaiqa Basin (Mataar Fm), Mashad region (Rubtayn Boulder member of the Rubtayn Formation), Jifn Basin (basal Jifn Fm), Antaq Basin (upper Rubtayn Fm), and Bir Sija Basins (Unit 4 polymict conglomerate). In this correlation, the proposed Upper Jibalah Group supersequence is equivalent to the Upper Nafun Group supersequence in Oman. Occurrence of possible dropstones in unspecified intervals of the Jifn Formation (Jifn Basin, Kusky, and Matsah 2003) and Nagr Formation (Vickers-Rich et al. 2010), in addition to the Intra-Dhaiqa diamictite (Miller et al. 2008) raise the possibility of post-Gaskiers glaciation in the ANS. Modified from Al-Husseini (2015)

Marinoan and/or Ediacaran glaciers. There seems to have been a major reorganization of drainage following the ~530 Ma Rum Unconformity. After this time drainage was dominated by vast fluvial systems that transported and deposited huge sediment volumes in giant sedimentary fans that seem to have been mostly transported to the north (Dabbagh and Rogers 1983). Before this time, drainage was more local, including ~600 Ma deposition of the Saramuj conglomerate of Jordan (Fig. 7.2, locality 21), which Jarrar et al. (1991) interpreted as deposited within a high velocity, braided stream/alluvial fan system, the Hammamat Group in NE Egypt (Fig. 7.2, locality 20; Jarrar et al. 1993; Wilde and Youssef 2002), and Jibalah Group sediments (Fig. 7.2, locality 18a–g). Pre-Rum Unconformity coarse sediments could be periglacial tillites of Marinoan or Ediacaran age, reworked by meltwater streams as glaciers receded, but deliberate studies are required to confirm or refute this suggestion. The >588 ± 10 Ma Elat Conglomerate of southern Israel (Fig. 7.2, locality 22) contains clasts up to 1.5 m and was deposited on a deeply dissected relief, suggesting that sea level was quite low (Be'eri-Shlevin 2008; Weissbrod and Sneh 2002). This timing is close to prospective glacial intervals in Morocco, SW Iberria, Bohemia, and N. Iran (Vernhet et al. 2012; Linneman et al. 2018; Etemad-Saeed et al. 2016), which would also have been situated along the northern Gondwana margin (present coordinates). The possibility that the Elat Conglomerate was deposited in a glacial or periglacial setting during an Ediacaran glacial episode, younger than the Gaskiers, is worthy of further study.

The >2 km thick Zenifim Formation of Israel (Fig. 7.2, locality 23) is constrained to have been deposited between ~550 and 600 Ma (Abdo et al. 2020). The Zenifim can be expected to record any glaciation impacting the area during this time but has not yet been studied for this purpose.

#### 7.5.3.3 Role of Glaciation in the Formation of the Afro-Arabian Peneplain

The Great Unconformity is a profound gap in Earth's stratigraphic record often evident below the base of the Cambrian system. Keller et al. (2020) argue that it was caused by multiple episodes of global glaciation that removed a global average of 3–5 vertical kilometers of crust and sediments. The age of the Great Unconformity in most places is difficult to constrain, but because tectonomagmatic activity and sedimentation continued throughout Neoproterozoic time, the age of Great Unconformity can be well-constrained in the ANS and environs (Fig. 7.2, localities 17 and 24—arbitrarily placed along the southern exposure limit of early Paleozoic sandstone; Fig. 7.13). The Jordan record, in particular, suggests that it formed as a result of multiple stages of downcutting over ~100 million years. The Ediacaran Araba Complex of Jordan is bracketed by two major erosional unconformities: the basal Araba Unconformity overlies ~605 Ma rocks and the overlying Ram unconformity, which is thought to have formed ~530 Ma (Powell et al. 2015). An unconformity like the Araba unconformity is also recognized in southern Israel, where Garfunkel (1999) documented a "Main Erosion Phase" at ~600 Ma, possibly involving 8–14 km of downcutting. Ediacaran glaciations may have contributed to downcutting of the Araba and Ram unconformities in Jordan. The compatible timing of the ~580 Ma Sub-Shuram Unconformity, separating the Khufai and Shuram formations in subsurface Oman, with deposition of conglomeratic units in the Jibalah Group of Arabia (Al-Husseini 2014; as discussed in Sect. 6.3.1), may further support regional scale glacial erosion linked to the Gaskiers and possibly younger Ediacaran glaciations along the peri-Gondwana margin.

Formation of the Great Unconformity in and around the ANS is likely related to alpine glaciation in the Transgondwanan Supermountain and set the stage for establishment of the peripheral superfan systems. Glacial activity was unlikely for final cutting as the presence of thick laterite immediately below the peneplain indicates a warm and humid climate (laterization could happen after glaciation). Erosion of this exceptional regional orogen would have been enhanced by the lack of terrestrial vegetation and also increased water-rock interaction (chemical weathering) in lower latitudes approaching the paleoequator (Squire et al. 2006). Orogen development would have transgressed both the Marinoan panglacial episode as well as regional scale Ediacaran glaciation, and its weathering intensity could have influenced carbon burial and greenhouse gas concentrations, perhaps even triggering glacial episodes. These continental glaciations would have greatly enhanced erosion and moved

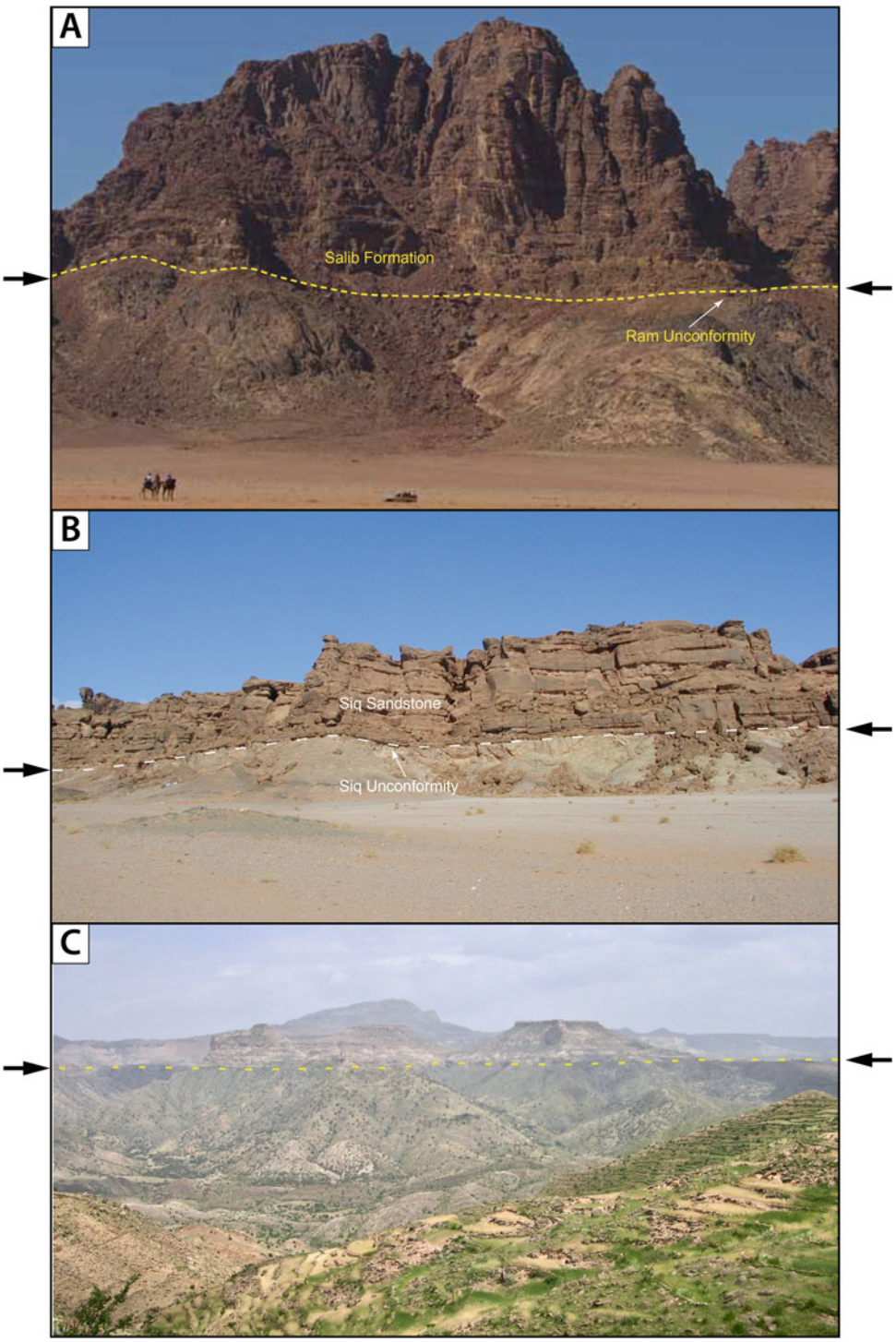


**Fig. 7.13** Expressions of the Great Unconformity (Afro-Arabian Peneplain) in the Arabian-Nubian Shield. **A** Southern Jordan (Wadi Ram). Ram Unconformity separating peneplained Neoproterozoic basement (Aqaba Complex granitoids) from overlying lower Cambrian sandstone (Ram Group). Photo from Powell et al. (2015). **B** Northern Arabia (25 km west of Al 'Ula) Siq Unconformity separating beveled Neoproterozoic granitic basement from overlying Cambrian-Ordovician sandstone. Horizontal field of view is ~130 m. **c** Northern Ethiopia (Adigrat region)—AAP separating Neoproterozoic basement from overlying Cambro-Ordovician sandstone

glacial till to lower elevations and ultimately marine margins. Alpine glacial environments are intrinsically transient, and preservation of Marinoan and Ediacaran glacial deposits may only have been possible in distal margin settings or within down-dropped basins. Some deposits in lowland settings may have developed secondarily from reworking of earlier glacigenic sediments. How the basal Cambrian peneplain formed has not been well studied, and the possible role of glaciation in its early cutting should be considered further.

The final episode in the latest Ediacaran time after final cutting of the peneplain was the establishment of a hot climate. This is shown by evaporites in eastern Arabia and Oman (Fig. 7.12A), where ash beds in evaporites of the Ara

Formation give U–Pb zircon ages of 541, 542, and 547 Ma (Bowring et al. 2007). This warm climate is also shown by a thick soil horizon at the base of the Great Unconformity in Israel (Sandler et al. 2012).

## 7.6 Conclusions

In many ways, the sedimentary and erosional history of the ANS has been ignored in international efforts to reconstruct the causes and events of Neoproterozoic glaciations. In spite of this, the diverse sedimentary environments and contemporary igneous activity combine to make the ANS a potentially excellent place to independently constrain Neoproterozoic climate evolution. There is some evidence for Tonian glaciation in the ANS, including ~770 Ma diamictite deposits on the southern margin of the Bi'r Umq-Nakasib Suture Zone in Sudan (Meritri Group) and Arabia (Mahd Group), but studies focused on these rocks are needed in order to confirm or refute this possibility. The ~717–659 Ma Sturtian glacial episode occurred when the ANS was mostly marine, so evidence for this episode is expected to be preserved in ANS rocks. There is increasing evidence for Sturtian glaciation in the form of diamictites in Egypt, Saudi Arabia, and Ethiopia and Banded Iron Formations of Egypt and Saudi Arabia. We have made good progress in constraining their age and understanding their significance, but further research is needed. There is an especially important opportunity in Sudan, where polymictic conglomerates of the Meritri Group in the Nakasib Suture Zone need to be studied to determine if these are glacigenic and if they are pre-Sturtian or Sturtian deposits.

Evidence for Marinoan and Ediacaran glaciations is less well preserved in the ANS because this was a time that the ANS was rising out of the sea as a result of continent-continent collision and formation of a huge mountain range in the EAO to the south, so erosion dominated over deposition. Consequently, evidence for Marinoan and Ediacaran glacial episodes is less clear. There was certainly glaciation in the high Transgondwanan Supermountains during the Marinoan panglacial episode and other times in the Ediacaran but when and where any of these glaciers reached the ANS is unclear. It is likely that much of the Great Unconformity was cut by multiple episodes of Marinoan and Ediacaran glaciation, including the ~605 Ma Araba Unconformity and ~530 Ma Rum Unconformity. Such evidence might be preserved in Ediacaran basins in the Arabian Shield, but such evidence must be sought for intentionally.

**Acknowledgements** We thank Peter Johnson and Yasser Abd El-Rahman for thoughtful reviews that improved the manuscript.

## References

Abd El-Rahman Y, Gutzmer J, Li X-H, Siefert T, Li C-F, Ling X-X, Li J (2020) Not all Neoproterozoic iron formations are glaciogenic: sturtian-aged non-Rapitan exhalative iron formations from the Arabian-Nubian Shield. Miner Deposita 55:577–596

Abdelsalam MG, Stern RJ (1993) Tectonic evolution of the Nakasib suture, Red Sea Hills, Sudan: evidence for a late Precambrian Wilson Cycle. J Geol Soc London 150:393–404

Abdelsalam MG, Stern RJ (1996) Sutures and shear zones in the Arabian-Nubian shield. J Afr Earth Sc 23:289–310

Abdelsalam MG, Stern RJ, Copeland P, El Faki EM, El Hur B, Ibrahim FM (1998) The Neoproterozoic Keraf Suture in NE Sudan: Sinistral transpression along the eastern margin of West Gondwana. J. Geology 106:133–147

Abdelsalam MG, Abdel-Rahman EM, El-Faki EM, Al-Hur B, El-Bashier FRM, Stern RJ, Thurmond AL (2003) Neoproterozoic deformation in the northeastern part of the Saharan Metacraton, northern Sudan. Precambr Res 123:203–221

Abdo A, Avigad D, Gerdes A, Morag N, Vainer S (2020) Cadomian (ca. 550 Ma) magmatic and thermal imprint on the North Arabian-Nubian Shield (south and central Israel): new age and isotopic constraints. Precambr Res 346:105804

Aftabi A (2001) Introduction of Bandar Abbas iron ore as the newest type of Rapitan banded iron formation. J Min Metall 60–70:53–66 (in Persian with English abstract)

Alene M, Jenkin GRT, Leng MJ, Darbyshire DP (2006) The Tambien Group, Ethiopia: an early Cryogenian (ca. 800–735 Ma) Neoproterozoic sequence in the Arabian-Nubian Shield. Precambr Res 149:79–89

Alessio B, Blades M, Murray G, Thorpe B, Collins AS, Kelsey D, Foden JD, Payne J, Al-Khirbash S, Jourdan F (2017) Origin and tectonic evolution of the NE basement of Oman: a window into the Neoproterozoic accretionary growth of India? Geol Mag 155:1150–1174

Al-Husseini MI (2000) Origin of the Arabian Plate structures: Amar collision and Najd rift. GeoArabia 5:527–542

Al-Husseini MI (2011) Ediacaran-Cambrian middle east geologic time scale 2014—late ediacaran to early Cambrian (Infracambrian) Jibalah Group of Saudi Arabia. GeoArabia 16:69–90

Al-Husseini MI (2014) Ediacaran-Cambrian middle east geologic time scale 2014—proposed correlation of Oman's Abu Mahara Supergroup and Saudi Arabia's Jibalah Group. GeoArabia 19:107–132

Al-Husseini MI (2015) Middle east geologic time scale 2015 Ediacaran and Cambrian Periods. J Middle East Petrol Geosci 20:511–528

Ali KA, Stern RJ, Manton WI, Kimura J-I, Khamees HA (2009) Geochemistry, Nd isotopes and U–Pb SHRIMP zircon dating of Neoproterozoic volcanic rocks from the Central Eastern Desert of Egypt: new insights into the ~750 Ma crust-forming event. Precambr Res 171:1–22

Ali KA, Stern RJ, Manton WI, Johnson PR, Mukherjee SK (2010a) Neoproterozoic diamictite in the Eastern Desert of Egypt and Northern Saudi Arabia: evidence of ~750 Ma glaciation in the Arabian-Nubian Shield. Int J Earth Sci 90:705–726

Ali KA, Stern RJ, Manton WI, Kimura J-I, Whitehouse M, Mukherjee SK, Johnson PR, Griffin WR (2010b) Geochemical, U–Pb zircon and Nd isotopic investigations of the Ghawjah Metavolcanic rocks, Northwestern Saudi Arabia. Lithos 120:379–392

Allen PA (2007) The Huqf Supergroup of Oman: basin development and context for Neoproterozoic glaciation. Earth-Sci Rev 84:139–185

Allen PA, Rieu R, Etienne JL, Matter A, Cozzi A (2011a) The Ayn formation of the Mirbat Group, Dhofar, Oman. In: Arnaud E et al. (eds) The geological record of Neoproterozoic glaciations. Geological Society of London Memoir 36, 239–249

Allen PA, Leather J, Brasier MD, Rieu R, Mccarron M, Le Guerroué E, Etienne JL, Cozzi A (2011b) The Abu Mahara Group (Ghubrah and Fiq formations), Jabal Akhdar, Oman. In: Arnaud E et al. (eds) The geological record of Neoproterozoic glaciations. Geological Society of London Memoir 36, 251–261

Antcliffe J (2013) Questioning the evidence of organic compounds called sponge biomarkers. Paleontology 56:917–925

Arkin Y, Beyth M, Dow DB, Levitte D, Haile T, Hailu T (1971) Geological map of Mekele Sheet area ND37-11 Tigre province. Imperial Ethiopian Government, Ministry of Mines. Geological Survey of Ethiopia. Scale 1:250,000

Asmerom Y, Jacobsen SB, Knoll AH, Butterfield NJ, Swett K (1991) Strontium isotopic variations of Neoproterozoic seawater: implications for crustal evolution. Geochim Cosmochim Acta 55:2883–2894

Asrat A, Barbey P, Ludden JN, Reisberg L, Gleizes G, Ayalew D (2004) Petrology and isotope geochemistry of the Pan-African Negash Pluton, northern Ethiopia: mafic-felsic magma interactions during the construction of shallow-level calc-alkaline plutons. J Petrol 45:1147–1179

Avigad D, Gvirtzman Z (2009) Late Neoproterozoic Arabian—rise and fall of the northern Nubian Shield: the role of lithospheric mantle delamination and subsequent thermal subsidence. Tectonophysics 477:217–228

Avigad D, Kolodner K, McWilliams M, Persing H, Weissbrod T (2003) Origin of northern Gondwana Cambrian sandstone revealed by detrital zircon SHRIMP dating. Geology 31:227–230

Avigad D, Sandler A, Kolodner K, Stern RJ, McWilliams M, Miller N, Beyth M (2005) Mass Cambro production of Ordovician quartz-rich sandstone as a consequence of chemical weathering of Pan-African terranes: environmental implications. Earth Planet Sci Lett 240:818–826

Avigad D, Stern RJ, Beyth M, Miller N, McWilliams M (2007) Detrital zircon U–Pb geochronology of Cryogenian diamictites and lower Palaeozoic sandstone in Ethiopia (Tigrai): age constraints on Neoproterozoic glaciation and crustal evolution of the southern Arabian-Nubian Shield. Precambr Res 154:88–106

Bailo E, Schandelmeier H, Franz G, Sun C-H, Stern RJ (2003) Plutonic and metamorphic rocks from the Keraf Suture (NE Sudan): a glimpse of the tectonic evolution of the NE margin of W. Gondwana during Neoproterozoic time. Precambr Res 123:67–80

Bartley JK, Semikhatov MA, Kaufman AJ, Knoll AH, Pope MC, Jacobsen SB, (2001) Global events across the Mesoproterozoic-Neoproterozoic boundary: C and Sr isotopic evidence from Siberia. Precambr Res 111:165–202

Be'eri-Shlevin Y (2008) The origin and evolution of neoproterzoic magmatism in the northern Arabian-Nubian-Shield (Sinai Peninsula, Egypt, and southern Israel): evidence from the stable and radiogenic isotope record. Thesis (Ph. D.)-Ben-Gurion University of the Negev, Department of Geological and Environmental Sciences, 2008, Beer-Sheva

Bentor YK (1985) The crustal evolution of the Arabo-Nubian massif with special reference to the Sinai peninsula. Precambr Res 28:1–74

Bertrand-Sarfati J, Moussine-Pouchkine A, Amard B, Ait Kaci Ahmed A (1995) First Ediacaran fauna found in Western Africa and evidence for an early Cambrian glaciation. Geology 23:133–136

Beyth M (1972) The geology of central western Tigre, Ethiopia. PhD thesis, Bonn, University of Bonn

Beyth M, Stern RJ, Matthews A (1997) Significance of highgrade metasediments from the Neoproterozoic basement of Eritrea. Precambr Res 86:45–58

Beyth M, Avigad D, Wetzel HU, Matthews A, Berhe SM (2003) Crustal exhumation and indications for snowball Earth in the East African Orogen: North Ethiopia and East Eritrea. Precambr Res 123:187–201

Bibolini A (1920) Risultali preliminary delle osservazioni faite nel Nord-est della Colona Eritrea. Asmara

Bibolini A (1921) Sui conglomerati di Rore Babla e dei Monti Haggar in Colonia Eritrea. Bollettino della Società Geologica Italiana 40:169–176

Bibolini A (1922) Contributions a l'étude de la géologi de l'Afrique orientale Italienne. 13th International Geological Congress (1922, Brussels, Belgium). Title Comptes rendus de la XIIIe session, en Belgique, parts 1–3:797–814

Blasband B, White S, Brooijmans P, de Brooder H, Viser W (2000) Late Proterozoic extensional collapse in Arabian-Nubian Shield. J Geol Soc London 157:615–628

Boger SD, Miller JM (2004) Terminal suturing of Gondwana and the onset of the Ross-Delamerian Orogeny: the cause and effect of an Early Cambrian reconfiguration of plate motions. Earth Planet Sci Lett 219:35–48

Bold U, Smith EF, Rooney AD, Bowring SA, Buchwaldt R, Dudás FÖ, Ramezani J, Crowley JL, Schrag DP, Macdonald FA (2016) Neoproterozoic stratigraphy of the Zavkhan terrane of Mongolia: the backbone for Cryogenian and early Ediacaran chemostratigraphic records. Am J Sci 316:1–63

Bonavia FF, Chorowicz J (1992) Northward expulsion of the Pan-African of northeast Africa guided by a reentrant zone of the Tanzania Craton. Geology 20:1023–1026

Bowring SA, Myrow PM, Landing E, Ramezani J (2003) Geochronological constraints on terminal Neoproterozoic events and the rise of metazoans. Geophys Res Abstr 5(13219):219

Bowring SA, Grotzinger JP, Condon DJ, Ramezani J, Newall MJ, Allen PA (2007) Geochronologic constraints on the chronostratigraphic framework of the Neoproterozoic Huqf Supergroup, Sultanate of Oman. Am J Sci 307:1097–1145

Brasier MD, Shields G, Kuleshov VN, Zhegallo EA (1996) Integrated chemo-and biostratigraphic calibration of early animal evolution: Neoproterozoic-Early Cambrian of southwest Mongolia. Geol Mag 133:445–485

Brasier M, McCarron G, Tucker T, Leather J, Allen P, Shields G (2000) New U–Pb zircon dates for the Neoproterozoic Ghubrah glaciation and for the top of the Huqf Supergroup, Oman. Geology 28:175–178

Burke K, Kraus JU (2000) Deposition of immense Cambro-Ordovician sandstone bodies, now exposed mainly in N. Africa and Arabia, during the aftermath of the final assembly of Gondwana. Geol Soc Am Abstr Program 32:249

Burke K, Sengör C (1986) Tectonic escape in the evolution of continental crust. In: Reflection seismology—the continental crust. Am Geophys Union, Geodynamic series 14:41–53

Burns SJ, Matter A (1993) Carbon isotopic record of the latest Proterozoic from Oman. Eclogae Geol Helv 86:595–607

Bussert R (2010) Exhumed erosional landforms of the Late Palaeozoic glaciation in northern Ethiopia: indicators of ice-flow direction, palaeolandscape and regional ice dynamics. Gondwana Res 18:356–369

Butterfield NJ (2015) The neoproterozoic. Curr Biol 25:R859–R863

Caby R, Fabre J (1981) Late proterozoic to early palaeozoic diamictites, tillites and associated glacigenic sediments in the Série Pourprée of western Hoggar, Algeria. In: Harland WB, Hambrey MJ (eds) Earth's pre-pleistocene glacial record, pp 140–145. Cambridge University Press

Calvez JY, Kemp J (1982) Geochronological investigations in the Mahd Adh Dhahab Quadrangle, Central Arabian Shield. Deputy Ministry for Mineral Resources: Jiddah, Saudi Arabia, BRGM-TR-02-5, pp 1–41

Canfield DE (2005) The early history of atmospheric oxygen: homage to Robert M. Garrels. Annu Rev Earth Planet Sci 33:1–36

Canfield DE, Poulton SW, Narbonne GM (2007) Late-neoproterozoic deep-ocean oxygenation and the rise of animal life. Science 315:92–95

Canfield DE, Poulton SW, Knoll AH, Narbonne GM, Ross G, Goldberg T, Strauss H (2008) Ferruginous Conditions dominated later neoproterozoic deep-water chemistry. Science 321:949–952

Canfield DE, Knoll AH, Poulton SW, Narbonne GM, Dunning GR (2020) Carbon isotopes in clastic rocks and the Neoproterozoic carbon cycle. Am J Sci 320:97–124

Cawood PA (2005) Terra Australis Orogen: rodinia breakup and development of the Pacific and Iapetus margins of Gondwana during the Neoproterozoic and Paleozoic. Earth Sci Rev 69:249–279

Cecioni G (1981) Precambrian pebbly mudstones in Eritrea, northeastern Ethiopia. In: Hambrey MJ, Harland WB (eds) Earth's pre-pleistocene glacial record. Cambridge University Press, A24, 150

Cohen KM, Finney SC, Gibbard PL, Fan J-X (2013) updated 2015. The ICS international chronostratigraphic chart. Episodes 36:199–204

Cohen PA, Strauss JV, Rooney AD, Sharma M, Tosca N (2017) Controlled hydroxyapatite biomineralization in an ~810 million-year-old unicellular eukaryote. Sci Adv 3:

Cole JC (1988) Geology of the Aban Al Ahmar Quadrangle, Sheet 25F, Kingdom of Saudi Arabia (explanatory notes). Deputy Ministry for Mineral Resources Map GM-105A, C

Collins AS, Pisarevsky SA (2005) Amalgamating eastern Gondwana: the evolution of the circum-Indian Orogens. Earth-Sci Rev 71:229–270

Collins AS, Windley BF (2002) The tectonic evolution of central and northern Madagascar and its place in the final assembly of Gondwana. J Geol 110:325–339

Condon D, Zhu M, Bowring S, Wang W, Yang A, Jin Y (2005) U-Pb ages from the Neoproterozoic Doushantuo Formation, China. Science 308:95–98

Cosca MA, Shimron A, Caby R (1999) Late Precambrian metamorphism and cooling in the Arabian-Nubian Shield: petrology and $^{40}Ar/^{39}Ar$ geochronology of metamorphic rocks of the Elat area (southern Israel). Precambr Res 98:107–127

Cox GM, Lewis CJ, Collins AS, Halverson GP, Jourdan F, Foden J, Nettle D, Kattan F (2012) Ediacaran terrane accretion within the Arabian-Nubian Shield. Gondwana Res 21:341–352

Cox GM, Halverson GP, Minarik WG, Le Heron DP, Macdonald FA, Bellefroid EJ, Strauss JV (2013) Neoproterozoic iron formation: an evaluation of its temporal, environmental and tectonic significance. Chem Geol 362:232–249

Cox GM, Halverson GP, Stevenson RK, Vokaty M, Poirier A, Kunzmann M, Li Z-X, Denyszyn SW, Strauss JV, Macdonald FA (2016) Continental flood basalt weathering as a trigger for Neoproterozoic Snowball Earth. Earth Planet Sci Lett 446:89–99

Cox GM, Foden J, Collins AS (2018) Late Neoproterozoic adakitic magmatism of the eastern Arabian Nubian Shield. Geosci Front 10:1981–1992

Cui H, Kaufman AJ, Zou H, Kattan FH, Trusler P, Smith J, Ivantsov A, Rich TH, Al Qubsani A, Yazedi A, Liu X-M, Johnson P, Goderis S, Claeys P, Vickers-Rich P (2020) Primary or secondary? A dichotomy of the strontium isotope anomalies in the Ediacaran carbonates of Saudi Arabia. Precambr Res 343:

Dabbagh ME, Rogers JJW (1983) Depositional environments and tectonic significance of the Wajid Sandstone of southern Saudi Arabia. J Afr Earth Sci 1:47–57

Dalziel IWD (1997) Neoproterozoic-paleozoic geography and tectonics: review, hypothesis, environmental speculation. Geol Soc Am Bull 109:16–42

Davies FB (1985) Explanatory notes to the geologic map of the Al Wajh Quadrangle, Kingdom of Saudi Arabia. Geoscience Map GM-83, scale 1:250,000, sheet 26B. Deputy Ministry for Mineral Resources, Ministry of Petroleum and Mineral Resources, Kingdom of Saudi Arabia, p 27

Davies J, Nairn AEM, Ressetar R (1980) The palaeomagnetism of certain late Precambrian and early Palaeozoic rocks from the Red Sea Hills, eastern desert, Egypt. J Geophys Res 85:3699–3710

De Souza Filho CR, Drury SA (1998) A Neoproterozoic supra-subduction terrane in northern Eritrea, NE Africa. J Geol Soc London 155:551–566

Delfour J (1970) Le Groupe de J'Balah, une nouvelle unite du Bouclier Arabe. Bureau de Recherche Geologique et Minieres Bulletin 4:19–32

Denèle Y, Leroy S, Pelleter E, Pik R, Talbot JY, Kahanbari K (2012) The Cryogenian juvenile Arc formation and successive high-K calc-alkaline plutons intrusion of Socotra Island Yemen. Arab J Geosci 5:903–924

Deynoux M, Affaton P, Trompette R, Villeneuve M (2006) Pan-African tectonic evolution and glacial events registered in Neoproterozoic to Cambrian cratonic and foreland basins of West Africa. J Afr Earth Sc 46:397–426

Dohrmann M, Wörheide G (2019) Dating early animal evolution using phylogenomic data. Nat Sci Reports 7:3599

Donnadieu Y, Goddéris Y, Ramstein G, Nédélec A, Meert J (2004) A 'snowball Earth' climate triggered by continental break-up through changes in runoff. Nature 428:303–306

Dor YB, Harlavan Y, Avigad D (2018) Provenance of the great Cambrian sandstone succession of northern Gondwana unraveled by strontium, neodymium and lead isotopes of feldspars and clays. Sedimentology 65:2595–2620

Drury SA, Berhe SM (1993) Accretion tectonics in northern Eritrea revealed by remotely sensed imagery. Geol Mag 130:177–190

El-Shazly AK, Khalil KI (2016) Metamorphic and geochronologic constraints on the tectonic evolution of the Central Eastern Desert of Egypt. Precambr Res 283:144–168

El-Shazly AK, Khalil KI, Helba HA (2019) Geochemistry of banded iron formations and their host rocks from the Central Eastern Desert of Egypt: a working genetic model and tectonic implications. Precambr Res 325:192–216

Ernst RE, Wingate MTD, Buchan KL, Li ZX (2008) Global record of 1600–700 Ma Large Igneous Provinces (LIPs): implications for the reconstruction of the proposed Nuna (Columbia) and Rodinia supercontinents. Precambr Res 160:59–178

Etemad-Saeed N, Hosseini-Barzi M, Adabi M, Miller NR, Sadeghi A, Stockli Houshmandzadeh DF (2016) Evidence for ~560 Ma Ediacaran glaciation in the Kahar Formation, Central Alborz Mountains, northern Iran. Gondwana Res 31:164–183

Evans D (2000) Stratigraphic, geochronological, and paleomagnetic-constraints upon the Neoproterozoic climatic paradox. Am J Sci 300:347–433

Evans D, Raub TD (2011) Neoproterozoic glacial palaeolatitudes: a global update. In: Arnaud E, Halverson GP, Shields-Shou G (eds) The geological record of Neoproterozoic glaciations. Geological Society of London, London, pp 93–112

Eyal M, Be'eri-Shlevin Y, Eyal Y, Whitehouse MJ, Litvinovsky B (2014) Three successive proterozoic island arcs in the northern arabian–nubian shield: evidence from SIMS U–Pb dating of zircon. Gondwana Res 25:338–357

Fairchild IJ, Spiro B, Herrington PM (2000) Controls on Sr and C isotope compositions of Neoproterozoic Sr-rich limestones of East Greenland and North China. In: Grotzinger JP, James NP (eds) Carbonate sedimentation and diagenesis in an evolving precambrian world, SEPM Special Publication vol 67, pp 297–313

Fairchild IJ, Spencer T, Ali D, Anderson R, Anderton R, Boomer I, Dove D, Evans J, Hambrey M, Howe J, Sawaki Y, Wang Z, Shields G, Zhou Y, Skelton A, Tucker M (2018) Tonian-Cryogenian boundary sections of Argyll, Scotland. Precambr Res 319:37–64

Feulner G (2012) The faint young Sun problem. Rev Geophys 50:364–370

Fike DA, Grotzinger JP, Pratt LM, Summons RE (2006) Oxidation of the Ediacaran Ocean. Nature 444:744–747

Fitzsimons ICW (2000) Grenville-age basement provinces in east Antarctica: evidence for three separate collisional orogens. Geology 28:879–882

Fowler A, Hassen I, Hassan M (2015) Tectonic evolution and setting of the Sa'al Complex, southern Sinai, Egypt: a Proterozoic continental back-arc rift model. J Afr Earth Sci 104:103–131

Fritz H, Abdelsalam M, Ali KA, Bingen B, Collins AS, Fowler AR, Ghebreab W, Hauzenberger CA, Johnson PR, Kusky TM, Macey P, Muhongo S, Stern RJ, Viola G (2013) Orogen styles in the East African Orogen: a review of the Neoproterozoic to Cambrian tectonic evolution. J Afr Earth Sci 86:65–106

Gad S, Kusky T (2007) ASTER spectral ratioing for lithological mapping in the Arabian-Nubian shield, the Neoproterozoic Wadi Kid area, Sinai, Egypt. Gondwana Res 11:326–335

Garfunkel Z (1999) History and paleogeography during the Pan-African orogen to stable platform transition: reappraisal of the evidence from the Elat area and the northern Arabian-Nubian Shield. Israel J Earth Sci 48:135–157

Garland CR (1980) Geology of the Adigrat area. Ministry of Mines Memoir No. 1, p 51. Addis Ababa 1:250,000 map

Gernon TM, Hincs TK, Tyrrell T, Rohling EJ, Palmer MR (2016) Snowball Earth ocean chemistry driven by extensive ridge volcanism during Rodinia breakup. Nat Geosci 9:242–248

Ghebreab W (1999) Tectono-metamorphic history of Neoproterozoic rocks in eastern Eritrea. Precambr Res 98:83–105

Glennie KW, Boeuf MGA, Hughes-Clarke MW, Moody-Stuart M, Pilaar WFH, Reinhardt BM (1974) Geology of the Oman mountains. Verhandelingen van het Koninklijk Nederlands geologisch mijnbouwkundig Genootschap 31:423

Goddéris Y, Donnadieu Y, Nédélec A, Dupré B, Dessert C, Grard A, Ramstein G, François LM (2003) The Sturtian "snowball" glaciation: fire and ice. Earth Planet Sci Lett 211:1–12

Gong Z, Kodama KP, Li YX (2017) Rock magnetic cyclostratigraphy of the Doushantuo Formation, South China and its implications for the duration of the Shuram carbon isotope excursion. Precambr Res 289:62–74

Gostin VA, McKirdy DM, Webster LJ, Williams GE (2010) Ediacaran ice-rafting and coeval asteroid impact, South Australia: insights into the terminal Proterozoic environment. Aust J Earth Sci 57:859–869

Gray DR, Foster DA, Meert JG, Goscombe BD, Armstrong R, Truow RAJ, Passchier CW (2008) A Damaran perspective on the assembly of southwestern Gondwana. Geol Soc London, Special Publications 294:257–278

Grotzinger JP, Fike DA, Fischer WW (2011) Enigmatic origin of the largest-known carbon isotope excursion in Earth's history. Nat Geosci 4:285–292

Guilbaud R, Poulton SW, Butterfield NJ, Zhu M, Shields-Zhou GA (2015) A global transition to ferruginous conditions in the early Neoproterozoic oceans. Nat Geosci 8:466–470

Hadley DG (1974) The taphrogeosynclinal Jubaylah Group in the Mashhad area, northwestern Hijaz. Saudi Arabian Directorate General of Mineral Resources Bulletin 10, p 18

Hadley DG (1986) Explanatory notes to the geologic map of the Sahl Al Matran Quadrangle, Kingdom of Saudi Arabia. Geoscience Map GM-86 C, scale 1:250,000, sheet 26C. Deputy Ministry for Mineral Resources, Ministry of Petroleum and Mineral Resources, Kingdom of Saudi Arabia. p 24

Hailu T (1975) Geological map of Adi Arkay. Adis Ababa, Geological Survey of Ethiopia Technical Report, scale 1:250,000

Halverson GP (2006) A Neoproterozoic chronology. In: Xiao S, Kaufman AJ (eds) Neoproterozoic geobiology and paleobiology: dordrecht. Springer, Netherlands, pp 231–271

Halverson GP, Hoffman PF, Schrage DP, Maloof AC, Rice AHN (2005) Toward a Neoproterozoic composite carbon-isotope record. Geol Soc Am Bull 117:1181–1207

Halverson GP, Dudás FÖ, Maloof AC, Bowring SA (2007a) Evolution of the 87Sr/86Sr composition of Neoproterozoic seawater. Palaeogeogr Palaeoclimatol Palaeoecol 256:103–129

Halverson GP, Maloof AC, Schrag DP, Dudás FÖ, Hurtgen M (2007b) Stratigraphy and geochemistry of a ca 800 Ma negative carbon isotope interval in northeastern Svalbard. Chem Geol 237:5–27

Halverson GP, Cox GM, Théou-Hubert L, Schmitz M, Hagadorn JW, Johnson P, Sansjofre P, Kunzmann M, Schumann D (2013) A multi-proxy geochemical record from a late Neoproterozoic volcano-sedimentary basin, eastern Arabian Shield. McGill University, Canada, unpublished poster

Halverson GP, Porter SM, Gibson TM (2018) Dating the late Proterozoic stratigraphic record. Emerg Top Life Sci 2:137–147

Hargrove US (2006a) Crustal evolution of the Neoproterozoic Bi'r Umq suture zone, Kingdom of Saudi Arabia. Geochronological, Isotopic, and Geochemical Constraints. Ph.D. Thesis, University of Texas, Dallas, TX, USA

Hargrove US, Stern RJ, Kimura J-I, Manton WI, Johnson PR (2006) How juvenile if the Arabian-Nubian Shield? Evidence from Nd isotopes and pre-Neoproterozoic inherited zircon in the Bi'r Umq suture zone, Saudi Arabia. Earth Planet Sci Lett 252:308–326

Harland WB (1964) Evidence of late Precambrian glaciation and its significance. In: Nairn AEM (ed) Problems in palaeoclimatology. Interscience, London, pp 119–149

Hassanlouei BT, Rajabzadeh MA (2019) Iron ore deposits associated with Hormuz evaporitic series in Hormuz and Pohl salt diapirs, Hormuzgan province, southern Iran. J Asian Earth Sci 172:30–55

Hebert CL, Kaufman AJ, Penniston-Dorland SC, Martin AJ (2010) Radiometric and stratigraphic constraints on terminal Ediacaran (post-Gaskiers) glaciation and metazoan evolution. Precambr Res 182:402–412

Hedge CE (1984) Precambrian geochronology of part of northwestern Saudi Arabia, Kingdom of Saudi Arabia. US Geological Survey Open File Report 83–381, p 12

Helmy HM, Morad AE, Abdel Rahman HB (2021) Um Zariq formation, southeast sinai, Egypt: a new record of the Sturtian Snowball Earth event in the Arabian Nubian Shield. J Afr Earth Sc 173:

Hill AC, Arouri K, Gorjan P, Walter MR (2000) Geochemistry of marine and nonmarine environments of a Neoproterozoic cratonic carbonate/evaporite: the Bitter Springs Formation, Central Australia. In: Grotzinger JP, James NP (eds) Carbonate sedimentation and diagenesis in the evolving precambrian world. SEPM, 327–344 (Spec. Pub. 67)

Hoffman PF (1999) The break-up of Rodinia, birth of Gondwana, true polar wander and the snowball earth. J Afr Earth Sci 29:17–33

Hoffman PF (2013) The great oxidation and a Siderian snowball Earth: MIF-S based correlation of Paleoproterozoic glacial epochs. Chem Geol 362:143–156

Hoffman PF, Schrag DP (2002) The snowball Earth hypothesis: testing the limits of global change. Terra Nova 14:129–155

Hoffman PF, Kaufman AJ, Halverson GP, Schrag DP (1998) A Neoproterozoic snowball earth. Science 281:1342–1346

Hoffman PF, Halverson GP, Domack EW, Husson JM, Higgins JA, Schrag DP (2007) Are basal Ediacaran (635 Ma) post-glacial "cap dolostones" diachronous? Earth Planet. Sci Lett 258:114–131

Hoffman PF, Abbot DS, Ashkenazy Y, Benn DI, Brocks JJ, Cohen PA, Cox GM, Creveling JR, Donnadieu Y, Erwin DH, Fairchild IJ, Ferreira D, Goodman JC, Halverson GP, Jansen MF, Le Hir G, Love GD, Macdonald FA, Maloof AC, Partin CA, Ramstein G, Rose BEJ, Sadler PM, Tziperman E, Voigt A, Warren SG (2017) Snowball earth climate dynamics and cryogenian geology-geobiology. Sci Adv 3:e1600983

Horton F (2015) Did phosphorus derived from the weathering of large igneous provinces fertilize the Neoproterozoic ocean? Geochem Geophys Geosystems 1:1723–1738

Husson JM, Maloof AC, Schoene B, Chen CY, Higgins JA (2015) Stratigraphic expression of Earth's deepest $\delta^{13}C$ excursion in the Wonoka Formation of South Australia. Am J Sci 315:1–45

Hyde WT, Crowley TJ, Baum SK, Peltier WR (2000) Neoproterozoic 'Snowball Earth' simulations with a coupled climate/icesheet model. Nature 405:425–429

Jacobs J, Thomas RJ (2004) Himalayan-type indenter-escape tectonics model for the southern part of the late Neoproterozoic-early Paleozoic East African-Antarctic orogen. Geology 32:721–724

Jacobs J, Bauer W, Fanning CM (2003) Late Neoproterozoic/Early Palaeozoic events in central Dronning Maud Land and significance for the southern extension of the East African Orogen into East Antarctica. Precambr Res 126:27–53

Jarrar GH, Wachendorf H, Zellmer D (1991) The Saramuj Conglomerate: evolution of a Pan-African molasse sequence from southwest Jordan. N Jb Geol Palaontol Mh 6:335–356

Jarrar GH, Wachendorf H, Zachmann D (1993) A Pan-African alkaline pluton intruding the Saramuj Conglomerate, southwest Jordan. Geol Rundschau 82:121–135

Javoy M, Pineau F, Delorme H (1986) Carbon and nitrogen isotopes in the mantle. Chem Geol 57:41–62

Johnson PR (1995) Proterozoic geology of Western Saudi Arabia—North-Central Sheet: explanatory notes on precambrian stratigraphic relations. Saudi Arabian Deputy Ministry for Mineral Resources, Jiddah, Saudi Arabia, USGS-OF-95-5, pp 1–44

Johnson PR (2003) Post-amalgamation basins of the NE Arabian shield and implications for Neoproterozoic III tectonism in the northern East African Orogen. Precambr Res 123:321–337

Johnson PR (2014) An expanding Arabian-Nubian Shield geochronologic and isotopic dataset: defining limits and confirming the tectonic setting of a Neoproterozoic accretionary orogen. Open Geol J 8:3–33

Johnson P, Kattan F (2008) Lithostratigraphic revision in the Arabian Shield: the impacts of geochronology and tectonic analysis. Arab J Sci Eng 33:3–16

Johnson PR, Kattan FH (2012) The geology of the Saudi Arabian Shield. Saudi Geological Survey, Jiddah, Saudi Arabia, pp 1–479

Johnson PR, Stewart ICF (1995) Magnetically inferred basement structure in central Saudi Arabia. Tectonophysics 245:37–52

Johnson PR, Woldehaimanot B (2003) Development of the Arabian-Nubian Shield: perspectives on accretion and deformation in the northern East African Orogen and the assembly of Gondwana. In: Yoshida M, Windley BF, Dasgupta S (eds) Proterozoic East Gondwana: supercontinent assembly and breakup, Geological Society, London, Spec. Pub. 206, pp 289–325

Johnson PR, Abdelsalam MG, Stern RJ (2003) The Bi'r Umq-Nakasib Suture Zone in the Arabian-Nubian Shield: a key to understanding crustal growth in the East African Orogen. Gondwana Res 6:523–530

Johnson PR, Andresen A, Collins AS, Fowler AR, Fritz H, Ghebreab W, Kusky T, Stern RJ (2011) Late cryogenian-ediacaran history of the Arabian-Nubian Shield: a review of depositional, plutonic, structural, and tectonic events in the closing stages of the northern East African Orogen. J Afr Earth Sci 61:167–232

Johnson PR, Halverson GP, Kusky TM, Stern RJ, Pease V (2013) Volcanosedimentary Basins in the Arabian-Nubian Shield: markers of repeated exhumation and denudation in a neoproterozoic accretionary orogen. Geosciences 3:389–445

Jones DS, Maloof AC, Hurtgen MT, Rainbird RH, Schrag DP (2010) Regional and global chemostratigraphic correlation of the early Neoproterozoic Shaler Supergroup, Victoria Island, Northwestern Canada. Precambr Res 181:43–63

Kaufman AJ, Jacobsen SB, Knoll AH (1993) TheVendian record of Sr and C isotopic variations in seawater: implications for tectonics and paleoclimate. Earth Planet Sci Lett 84:27–41

Kaufman AJ, Knoll AH, Narbonne GM (1997) Isotopes, ice ages, and terminal Proterozoic earth history. Proc Natl Acad Sci USA 94:6600–6605

Keller CB, Husson JM, Mitchell RN, Bottke WF, Gernon TM, Boehnke P, Bell EA, Swanson-Hysell NL, Peters SE (2020) Neoproterozoic glacial origin of the Great Unconformity. Proc Nat Academy Sci 116:1136–1145

Kemp J (1981) Geologic map of the Wadi Al Ays Quadrangle, Sheet 25C, Kingdom of Saudi Arabia, Saudi Arabian Deputy Ministry for Mineral Resources: Jiddah, Saudi Arabia, GM 53, pp 1–39

Kemp J, Gros Y, Prian JP (1982) Geologic Map of the Mahd adh Dhahab Quadrangle, Sheet 23E, Kingdom of Saudi Arabia, Saudi Arabian Deputy Ministry for Mineral Resources: Jiddah, Saudi Arabia, GM 64, pp 1–39

Kempf O, Kellerhals P, Lowrie W, Matter A (2000) Palaeomagnetic directions in late Precambrian glaciomarine sediments of the Mirbat Sandstone Formation, Oman. Earth Planet Sci Lett 175:181–190

Kennedy A, Johnson PR, Kattan FH (2004) SHRIMP geochronology in the Northern Arabian Shield Part I: data acquisition; Saudi geological survey: Jiddah, Saudi Arabia, SGS-OF-2004-11, pp 1–28

Kennedy A, Johnson PR, Kattan FH (2005) SHRIMP geochronology in the Northern Arabian Shield Part II: data acquisition 2004, Saudi Geological Survey: Jiddah, Saudi Arabia, SGS-OF-2005–10, pp 1–44

Kennedy A, Kozdroj W, Kattan FH, Ziolkowska-Kozdroj M, Johnson PR (2010a) SHRIMP Geochronology in the Arabian Shield (Midyan Terrane, Afif Terrane, Ad Dawadi Terrane) and Nubian Shield (Central Eastern Desert Terrane) Part IV: data acquisition 2008; Saudi Geological Survey: Jiddah, Saudi Arabia; SGS-OF-2010-10, pp 1–101

Kennedy A, Kozdroj W, Kadi K, Ziolkowska-Kozdroj M, Johnson PR (2010b) SHRIMP geochronology of the Arabian Shield (Midyan Terrane, Afif Terrane) and Nubian Shield (Central Eastern Desert Terrane), Part V: data acquisition 2009; Saudi Geological Survey, Jiddah, Saudi Arabia, SGS-OF-2010-11, p 80

Kidane T, Bachtadse V, Alene M (2014) Quaternary remagnetization of the Neoproterozoic limestone of Negash Synclinorium (Arabian–Nubian Shield, northern Ethiopia): With implications of no paleomagnetic testing for the proposed Snowball Earth events. Phys Earth Planet Inter 235:1–12

Kilner B, Conall MN, Brasier M (2005) Low-latitude glaciation in the Neoproterozoic of Oman. Geology 33:413–416

Kirschvink JL (1992) Late Proterozoic low-latitude global glaciation: the snowball Earth. In: Schopf JW, Klein C (eds) The Proterozoic biosphere—a multidisciplinary study. Cambridge University Press, Cambridge, pp 51–52

Kiyokawa S, Suzuki T, El-Dokouny HA, Dawoud M, Abuelhasan AA (2020) Stratigraphy, petrology, and geochemistry of a Neoproterozoic banded iron sequence in the El-Dabbah Group, central Eastern Desert, Egypt. J Afr Earth Sc 168:

Klaebe RM, Smith MP, Fairchild IJ, Fleming EJ, Kennedy MJ (2018) Facies-dependent $d^{13}C$ variation and diagenetic overprinting at the onset of the Sturtian glaciation in north-east Greenland. Precambr Res 319:96–113

Knoll AH, Walter MR, Narbonne GM, Christie-Blick N (2004) The Ediacaran Period: a new addition to the geologic time scale. Lethaia 39:13–30

Knoll AH, Walter MR, Narbonne GM, Christie-Blick N (2006) A new period the geologic time scale. Science 205:621–622

Kröner A (2001) The mozambique belt of East Africa and madagascar: significance of zircon and Nd model ages for Rodinia and Gondwana supercontinent formation and dispersal. S Afr J Geol 104:151–166

Kröner A, Muhongo S, Hegner E, Wingate MTD (2003) Single zircon geochronology and Nd isotopic systematics of Proterozoic high-grade rocks from the Mozambique belt of southern Tanzania (Masasi area): implications for Gondwana assembly. J Geol Soc London 160:645–757

Kusky TM, Matsah MI (2003) Neoproterozoic dextral faulting on the Najd fault system, Saudi Arabia, preceded sinistral faulting and escape tectonics related to closure of the Mozambique Ocean. Geol Soc Spec Publ 206:327–361

Küster D, Liégeois J-P, Matukov D, Sergeev S, Lucassen F (2008) Zircon geochronology and Sr, Nd, Pb isotope geochemistry of granitoids from Bayuda Desert and Sabaloka (Sudan): evidence for a Bayudian event (920–900 Ma) preceding the Pan-African orogenic cycle (860–590 Ma) at the eastern boundary of the Saharan Metacraton. Precambr Res 164:16–39

Kuznetsov AB, Semikhatov MA, Maslov AV, Gorokhov IM, Prasolov EM, Krupenin MT, Kislova IV (2006) New data on Sr-and C-isotopic chemostratigraphy of the Upper Riphean type section (Southern Urals). Stratigr Geol Correl 14:602–628

Le Guerroué E (2010) Duration and synchroneity of the largest negative carbon isotope excursion on Earth: the Shuram/Wonoka anomaly. CR Geosci 342:204–214

Letalenet J (1979) Explanatory notes to the geologic map of the 'Afif Quadrangle, Kingdom of Saudi Arabia. Geoscience Map GM-47C, scale 1:250,000, sheet 23F. Deputy Ministry for Mineral Resources, Ministry of Petroleum and Mineral Resources, Kingdom of Saudi Arabia, p 20

Li ZX, Bogdanova SV, Collins AS, Davidson A et al (2008) Assembly configuration and break-up history of Rodinia: a synthesis. Precambr Res 160:179–210

Li Z-X, Evans DAD, Halverson GP (2013) Neoproterozoic glaciations in a revised global palaeogeography from the breakup of Rodinia to the assembly of Gondwanaland. Sed Geol 294:219–232

Li X-H, Abd El-Rahman Y, Abu Anbar M, Li J, Ling X-X, Wu L-G, Masoud AE (2018) Old continental crust underlying juvenile oceanic arc: evidence from northern Arabian-Nubian Shield, Egypt. Geophys Res Lett 45:3001–3008

Linneman U, Pidal AP, Hofmann M, Drost K, Quesada C, Gerdes A, Marko L, Gärtner A, Zieger J, Ulrich J, Krause R, Vickers-Rich P, Horak J (2018) A ~565 Ma old glaciation in the Ediacaran of peri-Gondwanan West Africa. Int J Earth Sci https://doi.org/10.1007/s00531-017-1520-7

Liu Y, Peltier WR (2013) Sea level variations during snowball Earth formation: 1. A preliminary analysis. J Geophys Res 118:4410–4434

Love GD, Grosjean E, Stalvies C, Fike DA, Grotzinger JP, Bradley AS, Kelly AE, Bhatia M, Bowring SA, Condon DJ, Summons RE (2009) Fossil steroids record the appearance of demospongiae during the cryogenian. Nature 457:718–722

Macdonald FA, Schmitz MD, Crowley JL, Roots CF, Jones DS, Maloof AC, Strauss JV, Cohen PA, Johnston DT, Schrag DP (2010a) Calibrating the cryogenian. Science 327:1241–1243

Macdonald FA, Strauss JV, Rose CV, Dudas F, Schrag DP (2010b) Stratigraphy of the port Nolloth Group of Namibia and South Africa and implications for the age of neoproterozoic iron formations. Am J Sci 310:862–888

MacLennan SA, Park Y, Swanson-Hysell NL, Maloof AC, Schoene B, Gebreslassie M, Antilla E, Tesema T, Alene M, Haileab B (2018) The arc of the Snowball: U–Pb dates constrain the Islay anomaly and the initiation of the Sturtian glaciation. Geology 46:539–542

Maloof AC, Schrag DP, Crowley JL, Bowring SA (2005) An expanded record of early Cambrian carbon cycling from the Anti-Atlas Margin, Morocco. Can J Earth Sci 42:2195–2216

Maloof AC, Halverson GP, Kirschvink JL, Schrag DP, Weiss BP, Hoffman PF (2006) Combined paleomagnetic, isotopic, and stratigraphic evidence for true polar wander from the Neoproterozoic Akademikerbreen Group, Svalbard, Norway. GSA Bulletin 118:1024–1099

Master S, Wendorff M (2011) Neoproterozoic glaciogenic diamictites of the Katanga Supergroup, Central Africa. In: Arnaud E et al (eds) The geological record of neoproterozoic glaciations. Geol Soc London Memoir 36:173–183

McCaffrey MA, Moldowan JM, Lipton PA, Summons RE, Peters KE, Jeganathan A, Watt DS (1994) Paleoenvironmental implications of novel C30 steranes in Precambrian to Cenozoic age petroleum and bitumen. Geochimica et Cosmochimica Acta 58:529–532

Meert J (2003) A synopsis of events related to the assembly of eastern Gondwana. Tectonophysics 362:1–40

Meert JG, Lieberman BS (2008) The Neoproterozoic assembly of Gondwana and its relationship to the Ediacaran-Cambrian radiation. Gondwana Res 14:5–21

Meert JG, Van Der Voo R (1997) The assembly of Gondwana 800–550 Ma. J Geodyn 23:223–235

Miller NR, Alene M, Sacchi R, Stern R, Conti A, Kröner A, Zuppi G (2003) Significance of the Tambien Group (Tigre, N. Ethiopia) for snowball Earth events in the Arabian-Nubian Shield. Precambr Res 121:263–283

Miller N, Schilman B, Avigad D, Stern RJ, Beyth M (2006) Neoproterozoic Snowball Earth—the northern Ethiopia record. Abstract presented in the "Snowball Earth 2006" conference, Monte Verita, Switzerland, pp 74–75

Miller N, Johnson P, Stern R (2008) Marine versus non-marine environments for the Jibalah Group, NW Arabian Shield: a sedimentological and geochemical survey and report of possible Metazoa in the Dhaiqa Formation. Arab J Sci Eng 22:55–77

Miller NR, Stern RJ, Avigad D, Beyth M, Schilman B (2009) Neoproterozoic carbonate-slate sequences of the Tambien Group, N. Ethiopia (I): pre-'Sturtian' chemostratigraphy and regional correlation. Precambr Res 170:129–156

Miller NR, Avigad D, Stern RJ, Beyth M (2011) The Tambien Group, northern Ethiopia (Tigre). In: Arnaud E et al (eds) The geological record of Neoproterozoic glaciations. Geol Soc London Memoir 36:263–276

Moghazi A-KM, Ali KA, Wilde SA, Zhou Q, Andersen T, Andresen A, El-Enen MMA, Stern RJ (2012) Geochemistry, geochronology, and Sr–Nd isotopes of the Late Neoproterozoic Wadi Kid volcano-sedimentary rocks, Southern Sinai, Egypt: implications for tectonic setting and crustal evolution. Lithos 154:147–165

Morag N, Avigad D, Gerdes A, Belousova E, Harlavan Y (2011a) Crustal evolution and recycling in the northern Arabian-Nubian Shield: new perspectives from zircon Lu–Hf and U–Pb systematics. Precambr Res 186:101–116

Morag N, Avigad D, Gerdes A, Belousova E, Harlavan Y (2011b) Detrital zircon Hf isotopic composition indicates long-distance transport of North Gondwana Cambrian-Ordovician sandstones. Geology 39:955–958

Nairn AEM, Perry TA, Ressetar R, Rogers S (1987) A palaeomagnetic study of the Dokhan volcanic formation and younger granites, eastern desert of Egypt. J Afr Earth Sc 6:353–365

Nettle D (2009) A sequence stratigraphic, geochronological and chemostratigraphic investigation of the Ediacaran Antaq Basin,

Eastern Arabian Shield, Saudi Arabia. Unpublished Honours Thesis, Geology and Geophysics, University of Adelaide, Australia; Saudi Geological Survey Technical Report SGSTR-2010-5, p 83
Nettle D, Halverson GP, Cox GM, Collins AS, Schmitz M, Gehling J, Johnson PR, Kadi K (2013) A middle-late Ediacaran volcano-sedimentary record from the Eastern Arabian-Nubian Shield. Terra Nova 26:120–129
Newman MJ, Rood RT (1977) Implications of solar evolution for the Earth's early atmosphere. Science 198:1035–1037
Nicholson PG, Janjou DLA, Fanning CM, Heaman LM, Grotzinger JP (2008) Deposition, age, and Pan-Arabian correlation of late Neoproterozoic outcrops in Saudi Arabia (abstract), 8th Middle East Geoscience Conference and exhibition, GEO 2008, Manama, Bahrain AAPG Search and Discovery Magazine, article 90077
Och LM, Shields-Zhou GA (2012) The Neoproterozoic oxygenation event: environmental perturbations and biogeochemical cycling. Earth Sci Rev 110:26–57
Pallister JS, Stacey JS, Fischer LB, Premo WR (1988) Precambrian ophiolites of Arabia: geologic settings, U–Pb geochronology, Pb-isotope characteristics, and implications for continental accretion. Precambr Res 38:1–54
Park U, Swanson-Hysell NL, MacLennan SA, Maloof AC, Gebreslassie M, Tremblay MM, Schoene B, Alene M, Anttila ESC, Tesema T, Haileab B (2019) The lead-up to the Sturtian Snowball Earth: neoprotoerozoic chemostratigraphy time-calibrated by the Tambien Group of Ethiopia. GSA Bulletin 132:1119–1149
Patchett PJ, Chase CG (2002) Role of transform continental margins in major crustal growth episodes. Geology 30:39–42
Pellaton C (1979) Geologic map of the Yanbu'al Bahr Quadrangle, Sheet 24C, Kingdom of Saudi Arabia. Saudi Arabian Directorate General of Mineral Resources, Jiddah, Saudi Arabia
Pisarevsky SA, Murphy JB, Cawood PA, Collins AS (2008) Late Neoproterozoic and early Cambrian palaeogeography: models and problems. Geol Soc, London 294:9–31 Special Publications
Pisarevsky SA, McCausland PJ, Hodych JP, O'Brien SJ, Tait JA, Murphy JB, Colpron M (2011) Paleomagnetic study of the late Neoproterozoic Bull Arm and Crown Hill formations (Musgravetown Group) of eastern Newfoundland: Implications for Avalonia and West Gondwana paleogeography. Can J Earth Sci 49:308–327
Planavsky NJ, Reinhard CT, Wang X, Thomson D, McGoldrick P, Rainbird RH, Johnson T, Fischer WW, Lyons TW (2014) Low mid-Proterozoic atmospheric oxygen levels and the delayed rise of animals. Science 346:635–638
Pollard D, Kasting JF (2005) Snowball Earth: a thin-ice solution with flowing sea glaciers. J Geophys Res 110:C07010
Poulton SW, Canfield DE (2011) Ferruginous conditions: a dominant feature of the ocean through Earth's history. Elements 7:107–112
Powell JH, Abed A, Jarrar GH (2015) Ediacaran araba complex of jordan. GeoArabia 20:99–156
Pu JP, Bowring SA, Ramezani J, Myrow P, Raub TD, Landing E, Mills A, Hodgin E, Macdonald FA (2016) Dodging snowballs: geochronology of the Gaskiers glaciation and the first appearance of the Ediacaran biota. Geology 44:955–958
Ramsay CR (1986) Geologic Map of the Rabigh Quadrangle, Sheet 22D, Kingdom of Saudi Arabia. Saudi Arabian Deputy Ministry for Mineral Resources: Jiddah, Saudi Arabia, GM 84:1–49
Rieu R, Allen PA, Cozzi A, Kosler J, Bussy F (2007) A composite stratigraphy for the Neoproterozoic Huqf Supergroup of Oman: integrating new litho-, chemo- and chronolstratigraphic data of the Mirbat area, southern Oman. J Geol Soc, London 164:997–1009
Rooney AD, Chew DM, Selbey D (2011) Re–Os geochronology of the Neoproterozoic-Cambrian Dalradian Supergroup of Scotland and Ireland: Implications for Neoproterozoic stratigraphy, glaciations and Re–Os systematics. Precambr Res 185:202–214
Rooney AD, Macdonald FA, Strauss JV, Dudás FÖ, Hallmann C, Selby D (2014) Re-Os geochronology and coupled Os-Sr isotope constraints on the Sturtian snowball Earth. Proc Natl Acad Sci 111:51–56
Rooney AD, Strauss JV, Brandon AD, Macdonald FA (2015) A Cryogenian chronology: two long-lasting, synchronous Neoproterozoic snowball Earth glaciations. Geology 43:459–462
Rooney AD, Cantine MD, Bergmann KD, Gómez-Pérez I, Al Baloushi B, Boag TH, Busch JF, Sperling EA, Strauss JV (2020) Calibrating the coevolution of Ediacaran life and environment. Proc Nat Acad Sci 117:16824–16830
Rothman DH, Hayes JM, Summons RE (2003) Dynamics of the Neoproterozoic carbon cycle. Proc Natl Acad Sci 100:8124–8129
Runnegar B (2000) Loophole for snowball earth. Nature 405:403–404
Sahoo SK, Planavsky NJ, Kendall B, Wang X, Shi X, Scott C, Anbar AD, Lyons TW, Jiang G (2012) Ocean oxygenation in the wake of the Marinoan glaciation. Nature 489:546–549
Sandler A, Teutsch N, Avigad D (2012) Sub-Cambrian pedogenesis recorded in weathering profiles of the Arabian-Nubian Shield. Sedimentology 59:1305–1320
Sawaki Y, Kawai T, Shibuya T, Tahata M, Omori S, Tsuyoshi K, Yoshida N, Hirata T, Ohno T, Windley BF, Shigenori M (2010) $^{87}Sr/^{86}Sr$ chemostratigraphy of Neoproterozoic Dalradian carbonates below the Port Askaig Glaciogenic Formation, Scotland. Precambr Res 179:150–164
Schrag DP, Higgins JA, Macdonald FA, Johnston DT (2013) Authigenic carbonate and the history of the global carbon cycle. Science 339:540–543
Shang CK, Morteani G, Satir M, Taubald H (2010) Neoproterozoic continental growth prior to Gondwana assembly: constraints from zircon-titanite geochronology, geochemistry and petrography of ring complex granitoids, Sudan. Lithos 118:61–81
Shields GA, Mills BJW, Zhu M, Raub RD, Daines SJ, Lenton TM (2019) Unique Neoproterozoic carbon isotope excursions sustained by coupled evaporite dissolution and pyrite burial. Nat Geosci 12:823–827
Shields-Zhou GA, Denoux M, Och L (2011) The record of Neoproterozoic glaciation in the Taoudéni Basin, NW Africa. In: Arnaud E et al (eds) The geological record of Neoproterozoic glaciations. Geol Soc London Memoir 36:163–171
Shields-Zhou GA, Porter S, Halverson GP (2016) A new rock-based definition for the Cryogenian Period (circa 720–635 Ma). Episodes 39:3–8
Sifeta K, Roser BP, Kimura JI (2005) Geochemistry, provenance, and tectonic setting of Neoproterozoic metavolcanic and metasedimentary units, Werri area, Northern Ethiopia. J Afr Earth Sc 41:212–223
Spence GH, Le Heron DP, Fairchild IJ (2016) Sedimentological perspectives on climatic, atmospheric and environmental change in the Neoproterozoic Era. Sedimentology 63:253–306
Squire RJ, Campbell IH, Allen CM, Wilson CJ (2006) Did the Transgondwanan Supermountain trigger the explosive radiation of animals on Earth? Earth Planet. Sci Lett 250:116–133
Stein M (2003) Tracing the plume material in the Arabian-Nubian Shield. Precambr Res 123:223–234
Stern RJ (1985) The najd fault system, Saudi Arabia and Egypt: a late Precambrian rift-related transform system? Tectonics 4:497–511
Stern RJ (1994) Arc-assembly and continental collision in the Neoproterozoic African Orogen: implications for the consolidation of Gondwanaland. Annu Rev Earth Planet Sci 22:319–351
Stern RJ (2002) Crustal evolution in the East African Orogen: a neodymium isotopic perspective. J Afr Earth Sci 34:109–117
Stern RJ (2018) The evolution of plate tectonics. Philosophical Transactions A, 376, 20170406. https://doi.org/10.1098/rsta.2017.0406

Stern RJ, Abdelsalam MG (1998) Formation of juvenile continental crust in the Arabian-Nubian Shield: evidence from granitic rocks of the Nakasib suture. NE Sudan Geol Rundschau 87:150–160

Stern RJ, Johnson P (2010) Continental lithosphere of the Arabian Plate: a geologic, petrologic, and geophysical synthesis. Earth Sci Rev 101:29–67

Stern RJ, Miller NR (2018) Did the transition to plate tectonics cause Neoproterozoic snowball Earth? Terra Nova 30:87–94

Stern RJ, Miller NR (2019) Neoproterozoic glaciation—snowball earth hypothesis. Encyclopedia of geology, 2nd ed. https://doi.org/10.1016/B978-0-12-409548-9.12107-4

Stern RJ, Avigad D, Miller NR, Beyth M (2006) Geological society of Africa presidential review: evidence for the snowball earth hypothesis in the Arabian-Nubian Shield and the East African Orogen. J Afr Earth Sc 44:1–20

Stern RJ, Johnson PR, Ali KA, Mukherjee S (2011) Evidence for early and mid-cryogenian glaciation in the northern Arabian-Nubian Shield (Egypt, Sudan, and western Arabia). In: The geological record of neoproterozoic glaciation. In: Arnaud E, Halverson GP, Shield-Zhou G (eds) Geol Soc London, UK, 2011; Memoirs 36, 277–284

Stewart SA (2016) Structural geology of the Rub' Al-Khali Basin, Saudi Arabia. Tectonics 35:2417–2438

Stoeser DB, Stacey JS (1988) Evolution, U–Pb geochronology, and isotope geology of the Pan-African Nabitah orogenic belt of the Saudi Arabian Shield. In: El-Gaby S, Greiling RO (eds) The Pan-African Belt of NE Africa and adjacent areas, Friedr. Vieweg & Sohn, Braunschweig, pp 227–289

Sultan M, Arvidson RE, Duncan I, Stern RJ, El Kaliouby M (1988) Extension of the Najd Shear System from Saudi Arabia to the Central Eastern Desert of Egypt based on Integrated Field and Landsat Observations. Tectonics 7:1291–1306

Swanson-Hysell NL, Rose CV, Calmet CC, Halverson GP, Hurtgen MT, Maloof AC (2010) Cryogenian glaciation and the onset of carbon-isotope decoupling. Science 328:608–611

Swanson-Hysell NL, Maloof AC, Condon DJ, Jenkin GR, Alene M, Tremblay MM, Tesema T, Rooney AD, Haileab B (2015) Stratigraphy and geochronology of the Tambien Group, Ethiopia: evidence for globally synchronous carbon isotope change in the Neoproterozoic. Geology 43:323–326

Tadesse T (1997) The geology of axum area (ND 37-6). Ethiopian Institute of Geological Surveys, Addis Ababa (Memoir No. 9)

Tadesse T (1999) Axum sheet geological map. Geological Survey of Ethiopia, Addis Ababa, Ethiopia. 1:250,000 map

Tadesse T, Hoshino M, Suzuki K, Iizumi S (2000) Nd, Rb–Sr and Th–U–Pb zircon ages of syn- and post-tectonic granitoids from the Axum area of northern Ethiopia. J Afr Earth Sci 30:313–327

Tait J, Delpomdor F, Préat A, Tack A, Straathof G, Nkula VK (2011) Neoproterozoic sequences of the West Congo and Lindi/Ubangi Supergroups in the Congo Craton, Central Africa. In: Arnaud E et al (eds) The geological record of Neoproterozoic glaciations. Geol Soc London Memoir 36:185–193

Teklay M, Kröner A, Mezger K (2001) Geochemistry, geochronology and isotope geology of Nakfa intrusive rocks, northern Eritrea: products of a tectonically thickened Neoproterozoic arc crust. J Afr Earth Sci 33:283–301

Tostevin R, Clarkson MO, Gangl S, Shields GA, Wood RA, Bowyer F, Penny AM, Stirling CH (2019) Uranium isotope evidence for an expansion of anoxia in terminal Ediacaran oceans. Earth Planet Sci Lett 506:104–112

Trindade RIF, Macouin M (2007) Palaeolatitude of glacial deposits and palaeogeography of Neoproterozoic ice ages. CR Geosci 339:200–211

Tschopp RH (1967) The general geology of Oman. In: Proceedings of the 7th world petroleum congress 2, pp 231–242

Tsige L, Abdelsalam MG (2005) Neoproterozoic-early Paleozoic gravitational tectonic collapse in the southern part of the Arabian-Nubian Shield: the Bulbul Belt of southern Ethiopia. Precambr Res 38:31–297

Tziperman E, Halevy I, Johnston DT, Knoll AH, Schrag DP (2011) Biologically induced initiation of Neoproterozoic snowball-Earth events. Proc Natl Acad Sci USA 108:15091–15096

Vail JR (1983) Pan-African crustal accretion in northeast Africa. J Afr Earth Sci 1:285–294

Veevers JJ (2003) Pan-African is Pan-Gondwanaland: oblique convergence drives rotation during 650–500 Ma assembly. Geology 31:501–504

Vernhet R, Youbi N, Chellai EH, Villeneuve M El, Archi A (2012) The Bou-Azzer glaciation: evidence for an Ediacaran glaciation on the West African Craton (Anti-Atlas, Morocco). Precambr Res 196–197:106–112

Verri P (1909) Contributo allo studio geografio Della Colonia Eritrea. Bollettino della Societa' Geografica Italiana, 10, pp 251–320. Carta Geologica 1:1,500,000

Vickers-Rich P, Kozdroj W, Kattan FH, Leonov M, Ivantsov A, Johnson PR, Linnemann U, Hofmann M, Al Garni SM, Al Qubsani A, Shamari A, Al Baraki A, Al Kaff MH, Ziolkowska-Kozdroj M, Rich TH, Trusler P, Rich B (2010) Reconnaissance for an Ediacaran fauna, Kingdom of Saudi Arabia. Saudi Geological Survey, Technical Report, SGS-TR-2010-8, p 42, 74 figs., 1 table, 1 pl

Vickers-Rich P, Ivantsov A, Kattan FH, Johnson PR, Al Qubsani A, Kashghari W, Leonov M, Rich R, Linnemann U, Hofmann M, Trusler P, Smith J, Yazidi A, Rich B, Al Garni SM, Shamari A, Al Barakati A, Al Kaff MH (2013) In search of the Kingdom's Ediacarans: the first genuine Metazoans (macroscopic body and trace fossils) from the Neoproterozoic Jibalah Group (Vendian/Ediacaran) on the Arabian Shield. Saudi Geological Survey Technical Report SGS-TR-2013-5, p 21., 19 figs., 1 table

Weissbrod T, Sneh A (2002) Sedimentology and paleogeography of the Late Precambrian–Early Cambrian arkosic and conglomeratic facies in the northern margins of the Arabo-Nubian Shield Bulletin. Geol Survey Israel 87:44

Whitehouse MJ, Pease V, Al-Khirbash S (2016) Neoproterozoic crustal growth at the margin of the East Gondwana continent—age and isotopic constraints from the easternmost inliers of Oman. Int Geol Rev 58:2046–2064

Wilde SA, Youssef K (2000) Significance of SHRIMP dating of the imperial porphyry and associated Dokhan volcanics, Gebel Dokhan, northeastern desert, Egypt. J Afr Earth Sci 31:403–413

Wilde SA, Youssef K (2002) A re-evaluation of the origin and setting of the late Precambrian Hammamat Group based on SHRIMP U–Pb dating of detrital zircons from Gebel Umm Tawat, North Eastern Desert, Egypt. J Geol Soc London 159:595–604

Williams GE (2008) Proterozoic (pre-Ediacaran) glaciation and the highobliquity, low-latitude ice, strong seasonality (HOLIST) hypothesis: principles and tests. Earth Sci Rev 87:61–93

Williams GE, Schmidt PW, Young GM (2016) Strongly seasonal Proterozoic glacial climate in low palaeolatitudes: radically different climate system on the pre-Ediacaran Earth. Geosci Front 7:555–571

Wu C, Yang T, Shields GA, Bian X, Bao B, Ye H, Li W (2020) Termination of Cryogenian ironstone deposition by deep ocean euxinia. Geochem Perspect Lett 15:1–5

Yin Z, Zhu M, Davidson EH, Bottjer DJ, Zhao F, Tafforeau P (2015) Sponge grade body fossil with cellular resolution dating 60 Myr before the Cambrian. Proc Nat Acad Sci 141:E1453–E1460

Zhou MT, Luo T, Huff WD, Yang Z, Zhou G, Gan T, Yang H, Zhange D (2018) Timing the termination of the Doushantuo negative carbon isotope excursion: evidence from U–Pb ages from

the Dengying and Liuchapo formations, South China. Sci Bull 63:1431–1438

Zhou Y, Pogge von Strandmann PAE, Zhu M, Ling H, Manning C, Li D, He T, Shields GA (2020) Reconstructing Tonian seawater $^{87}Sr/^{86}Sr$ using calcite microspar. Geology 48:462–467

Zimmer M, Kröner A, Jochum KP, Reischmann R, Todt W (1995) The Gabal Gerf complex: a Precambrian N-MORB ophiolite in the Nubian Shield, NE Africa. Chem Geol 123:29–51